

ANL/APS/TB-50

**THERMAL ANALYSIS OF THE COMPONENTS OF
THE INSERTION DEVICE FRONT ENDS
FEv1.2 AND FEv1.5**

**Yifei Jaski
XFD Division
Advanced Photon Source**

July 2005

**Work sponsored by
U.S. DEPARTMENT OF ENERGY
Office of Science**

Table of Contents

1. INTRODUCTION	1
2. GENERAL INFORMATION	2
2.1. Front-End Description and Components List	2
2.2. Source Parameters	3
2.3. Material Properties	4
2.4. Failure Criteria	4
3. THERMAL ANALYSIS OF COMPONENTS OF FEV1.5	6
3.1. Thermal Analysis of Pre-Mask B7-70	6
3.1.1. B7-70 General Information	6
3.1.2. Bending Magnet Power Calculation	7
3.1.3. Thermal and Stress Analysis of B7-70	7
3.2. Thermal Analysis of the First Fixed Mask M1-40	9
3.2.1. M1-40 Model and Mesh	9
3.2.2. M1-40 Power Calculation	11
3.2.3. M1-40 Thermal and Stress Analyses for 100 mA Operation	12
3.2.4. M1-40 Temperature and Stress at Higher Beam Current	16
3.2.5. Sensitivity Study of Film Coefficient and Cooling Water Set Point	17
3.3. Thermal Analysis of the Second Fixed Mask M2-40	18
3.3.1. M2-40 Model and Mesh	18
3.3.2. M2-40 Power Calculation	21
3.3.3. M2-40 Thermal and Stress Analysis for 100 mA Operation	22
3.4. Thermal Analysis of the Third Fixed Mask M2-50	26
3.4.1. M2-50 Model and Mesh	26
3.4.2. M2-50 Power Calculation	29
3.4.3. M2-50 Thermal and Stress Analysis for 100 mA Operation	30
3.5. Thermal Analysis of the Photon Shutters P2-30	34
3.5.1. P2-30 Model and Mesh	34
3.5.2. P2-30 Power Calculation	36
3.5.3. P2-30 Thermal and Stress Analysis for 100 mA Operation	37
3.6. Thermal Analysis of the Exit Mask M4-40	39
3.6.1. M4-40 Model and Mesh	39
3.6.2. M4-40 Power Calculation	41
3.6.3. M4-40 Thermal and Stress Analysis for 100 mA Operation	42
3.7. Summary of the Results for Front End v1.5	45
4. THERMAL ANALYSIS OF COMPONENTS OF FRONT END V1.2U	47
4.1. Thermal Analysis of Premasks B7-50 and B7-60	47

4.2.	Thermal Analysis of the First Fixed Mask M1-30	49
4.2.1.	M1-30 Model and Mesh	49
4.2.2.	M1-30 Power Calculation	51
4.2.3.	M1-30 Thermal and Stress Analyses for 100 mA Operation	52
4.3.	Thermal Analysis of the Second Fixed Mask M2-20	56
4.3.1.	M2-20 Model and Mesh	56
4.3.2.	M2-20 Power Calculation	58
4.3.3.	M2-20 Thermal and Stress Analysis for 100 mA Operation	59
4.4.	Thermal Analysis of Photon Shutters P1-20 and P2-20	61
4.4.1.	P1-20 and P2-20 Model	61
4.4.2.	P1-20 and P2-20 Power Load	62
4.4.3.	P1-20 and P2-20 Thermal Analysis at 100 mA	64
4.5.	Thermal Analysis of the Exit Mask L5-83	67
4.5.1.	L5-83 Model and Mesh	67
4.5.2.	L5-83 Power Calculation	69
4.5.3.	L5-83 Thermal and Stress Analysis for 100 mA Operation	70
4.6.	Thermal Analysis of the Exit Mask M4-30	73
4.6.1.	M4-30 Model and Mesh	73
4.6.2.	M4-30 Power Calculation	75
4.6.3.	M4-30 Thermal and Stress Analyses for 100 mA Operation	76
4.7.	Summary of the Results for Front End v1.2u	79
5.	SPECIAL CASE: 3-ID FRONT END	81
5.1.	Thermal Analysis of the 3-ID Photon Shutters	81
6.	SPECIAL CASE: 4-ID FRONT END	85
6.1.	4-ID General Information	85
6.2.	Thermal Analysis of the 4-ID P1-20 and P2-20	85
6.3.	Thermal Analysis of the 4-ID Exit Mask M7-20	89
6.3.1.	M7-20 Model and Mesh	89
6.3.2.	M7-20 Power Calculation	91
6.3.3.	M7-20 Thermal and Stress Analysis for 100 mA Operation	93
7.	SUMMARY AND CONCLUSION	96
7.1.	FE Components and Source Summary	96
	ACKNOWLEDGMENTS	98
	REFERENCES	98

1. Introduction

In order to prepare for higher beam current operation and to establish the maximum allowed beam current, thermal and stress analyses of the components of the existing front ends (FEv1.2 and FEv1.5 plus special cases) were carried out. This report contains analyses of the beam confining and stopping components including all fixed masks, photon shutters and exit masks of the existing front ends. It excludes the newly installed canted-undulator front ends (21-ID, 23-ID, and 24-ID) and the high-heat-load front ends (26-ID and 30-ID). Separate analyses exist for the canted-undulator front ends and the high-heat-load front ends. In this report the analysis of each component is comprehensive. It contains details of each component's modeling, meshing, load cases, maximum temperature and stress results. All mask analyses include details of the aperture profile and beam-missteering scenarios. This report illustrates the finite element analysis (FEA) method step by step in each component's analysis. It will serve as the front-end engineering analysis data archive for the existing front ends. The report is organized by the type of front end and name of the components. The temperature and stress data for 100 mA operation are calculated. Once the temperature and stress data for 100 mA beam current are calculated, linear extrapolation is used to derive the temperature and stress data for higher beam currents. By comparing the temperature and stress data to the failure criteria, the maximum allowed beam current is derived.

2. General Information

2.1. Front-End Description and Components List

There are mainly two types of existing front ends (FEv1.2 and FEv1.5) plus some variations. Most sectors have a single 2.4-m-long 3.3-cm-period undulator (undulator A) with a minimum gap of 11 mm ($k=2.62$). Unless specifically noted, the source is assumed to be undulator A at $k=2.62$. The front-end components list is shown in Table 2.1-1

Table 2.1-1 Front-end description and components list.

Type of FE	Components	Description	Installed in sectors	Source
FEv1.5	B7-70	BM mask	16, 22, 31, 32	Bending Magnet 3.3 cm, N=72 undulator at 11 mm gap ($K_{\max}=2.62$)
	M1-40	1 st Fixed Mask		
	M2-40	2 nd Fixed Mask		
	M2-50	3 rd Fixed Mask		
	P2-30	1 st Photon Shutter		
	P2-30	2 nd Photon Shutter		
	M4-40	Exit Mask		
FEv1.2u	B7-60	BM mask	1,5,6,7,8,9,10, 12,13,14,15, 17,18,19,20,3 3,34	Bending Magnet 3.3 cm, N=72 undulator at 11 mm gap ($K_{\max}=2.62$)
	M1-30	1 st Fixed Mask		
	M2-20	2 nd Fixed Mask		
	P1-20	1 st Photon Shutter		
	P2-20	2 nd Photon Shutter		
	L5-83	Exit Mask		
	M4-30	Mask down stream of L5-83 for change exit aperture from 4.5×4.5 mm to 3×2 mm	1,7,10	
2-ID	Same components as FEv1.2u with different source		2	undulator A, plus 5.5 cm, 2.4 m undulator
3-ID	Same components as FEv1.2u with different source		3	Two U2.7 N=88 $k_{\max}=1.697$
4-ID (FEv1.5 masks and FEv1.2 shutters with a special exit mask)	B7-70	BM mask	4	3.3 cm N=72 undulator at 9.5 mm gap ($K_{\max}=3.175$) plus CPU
	M1-40	1 st Fixed Mask		
	M2-40	2 nd Fixed Mask		
	M2-50	3 rd Fixed Mask		
	P1-20	1 st Photon Shutter		
	P2-20	2 nd Photon Shutter		
M7-20	Exit Mask			
11-ID (FEv1.2w)	Same components as FEv1.2u except the 1 st Fixed Mask is M1-20 instead of M1-30		11	Elliptical multipole wiggler ($\lambda=16$ cm) $K_{y,\max}=14.3$, N=18

2.2. Source Parameters

For undulator power calculations, the source size and divergence were used. The smaller source size and divergence will result in a slightly higher peak power density. Zero emittance will result in the highest peak power density. Some calculations done over a year ago used the standard emittance, which is the default emittance for the source calculation software such as XOP [1] and SRUFF [2]. The current operation has a lower emittance. The peak power density difference between using the standard emittance and the lower emittance is about 2%. The peak power density difference between using the standard emittance and zero emittance is about 3%. The APS nominal storage ring parameters are shown in Table 2.2-1. The insertion device parameters are listed in Table 2.2-2.

Table 2.2-1 APS nominal storage ring parameters.

		Low emittance: 3.0 nm-rad Coupling: 2%	Standard emittance (Default in XOP and SRUFF)
Source size	σ_x	239.5 μm	352 μm
	σ_y	15.4 μm	18 μm
Divergence	$\sigma_{x'}$	14.4 μrad	22 μrad
	$\sigma_{y'}$	3.9 μrad	4.2 μrad

Table 2.2-2 Insertion device parameters at 100 mA beam current.

Location	ID type	description	K_{max} (gap)	Total power (Watts)	Peak power density (kW/mrad ²)
FEv1.2 and FEv1.5	Undulator A	$\lambda=3.3$ cm, N=72	2.62 (11 mm)	5327	157
2-ID upstream	Undulator A	$\lambda=3.3$ cm, N=72	2.62 (11 mm)	5327	157
2-ID downstream	Undulator	$\lambda=5.5$ cm, N=44	6.57	12280	146.3
3-ID	Undulator	$\lambda=2.7$ cm, N=176	1.697	6676	297
4-ID upstream	Circularly Polarized Undulator (CPU)	$\lambda=12.8$ cm, N=34	2.75	714	19.9
4-ID downstream	Undulator A	$\lambda=3.3$ cm, N=72	3.175 (9.5 mm)	7822	189
11-ID	Elliptical Multipole Wiggler (EMW)	$\lambda=16$ cm, N=18	$K_x=1.1$ $K_y=14.3$	8182	44.8

2.3. Material Properties

All masks and P2-30 shutters are made by electro-discharge machining (EDM) from solid blocks of GlidCop [3]. The P1-20 and P2-20 photon shutters are made by explosion bonding a GlidCop plate to the OFHC copper base. The properties relevant for the analysis for GlidCop and OFHC copper are shown in Table 2.3-1.

Table 2.3-1 Material properties of GlidCop and OFHC copper.

Material properties required for analysis	GlidCop AL-15	OFHC copper	Comments
Thermal conductivity (w/mm°C)	0.365	0.391	Required as input data
Thermal expansion coefficient (µm/m/°C)	16.6	17.7	Required as input data
Young's modulus (GPa)	130	115	Required as input data
Poisson's ratio	0.326	0.323	Required as input data
Yield strength (MPa)	331~455 (as consolidated to 75% cold worked)	41 (annealed) 324 ~ 372 (75% cold worked)	Not required as input data for linear analysis
Ultimate tensile strength (MPa)	413 ~ 483 (as consolidated to 75% cold worked)	220 (annealed) 344 ~ 381 (75% cold worked)	Not required as input data for linear analysis

2.4. Failure Criteria

The APS has, over the past 10 years, used conservative criteria for establishing the maximum thermal load acceptable for x-ray beam-intercepting components:

- 1) Maximum temperature on GlidCop < 300°C to prevent material creep.
- 2) Maximum temperature on the cooling wall < water boiling temperature at channel pressure to prevent water from boiling and to maintain single-phase heat transfer. The typical pressure after going through two-thirds of the length of a component is about 60 psig, and the corresponding water boiling temperature at 60 psig is 153°C.
- 3) Maximum von Mises stress < 400 MPa for photon shutters (the yield strength of the plate stock of GlidCop at room temperature). The maximum stress allowed on fixed masks at extreme missteering conditions is relatively relaxed since such missteering cases are very rare.

Recently, efforts have been underway to re-examine these criteria. A committee has been formed to re-evaluate the failure criteria, especially the stress limit. Tests are underway in collaboration with ESRF to obtain operational fatigue strength data. Since masks are only exposed to beam during beam missteering, while shutters are intercepting the beam fully during normal operation, the criteria for masks and shutters will be different.

3. Thermal Analysis of Components of FEv1.5

The FEv1.5 components have never been analyzed before. We took advantage of newly obtained software (ANSYS/ProE geometry connection) to have geometries modeled in ProE and transferred to ANSYS via this interface. All components in FEv1.5 were modeled in ProE by various designers to the fabrication level. Then the analyst examined the model and suppressed the features that are not relevant for the analysis, such as external chamfers, rounds and screw holes. The cleaned-up model was then read into ANSYS via an ANSYS/ProE geometry connection that is part of the ANSYS package. Next, a mesh was generated in ANSYS. For masks, the mesh control was set to have fine mesh in the aperture region, where the beam may strike, and a coarse mesh elsewhere to save computational time. The heat loads were calculated precisely based on the source parameters using SRUFF and fitted into a 4th-order Gaussian formula. The Gaussian formula was then applied as the heat flux distribution in ANSYS. The temperature field is calculated; then, using the temperature as the body load, the stress field is calculated. The beam was moved around within the aperture to simulate vertical, horizontal, and corner missteering, with temperature and stress calculations repeated to cover all load cases.

3.1. Thermal Analysis of Pre-Mask B7-70

3.1.1. B7-70 General Information

Pre-mask B7-70 is used to block the bending magnet (BM) radiation from AM bending magnet coming down the same pipe with the undulator beam. The B7-70 pre-mask is to protect the first fixed mask inlet flange from being struck by the bending magnet beam. This mask is machined from solid GlidCop rounds, and the BM radiation is normal incidence to the mask. The key information for B7-70 is listed in Table 3.1-1.

Table 3.1-1 Key information for pre-mask B7-70.

Name	B7-70
Distance to the center of the straight section (m)	16.0
Distance to the start of the AM bending magnet (m)	8.27
Inlet aperture H×V (mm×mm)	(+31/-17)× 25
Outlet aperture H×V (mm×mm)	(+31/-17)× 25
Total BM fan exit from SR valve in undisplaced sector	5.5 mrad (refer to drawing 310308-920015-02)
Total BM fan intercepted by B7-70 in undisplaced sector	3.5 mrad (inbound)
Total BM fan exit from SR valve in displaced sector	4.0 mrad (refer to drawing 310308-920016)
Total BM fan intercepted by B7-70 in displaced sector	3.5 mrad (inbound)
B7-70 reference drawing number	B7-710001-00

3.1.2. Bending Magnet Power Calculation

For both an undisplaced and a displaced sector, the B7-70 mask will intercept 3.5 mrad of the BM horizontal radiation fan. At 300 mA, the total power/mrad horizontal beam and peak power density is shown in the following equations.

$$P_{total} (w/mrad) = 4.22B(Tesla)E^3(GeV)I(Amp) = 4.22 \times 0.6 \times 7^3 \times 0.3 = 260.5w/mrad$$

$$P_{peak} (w/mrad^2) = 5.42B(Tesla)E^4(GeV)I(Amp) = 5.42 \times 0.6 \times 7^4 \times 0.3 = 2342w/mrad^2.$$

The power density distribution can be calculated as

$$P = P_{peak} \left[\frac{1}{7} \left(\frac{12}{(1+(\gamma\psi)^2)^{\frac{5}{2}}} - \frac{5}{(1+(\gamma\psi)^2)^{\frac{7}{2}}} \right) \right] \approx P_{peak} e^{-\frac{\psi^2}{2\sigma^2}},$$

where $\gamma = 1957E(GeV) = 1957 \times 7 = 13700$

$$\sigma = 0.608 \times \frac{1}{\gamma} = 0.044mrad$$

$$\psi = \frac{y(mm)}{D(m)}, \text{ D is the distance to source.}$$

3.1.3. Thermal and Stress Analysis of B7-70

The B7-70 pre-mask was modeled in ProE and read in by ANSYS. A 300 mA beam current was used for the analysis. The mask is cooled via two clear 3/8-inch-diameter horizontal cooling holes. The beam is normal incidence to the mask and only on the inbound side of the mask. The temperature plot is shown in Figure 3.1-1, and the von Mises stress plot is shown in Figure 3.1-2. The results are summarized in Table 3.1-2.

Table 3.1-2 B7-70 results with 300 mA beam current, film coefficient $h=0.01 \text{ w/mm}^2\text{C}$, $T_0=25.6\text{C}$

Total power absorbed in the B7-70 pre-mask model (w)	913
Peak power density (w/mm^2)	34.2
Maximum temperature ($^{\circ}\text{C}$)	208.5
Maximum cooling wall temperature ($^{\circ}\text{C}$)	74.9
Maximum von Mises stress (MPa)	180.2

B7-70 is made of GlidCop, and the maximum temperature and stress data are well within the current limit. So B7-70 can safely operate at 300 mA.

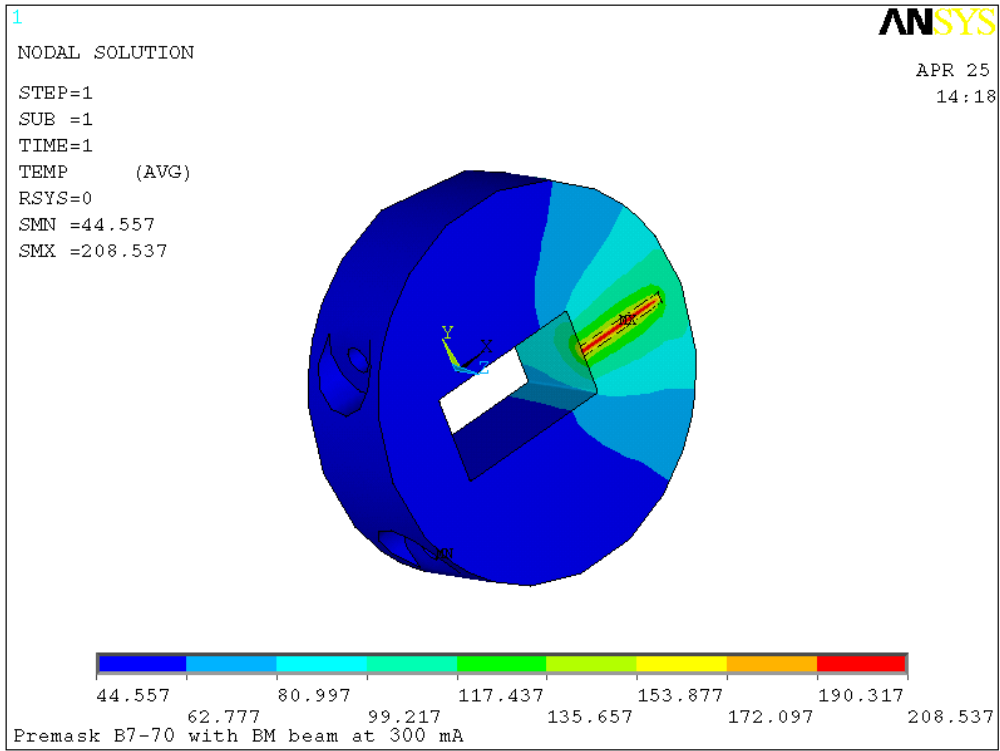


Figure 3.1-1 B7-70 pre-mask temperature plot ($^{\circ}\text{C}$) with 300 mA, $h=0.01 \text{ w/mm}^2$, $T_0=25.6^{\circ}\text{C}$.

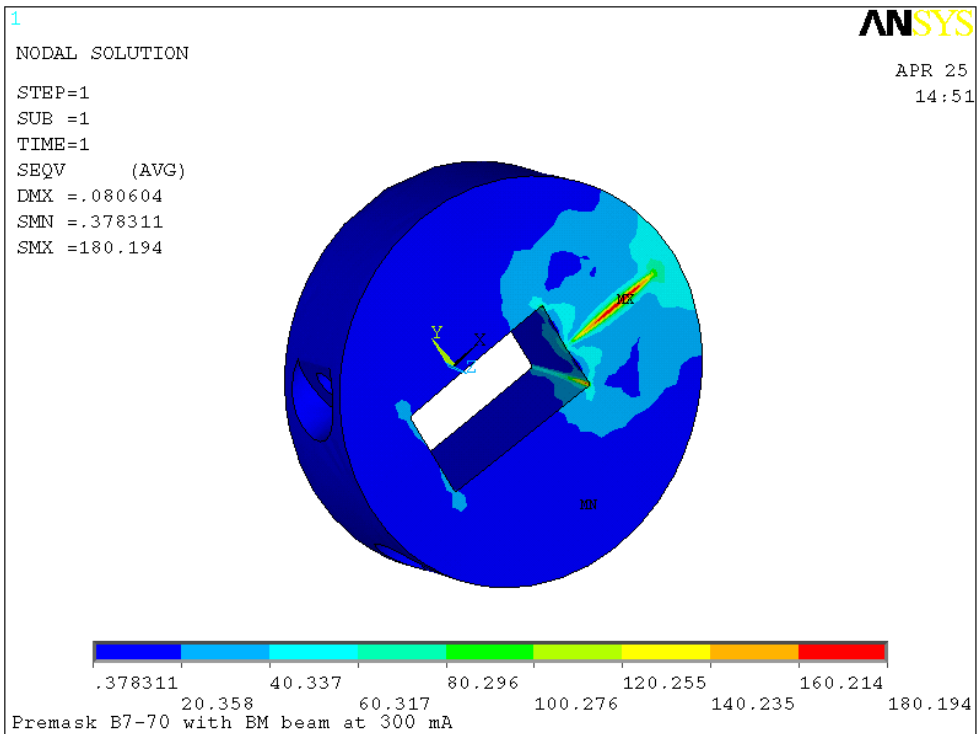


Figure 3.1-2 B7-70 pre-mask von Mises stress plot (MPa) with 300 mA, $h=0.01 \text{ w/mm}^2$, $T_0=25.6^{\circ}\text{C}$.

3.2. Thermal Analysis of the First Fixed Mask M1-40

3.2.1. M1-40 Model and Mesh

The M1-40 mask is manufactured from a solid round billet of GlidCop. The M1-40 was modeled in ProE, and the model was read in by ANSYS for analysis. Within ANSYS, the original model was divided into two volumes lengthwise to simplify the meshing of the model.

Volume 1: from the inlet to the narrowest aperture (the neck of the mask). This volume can be meshed with a brick mesh because the cross section is topologically similar. A brick mesh is desired when possible because it results in better accuracy and less computation time.

Volume 2: from the narrowest aperture to the exit end of the mask. This volume can not be meshed with a brick mesh and so is meshed with a tetrahedron mesh due to the cooling channels stop within this volume. Key information for M1-40 is shown in Table 3.2-1. The model and mesh are shown in Figure 3.2-1 and Figure 3.2-2, respectively.

Table 3.2-1 Key dimensions and reference information for M1-40.

Name	M1-40
Distance to the center of the straight section (m)	16.75
Distance to the center of undulator installed 1.25 m downstream (m)	15.50
Total power (watts)	5327
Peak power density (w/mm ²)	648.3
Inlet aperture H×V (mm×mm)	38 × 26
Outlet aperture H×V (mm×mm)	20 × 12
Active length (mm)	344
Horizontal taper angle	1.5°
Vertical taper angle	1.17°
Aperture corner radius (mm)	1.0
Reference drawing number	4102010101-410000

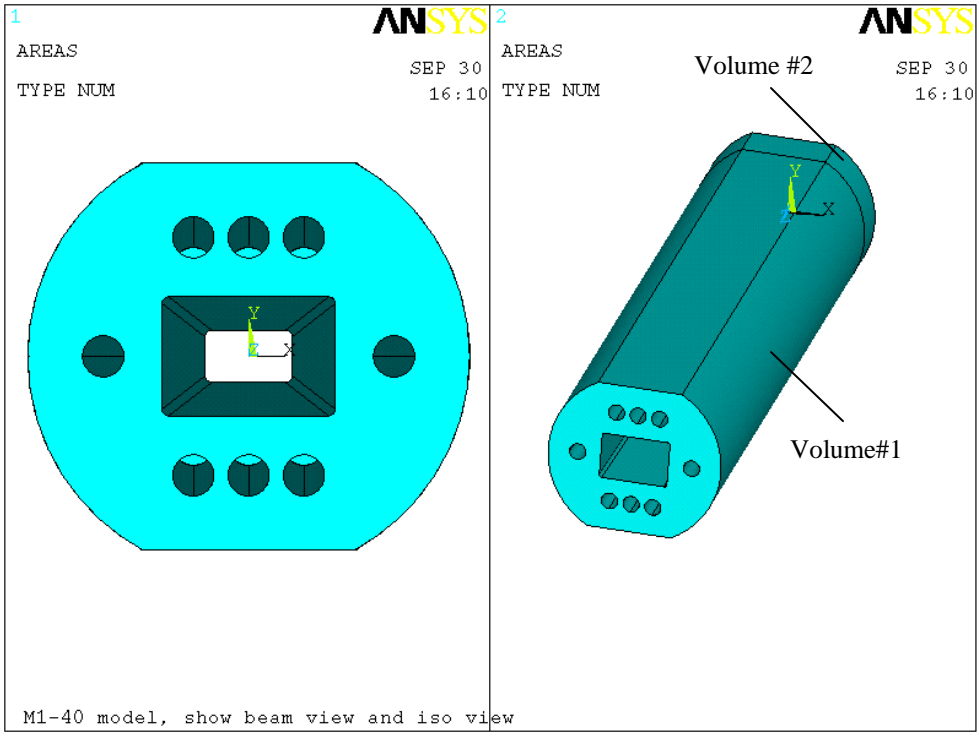


Figure 3.2-1 M1-40 model read in from ProE, and then divided into two volumes.

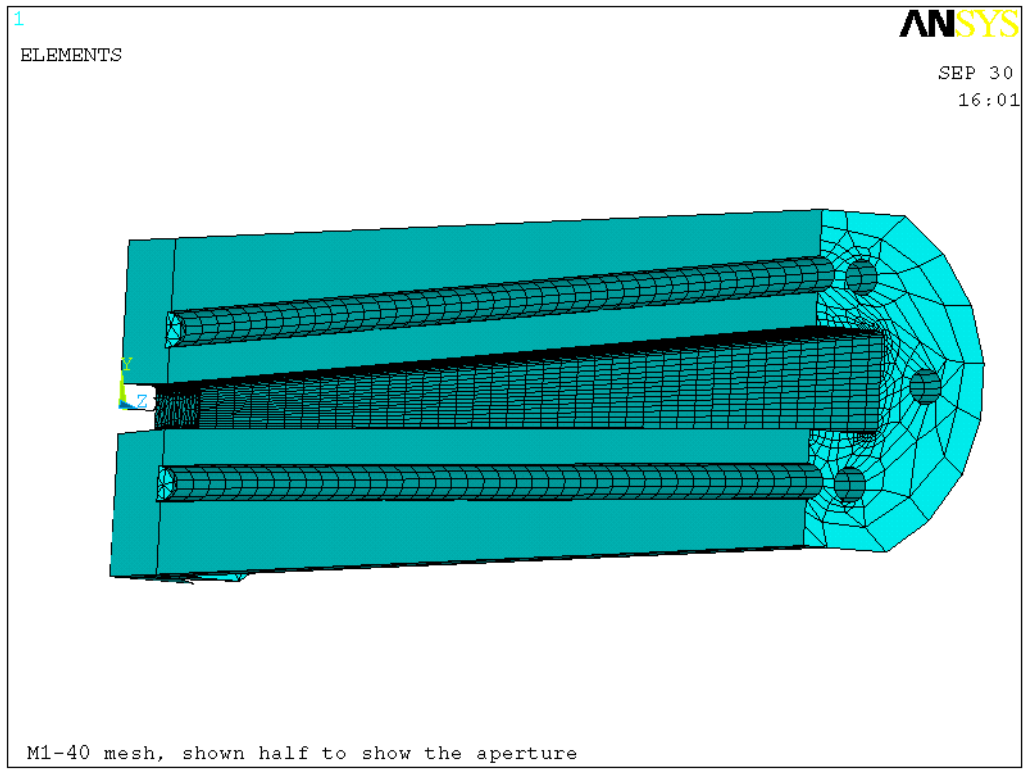


Figure 3.2-2 M1-40 mesh, cross section is shown in order to show the aperture.

3.2.2. M1-40 Power Calculation

The power density distribution from one undulator A at 100 mA and 11 mm gap ($k=2.62$) at 15.5 m was calculated using SRUFF. The power density distribution and the curve fit are shown in Figure 3.2-3 and Figure 3.2-4, respectively. The fitted formula was used in ANSYS for the thermal load application.

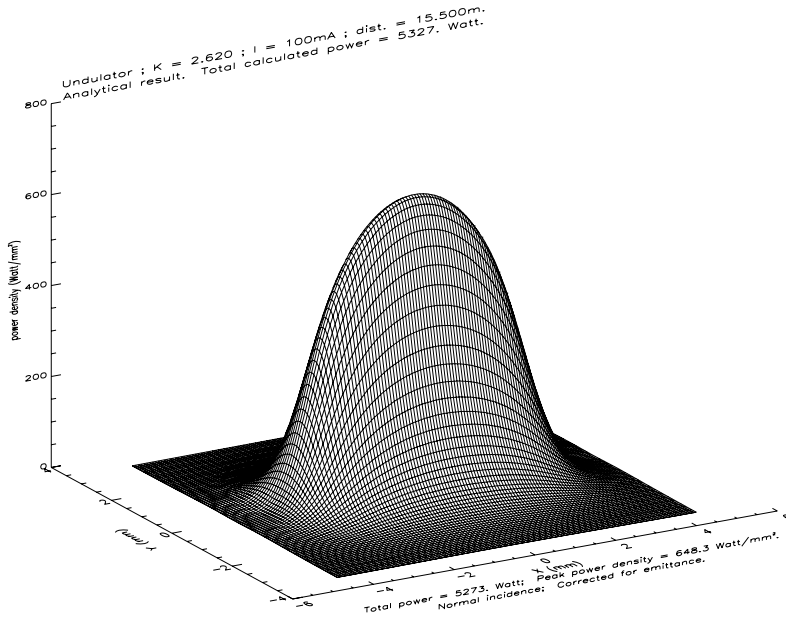


Figure 3.2-3 Undulator A power density distribution at 100 mA, $k=2.62$ at 15.5 m.

$$\text{Fit} = \exp(6.4743 - 0.045472x^2 - 1.2597y^2 - 0.013699x^4 + 0.10310y^4 + 0.014556x^2y^2)$$

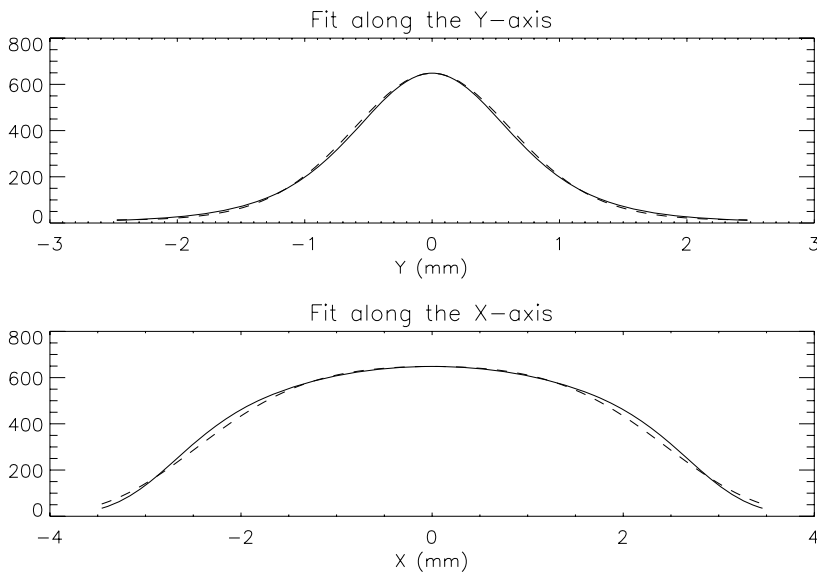


Figure 3.2-4 Power density distribution at 15.5 m from the Gaussian fitting formula. The solid line is the calculated data and the dashed line is the fitted formula.

3.2.3. M1-40 Thermal and Stress Analyses for 100 mA Operation

Under normal operating conditions, the beam will not strike the mask. The beam will strike the mask only when it is missteered. Missteering can be vertical, horizontal or a combination. Vertical missteering projects the beam on the upper or lower surface of the aperture, and the resulting footprint has the same width as the beam width. Horizontal missteering projects the beam on the left- or right-side surface of the aperture, and the resulting footprint has the same width as the beam height. The beam footprint is wider and shorter in vertical missteering compared to narrower and longer in horizontal missteering. As heat transfer depends on the perimeter of the beam footprint, typically, vertical missteering, which has shorter beam footprint perimeter, results in higher temperature and stress compared to horizontal missteering. With combination missteering, while the beam is still projected on either the upper or lower face of the aperture, it is closer to the corner, and the temperature will be lower because there is more material in the corner to help with heat transfer. Although the temperature is lower, the stress could be higher because the corner region is more constrained. So several spots need to be checked to find the highest stressed spot. Figure 3.2-5 shows various beam center locations used to locate the highest stressed spot.

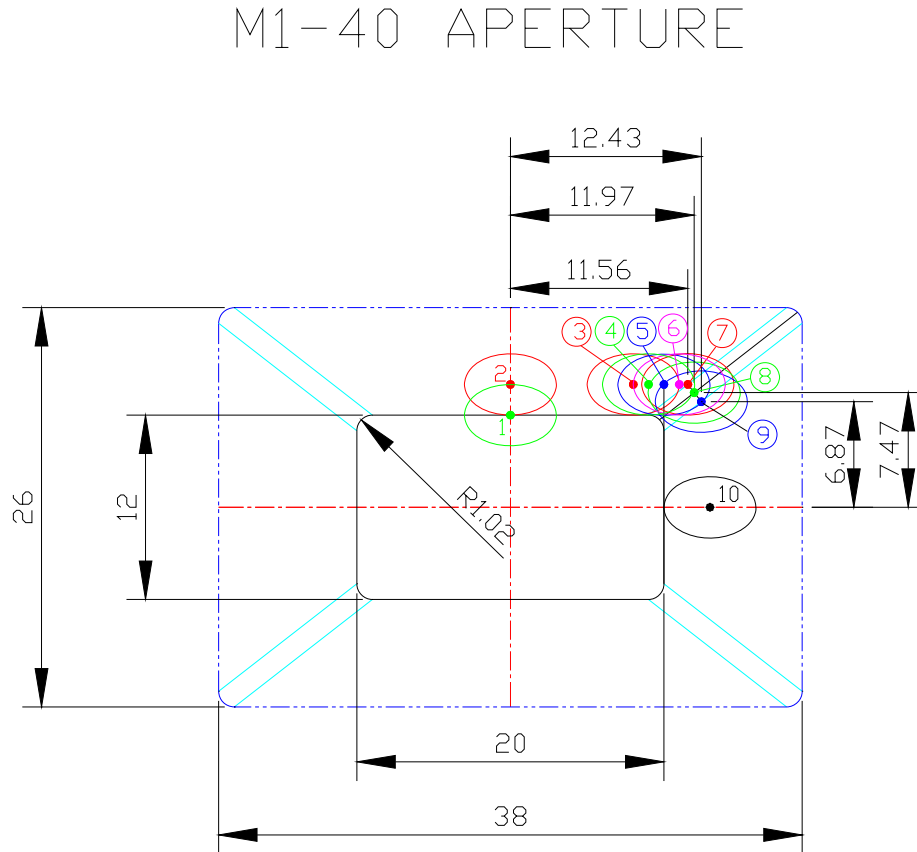


Figure 3.2-5 M1-40 aperture, round dots stand for the beam center, ovals stand for the beam footprint of 6x4 mm.

Temperature and stress data for beam at various locations are tabulated in Table 3.2-2.

Table 3.2-2 Temperature and stress results for M1-40 with beam center at various locations (100 mA, $k=2.62$, $h=0.015$ w/mm²°C, $T_0=25.6$ °C).

Beam center position	Beam center coordinates [x,y] mm	Missteering case	Max. temperature (°C)	Max. von Mises stress (MPa)	Comments
1	[0,6]	Vertical, beam center hits the neck, only half of beam on the top surface, other half of beam passes the aperture	179.5	n/a	Temperature too low to warrant stress calculation
2	[0,8]	Vertical, full beam on the top surface	204.8	319.4	Highest temperature
3	[8,8]	Vertical, approaching corner, full beam on the top surface	197.5	313.0	
4	[9,8]	Vertical, approaching corner, partial beam on the corner fillet	195.3	323.3	
5	[10,8]	Vertical, approaching corner, partial beam on the corner fillet	191.2	346.7	
6	[11,8]	Vertical approaching corner	182.0	349.1	Highest stress
7	[11.56,8]	Corner, beam center on the intersection of the top surface and corner fillet	174.3	342.1	
8	[11.97,7.47]	Corner, beam center on the center of the corner fillet	159.5	306.9	
9	[12.43,6.87]	Corner, beam center on the intersection of the right side surface and corner fillet	140.5	n/a	Temperature too low to warrant stress calculation
10	[13,0]	Horizontal, full beam on the right side surface	132.8	n/a	Temperature too low to warrant stress calculation

As predicted, the vertical missteering (position 2) results in the highest temperature. As the beam moves closer to the corner, the temperature decreases because there is more material to conduct heat, while the stress increases due to more constraints at the corner. The highest stress results when the beam hits position 6 (top surface very close to the intersection of the top and corner fillet). The neighboring positions of 5 and 7 have similar stress values. So the spacing of the positions is good enough.

The temperature and stress for the vertical and near-corner missteering cases are plotted in Figure 3.2-6 through Figure 3.2-9.

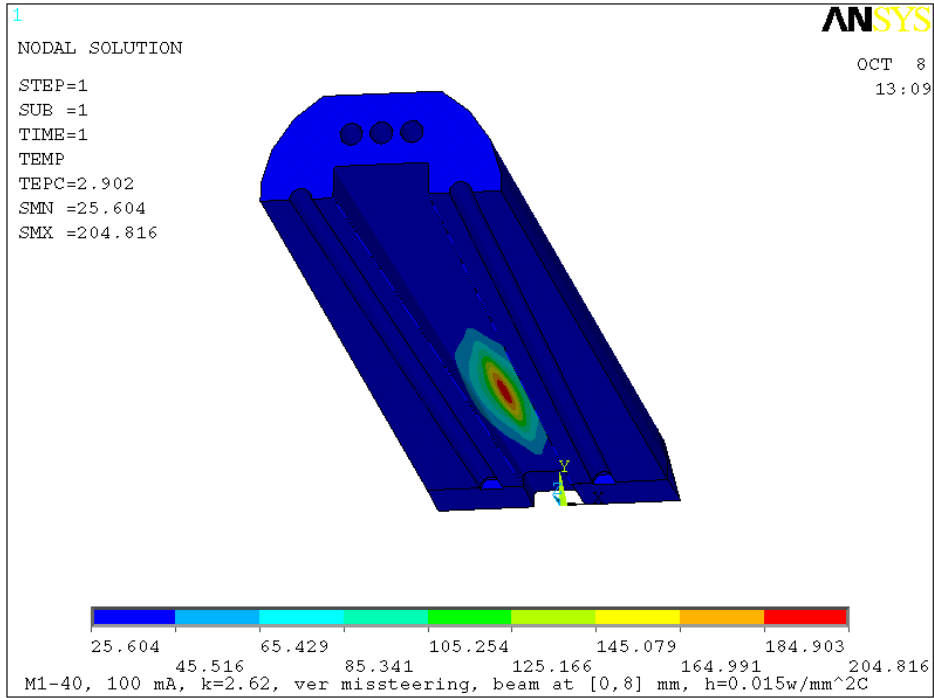


Figure 3.2-6 Temperature plot(°C), vertical missteering for M1-40 mask.

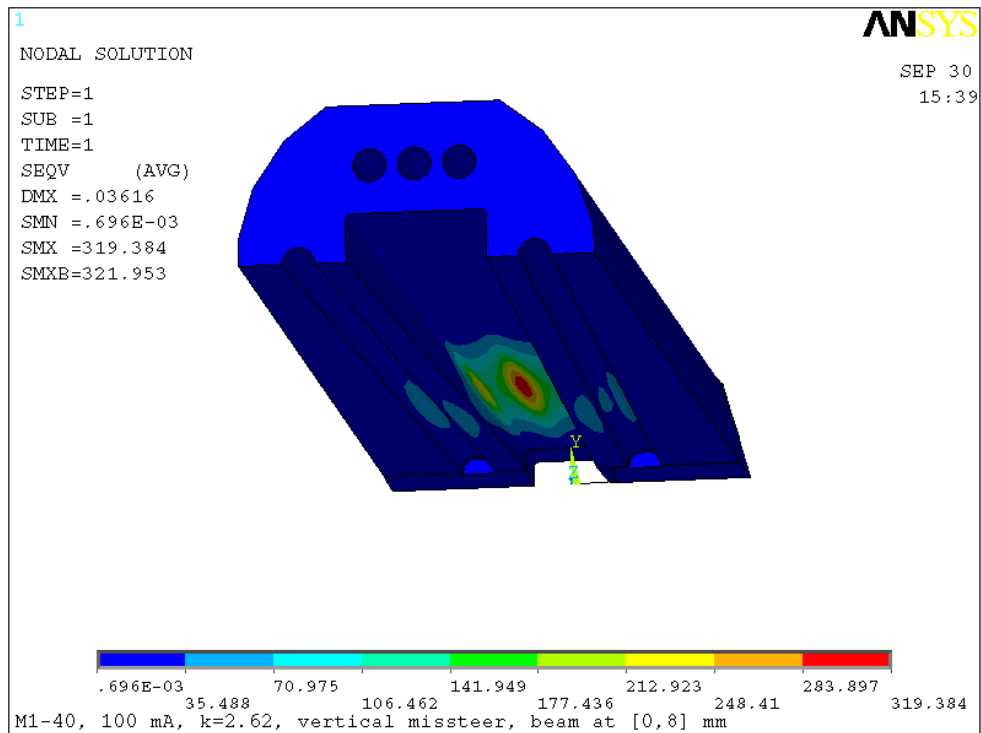


Figure 3.2-7 von Mises stress plot (MPa), vertical missteering for M1-40 mask.

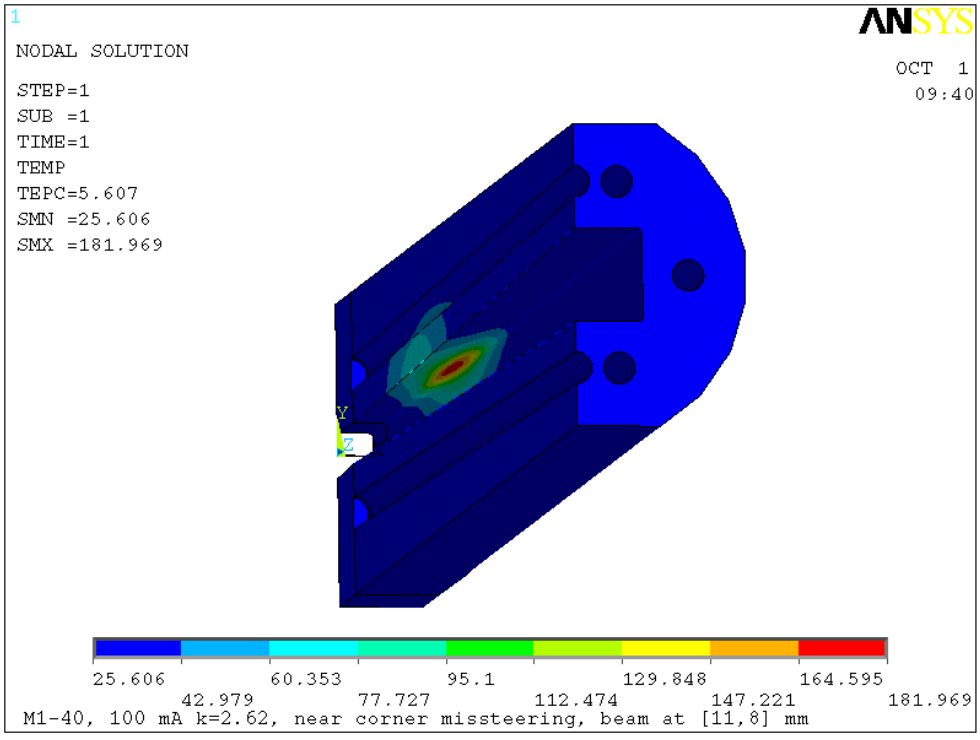


Figure 3.2-8 Temperature plot (°C), near-corner missteering for M1-40 mask.

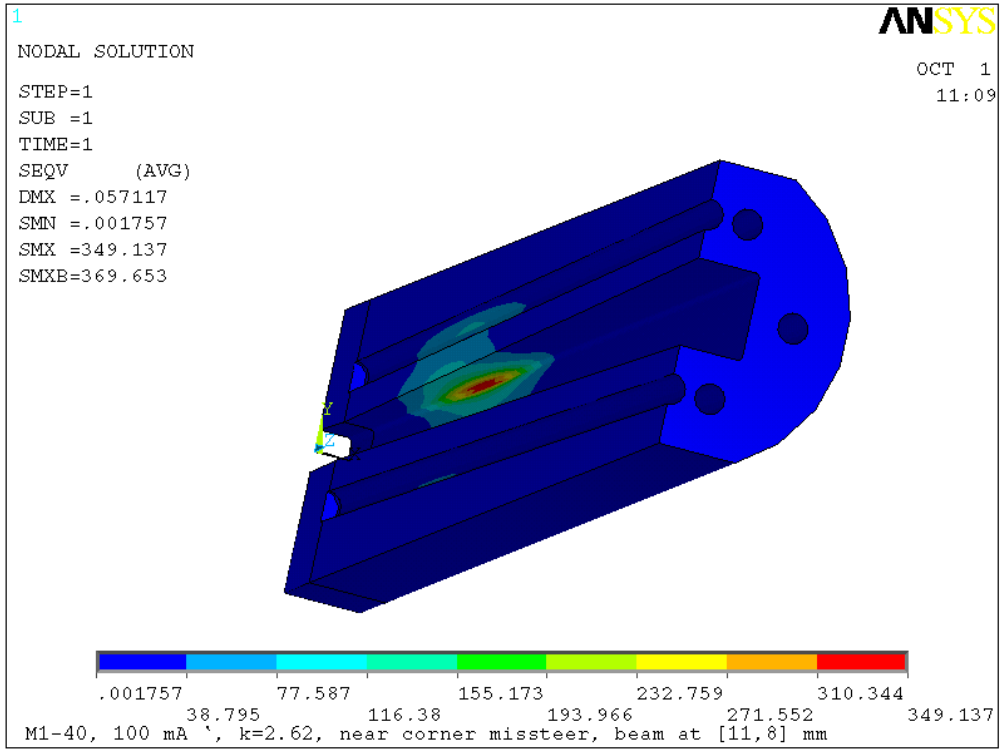


Figure 3.2-9 von Mises stress plot (MPa), near- corner missteering for M1-40 mask.

3.2.4. M1-40 Temperature and Stress at Higher Beam Current

It is only necessary to calculate the 100 mA case because an increasing beam current has a linear effect on the component's response. The following formula can precisely predict the higher current results, such as 130 mA or 150 mA.

$$T_{150mA} = (T_{100mA} - T_{water}) \times \left(\frac{150mA}{100mA}\right) + T_{water}$$

$$S_{150mA} = S_{100mA} \times \left(\frac{150mA}{100mA}\right),$$

where T_{water} is the cooling water temperature.

To illustrate this method, the temperature and stress at a beam corner missteering of 150 mA is calculated both by the above formula and by ANSYS, and the results are shown in Table 3.2-3.

Table 3.2-3 M1-40 with one undulator A at 11 mm gap (k=2.62) at 150 mA, corner missteering at position #6. Results from the above formula are compared with those from ANSYS calculation (h=0.015 w/mm²°C, T₀=25.6°C).

At position #6	Max. temperature (°C)	Max. von Mises stress (MPa)
100 mA results	182.0	349.1
150 mA results predicted by formula	260.2	523.7
150 mA results calculated by ANSYS	260.2 (Figure 3.2-10)	523.7 (Figure 3.2-11)

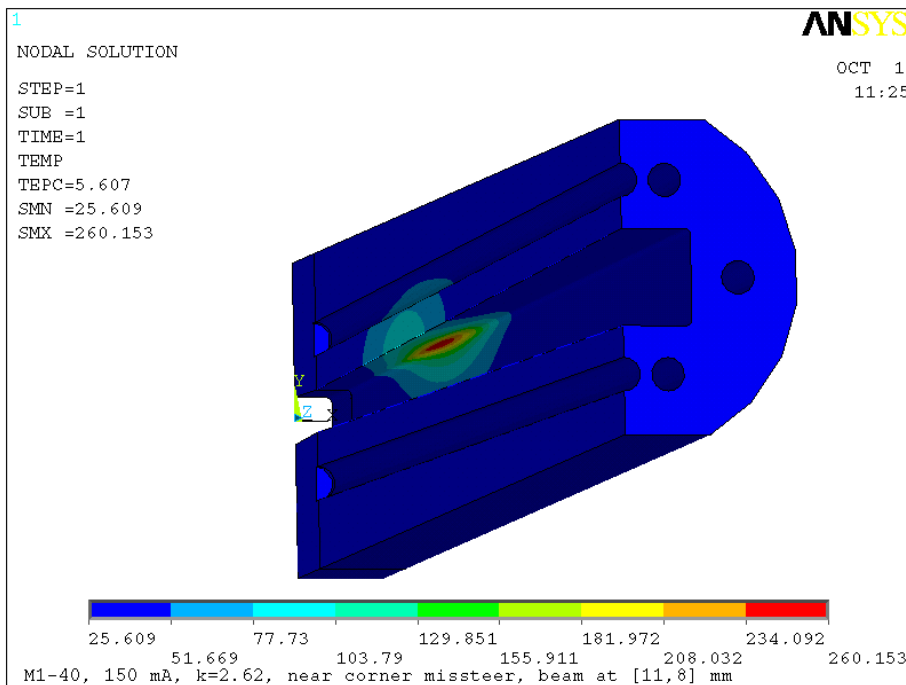


Figure 3.2-10 Temperature plot (°C) at 150 mA of M1-40 mask.

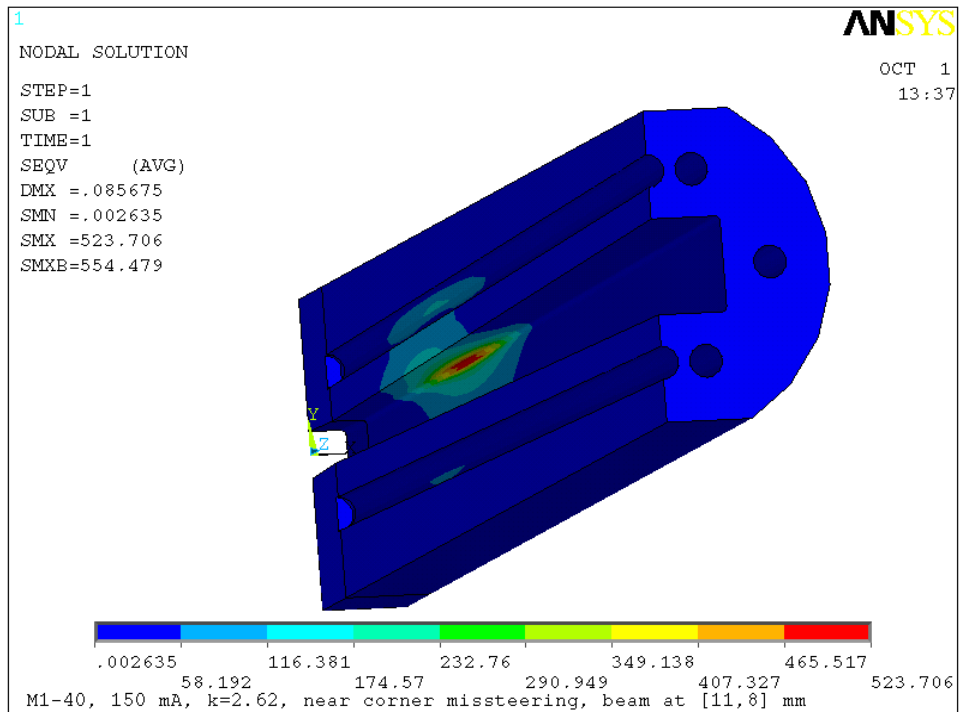


Figure 3.2-11 von Mises stress (MPa) plot at 150 mA of M1-40 mask.

3.2.5. Sensitivity Study of Film Coefficient and Cooling Water Set Point

M1-40 mask has copper mesh in the cooling channel to enhance the cooling coefficient. Under normal operating conditions the cooling coefficient is between 0.015 ~ 0.02 w/mm²°C. Sensitivity to the cooling coefficient depends on the cooling wall thickness (the beam striking surface to the cooling surface): the thinner the wall, the more sensitive it will be. So the vertical missteering is most sensitive to the cooling coefficient. Table 3.2-4 shows the peak temperature and wall temperature change based on changing the film coefficient h.

Table 3.2-4 M1-40 with different cooling coefficients at vertical missteering (100 mA, k=2.62)

Film coefficient (w/mm ² °C)	Max. temperature (°C)	Max. wall temperature (°C)	% change of peak temperature compared to nominal operating conditions
h=0.02	199.2	81.1	2.7% decrease
h=0.015	204.8	88.2	Nominal operating conditions
h=0.001	213.7	98.8	4.3% increase
h=0.005	232.3	119.8	13.4% increase

The M1-40 mask is not very sensitive to the h value. As long as h is maintained above 0.01 w/mm²°C, the change in the peak temperature is less than 5%.

3.3. Thermal Analysis of the Second Fixed Mask M2-40

3.3.1. M2-40 Model and Mesh

The M2-40 mask is manufactured from a solid round billet of GlidCop. The M2-40 was modeled in ProE, and the model was read in by ANSYS for analysis. Because the model's cross section is not topologically similar, it was not possible to use the brick mesh as is. A tetrahedron mesh was required, which is computationally expensive (takes a long time to run one case and takes up a lot of disk space). However if the external mounting grooves are removed, then the model can be divided in two regions, just as was the M1-40, and meshed in bricks mostly. So we did one case of thermal analysis of both the exact model and the simplified model with the external mounting grooves removed to see how different the results would be. If the difference is negligible, then we will use the simplified model to do case studies. The exact model and its tetrahedron mesh are shown in Figure 3.3-1 and Figure 3.3-2, and the simplified model and brick mesh are shown in Figure 3.3-3 and Figure 3.3-4. The key information for the M2-40 mask is shown in Table 3.3-1.

Table 3.3-1 Key dimensions and reference information for the M2-40 mask.

Name	M2-40
Distance to the center of the straight section (m)	17.4
Distance to the center of undulator installed 1.25 m downstream (m)	16.15
Total power (watts)	5327
Peak power density (w/mm ²)	597.3
Inlet aperture H×V (mm×mm)	25.8 × 17.4
Outlet aperture H×V (mm×mm)	11 × 6
Active length (mm)	261
Horizontal taper angle	1.6°
Vertical taper angle	1.23°
Aperture corner radius (mm)	1.0
Top and bottom cooling wall thickness (mm)	9.0 (inlet) ~ 9.6 (outlet)
Left and right cooling wall thickness (mm)	8.8 (inlet) ~ 9.6 (outlet)
Reference drawing number	M2-410001-02-2

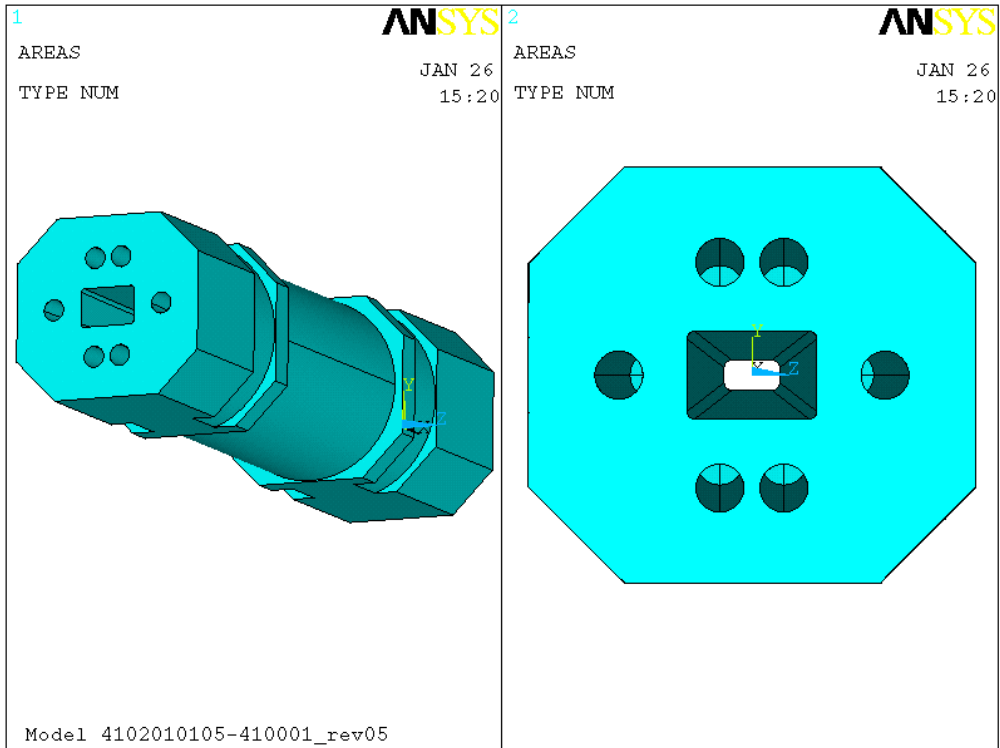


Figure 3.3-1 M2-40 exact model read in from ProE.

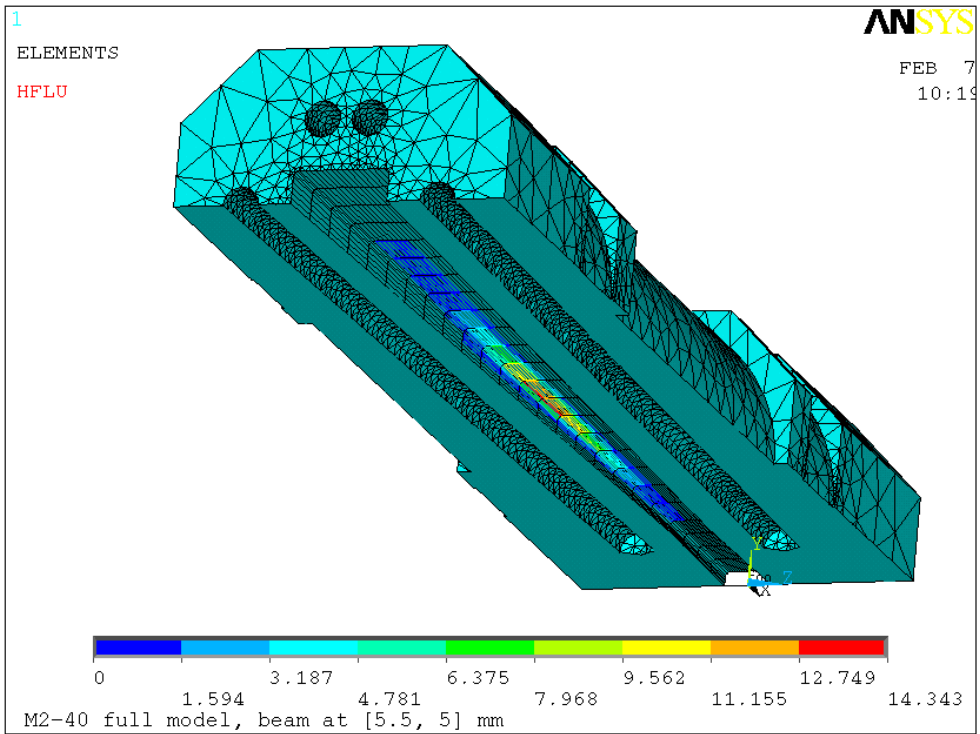


Figure 3.3-2 M2-40 exact model mesh, only half is shown to show the aperture, with the beam center at [5.5, 5] mm.

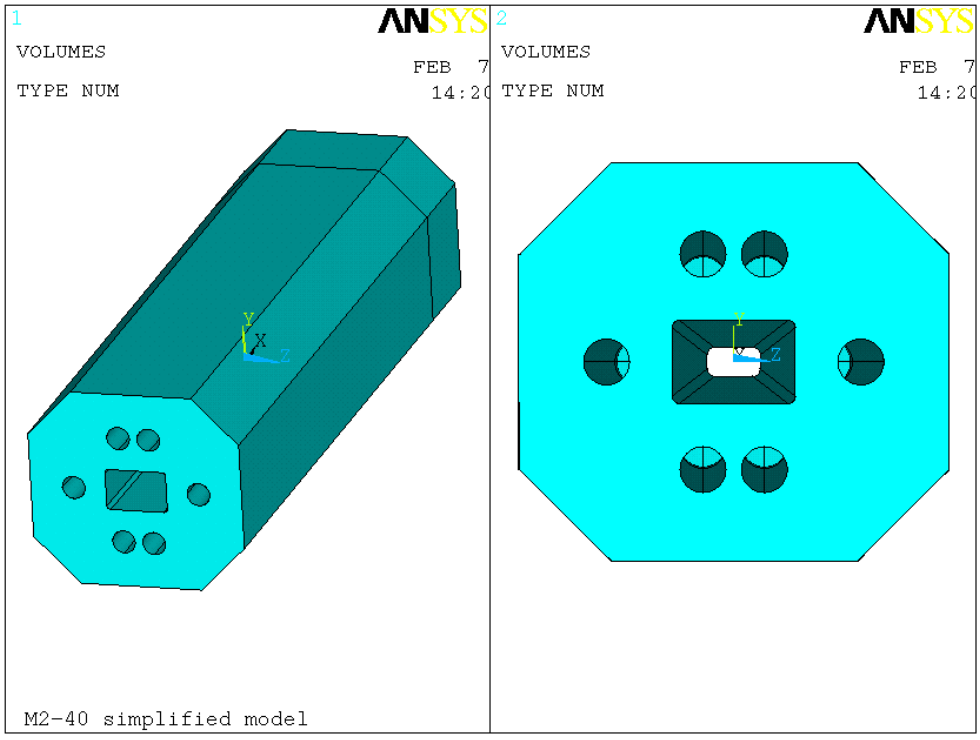


Figure 3.3-3 M2-40 simplified model with external grooves removed.

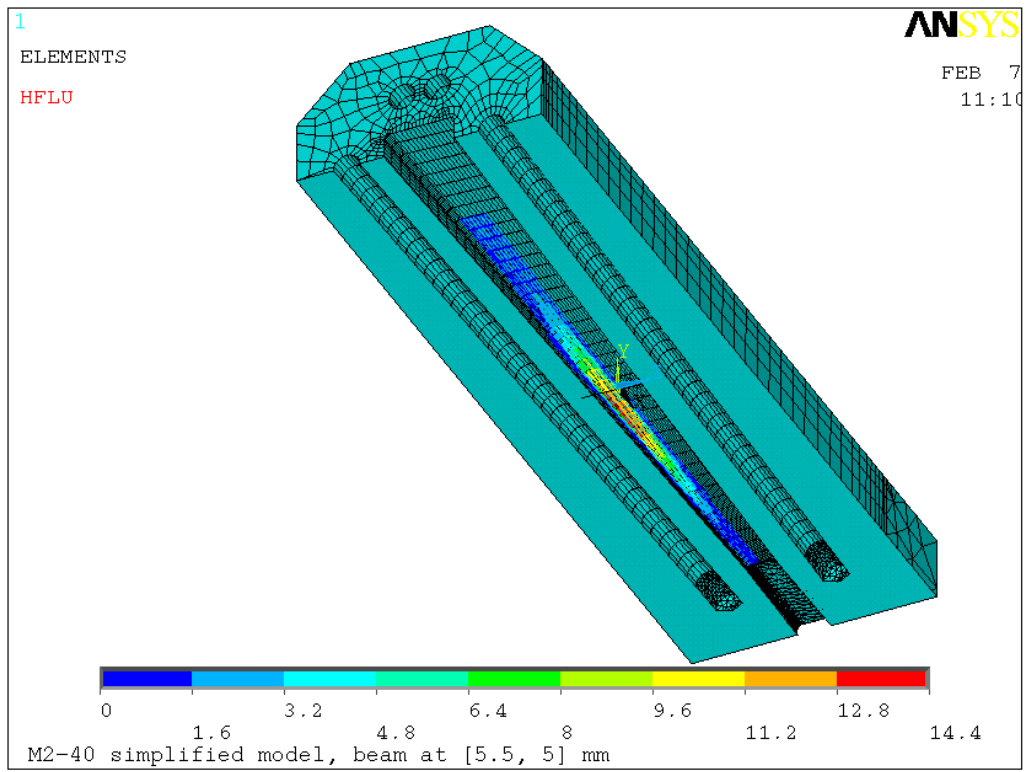


Figure 3.3-4 M2-40 simplified model with brick mesh and the beam center at [5.5, 5] mm.

3.3.2. M2-40 Power Calculation

The power of one undulator A at 100 mA and 11 mm gap (k=2.62) at 16.15 m was calculated using SRUFF. The power density distribution and the curve fit are shown in Figure 3.3-5 and Figure 3.3-6, respectively. The fitted formula will be used in ANSYS for the thermal load application.

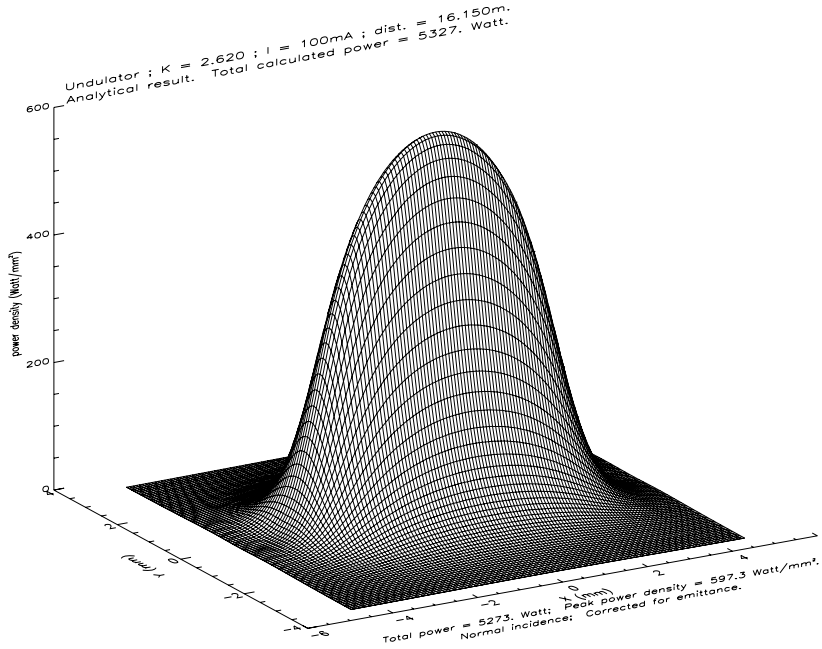


Figure 3.3-5 Undulator A power density distribution at 100 mA, k=2.62 at 16.15 m.

$$\text{Fit} = \exp(6.3925 - 0.034235x^2 - 1.2422y^2 - 0.012211x^4 + 0.12309y^4 + 0.011490x^2y^2)$$

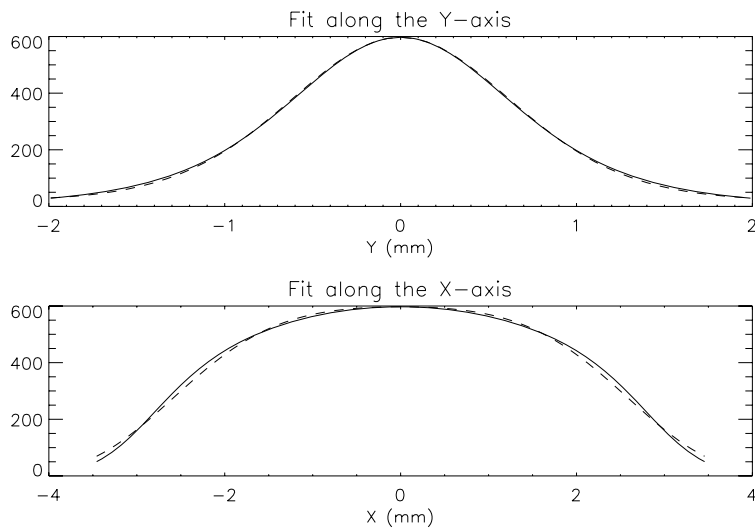


Figure 3.3-6 M2-40 power density distribution at 16.15 m from the Gaussian fitting formula. The solid line is the calculated data, and the dashed line is the fitted formula.

3.3.3. M2-40 Thermal and Stress Analysis for 100 mA Operation

The temperature distribution of M2-40 for the beam center at the [5.5, 5] mm corner missteering case were calculated for both the exact model (Figure 3.3-1) and the simplified model (Figure 3.3-2). The temperature distribution for the exact model is shown in Figure 3.3-7 and, for the simplified model, is shown in Figure 3.3-8. The thermal analysis results are also tabulated in Table 3.3-2.

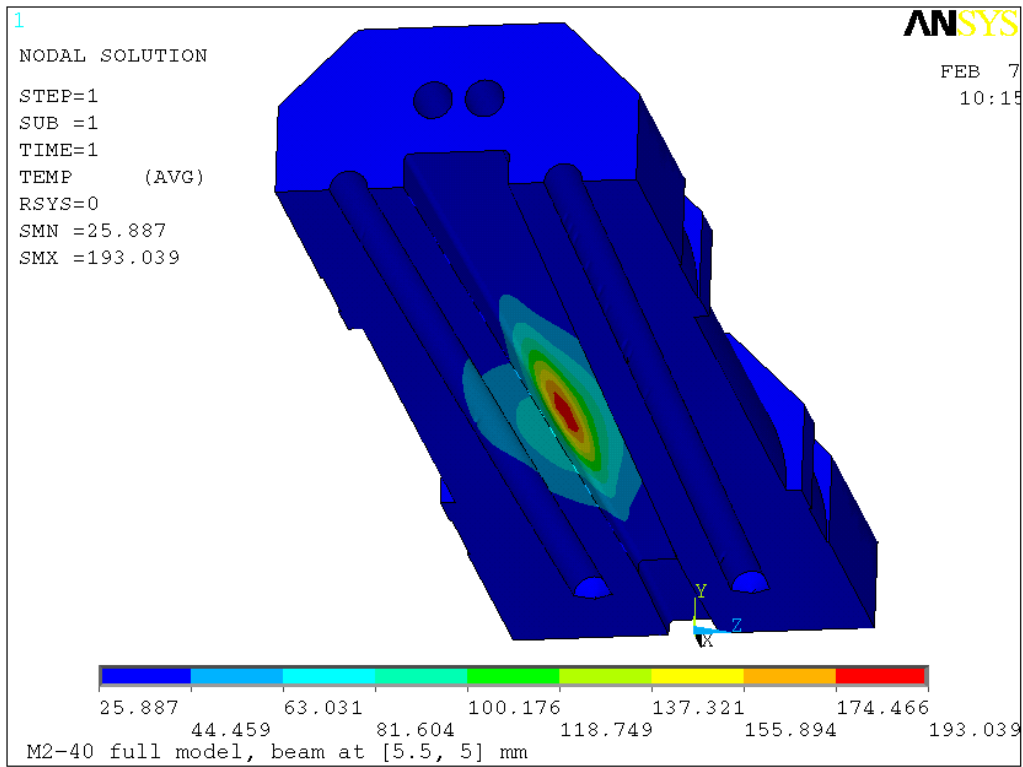


Figure 3.3-7 Temperature distribution (°C) for the M2-40 exact model, beam center at [5.5, 5.0] mm, $h=0.015$ w/mm²°C, $T_0=25.6$ °C.

Table 3.3-2 Thermal analysis comparison of the exact model and the simplified model for M2-40, $h=0.015$ w/mm²°C, $T_0=25.6$ °C.

	M2-40 exact model	M2-40 simplified model with external features suppressed
T_{\max} (°C)	193.04	191.57
T_{wall} (°C)	83.6	83.2

From Table 3.3-2, we see the temperature difference between the exact model and the simplified model is less than 1%. Typically the stress mainly depends on the profile of the aperture and depends very little on the external features, so using the simplified model for the full analysis is sufficient.

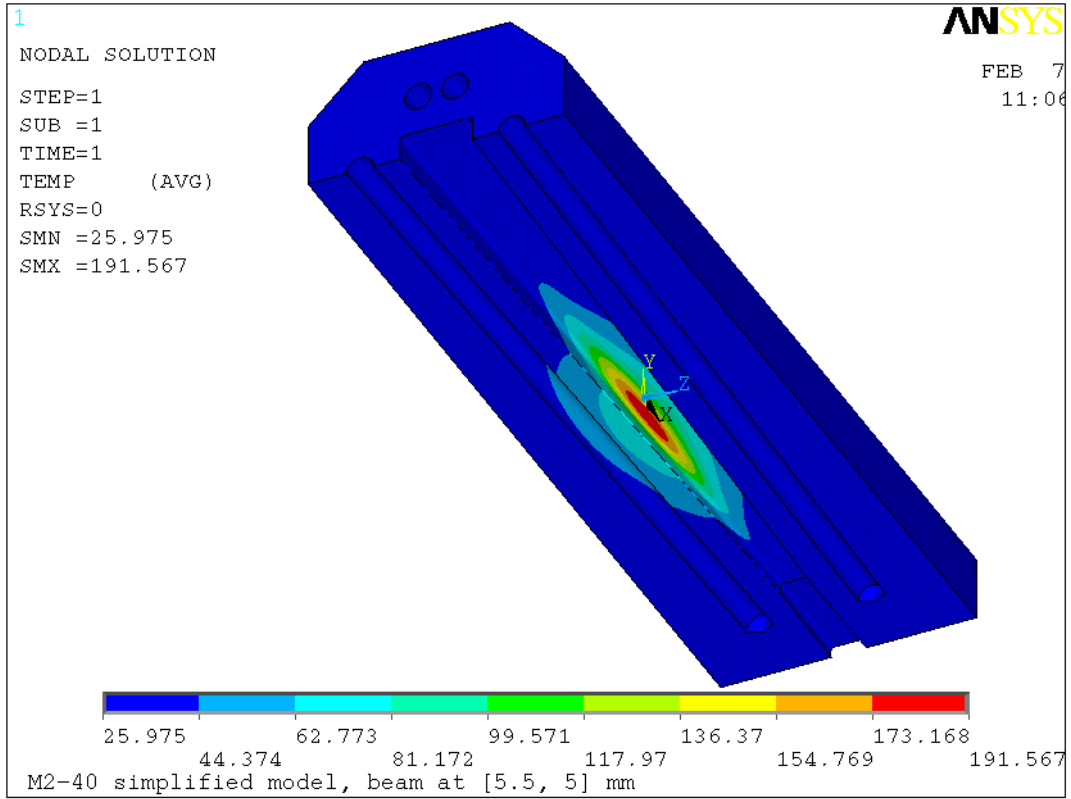


Figure 3.3-8 Temperature distribution ($^{\circ}\text{C}$) of the M2-40 simplified model, beam center at [5.5, 5.0] mm, $h=0.015 \text{ w/mm}^2\text{C}$, $T_0=25.6^{\circ}\text{C}$.

The M2-40 mask aperture is very similar to the M1-40 aperture; the M2-40 aperture and the beam missteering locations used in the analysis are shown in Figure 3.3-9.

M2-40 APERTURE (mm)

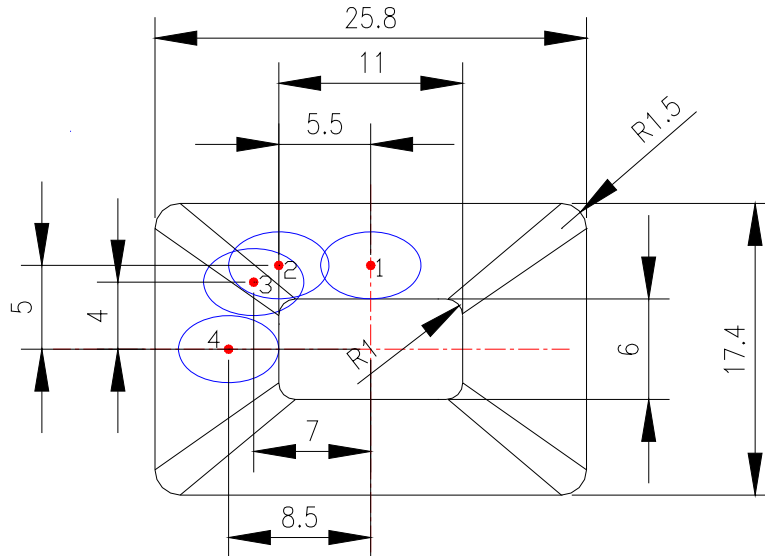


Figure 3.3-9 M2-40 aperture, round dots stand for the beam center, ovals stand for the beam footprint of 6×4 mm.

Temperature and stress data for M2-40 with the beam at various locations are tabulated in Table 3.3-3.

Table 3.3-3 Temperature and stress results for M2-40 with beam center at various locations (100 mA, $k=2.62$, $h=0.015$ w/mm²°C, $T_0=25.6$ °C).

Beam center position	Beam center coordinates [x,y] mm	Missteering case	T_{max} (°C)	T_{wall} (°C)	σ_{vm} (MPa)
1	[0, 5.0]	Vertical	200.3	78.0	312.0
2	[5.5, 5.0]	Near corner	191.6 (Figure 3.3-8)	83.2	326.5 (Figure 3.3-10)
3	[7.0, 4.0]	At corner	155.0	67.3	n/a*
3	[8.5, 0]	Horizontal	128.3	57.0	n/a*

* Temperature is too low to warrant a stress analysis

As predicted, the vertical missteering (position 1) results in the highest temperature; the near-corner (position 2) missteering has a lower temperature but higher stress. The cooling wall temperature is low, which means the cooling channel is positioned far from the heating surface. The temperature of M2-40 will not be sensitive to the film coefficient h . Thus it is not necessary to study the temperature change versus a change in the h value.

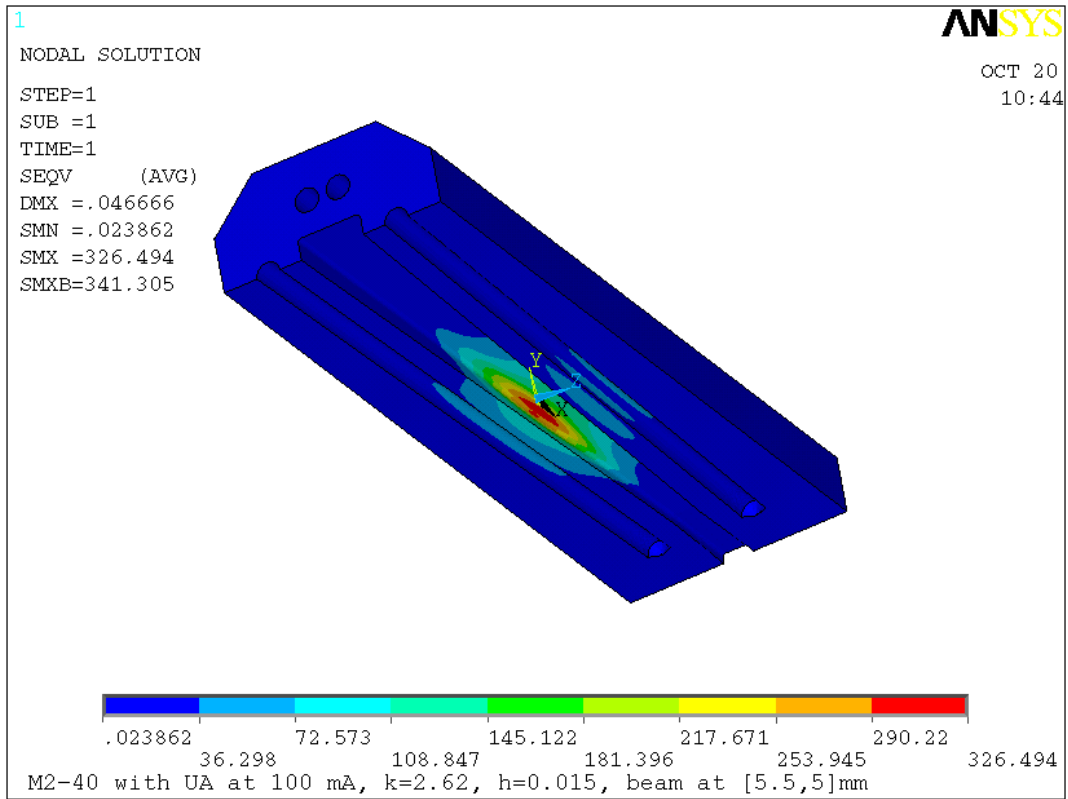


Figure 3.3-10 Von Mises stress plot (MPa), corner missteering, beam center at [5.5, 5.0] mm.

3.4. Thermal Analysis of the Third Fixed Mask M2-50

3.4.1. M2-50 Model and Mesh

Mask M2-50 is very similar to M2-40; it is manufactured from a solid round billet of GlidCop. The M2-50 was modeled in ProE, and the model was read in by ANSYS for analysis. Due to the model's cross section, it is not topologically similar, the meshing of the as-is model with a brick mesh is impossible. A tetrahedron mesh will be required, and it is computationally expensive. However if the external features, such as mounting grooves, are removed, then the model can be divided into two regions just as with M2-40 and mostly meshed in a brick mesh. So we will again do one case of thermal analysis for both the exact model and the simplified model with the external mounting grooves removed to see how different the results will be. If the difference is negligible, then we will use the simplified model to do our case studies. The exact model and its tetrahedron mesh are shown in Figure 3.4-1 and Figure 3.4-2 and the simplified model and brick mesh are shown in Figure 3.4-3 and Figure 3.4-4. The key information for the model is shown in Table 3.4-1.

Table 3.4-1 Key dimensions and reference information for M2-50.

Name	M2-50
Distance to the center of the straight section (m)	21.1
Distance to the center of undulator installed 1.25 m downstream (m)	19.85
Total power (watts)	5327
Peak power density (w/mm ²)	393.0
Inlet aperture H×V (mm×mm)	23.5 × 15.9
Outlet aperture H×V (mm×mm)	12.7 × 5.2
Active length (mm)	181
Horizontal taper angle	1.6°
Vertical taper angle	1.6°
Aperture corner radius (mm)	1.5
Top and Bottom cooling wall thickness (mm)	9.7 (inlet) ~ 10.1 (outlet)
Left and right cooling wall thickness (mm)	10.0 (inlet) ~ 10.7 (outlet)
Reference drawing number	M2-510001-03-2

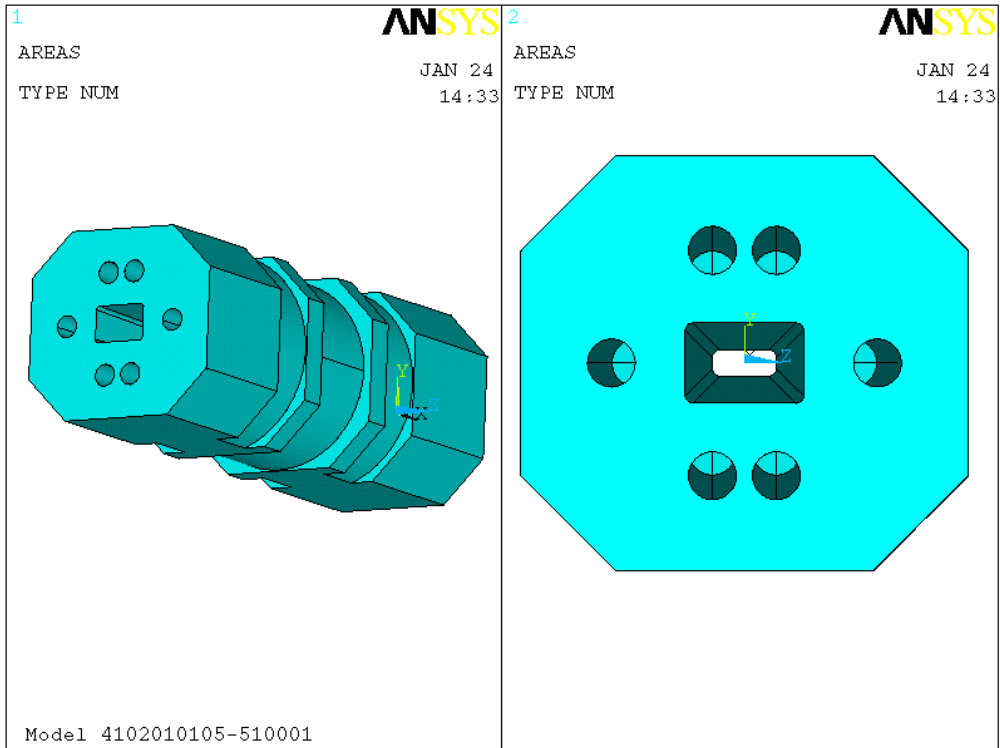


Figure 3.4-1 M2-50 exact model read in from ProE.

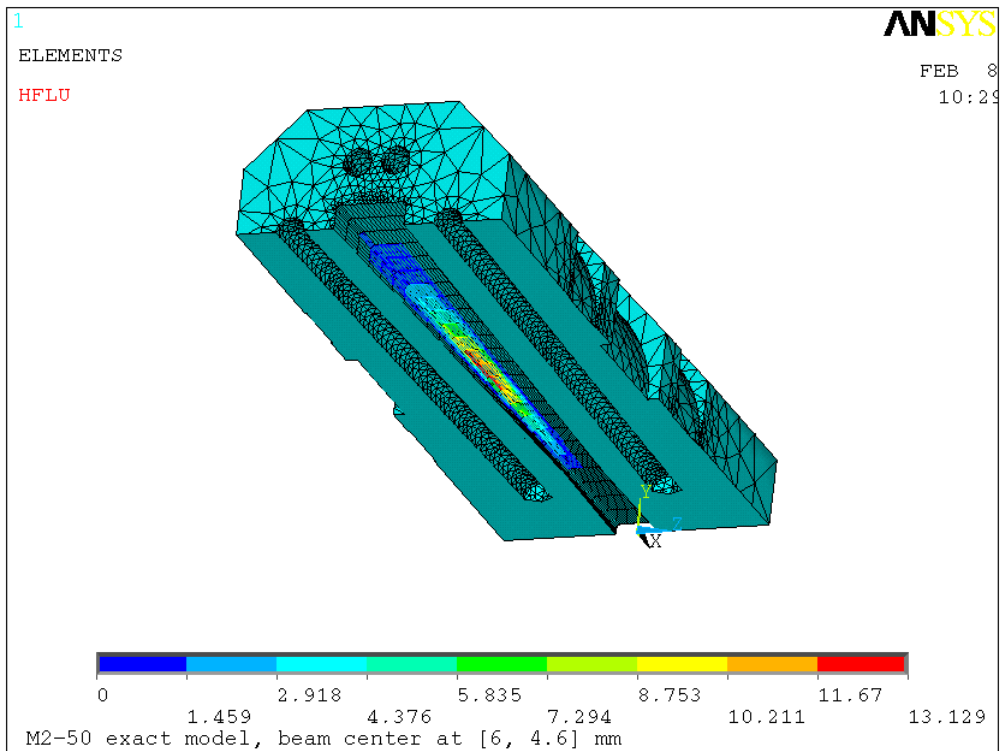


Figure 3.4-2 Cross section of the M2-50 exact model mesh, with beam center at [5.5, 5] mm showing heat flux.

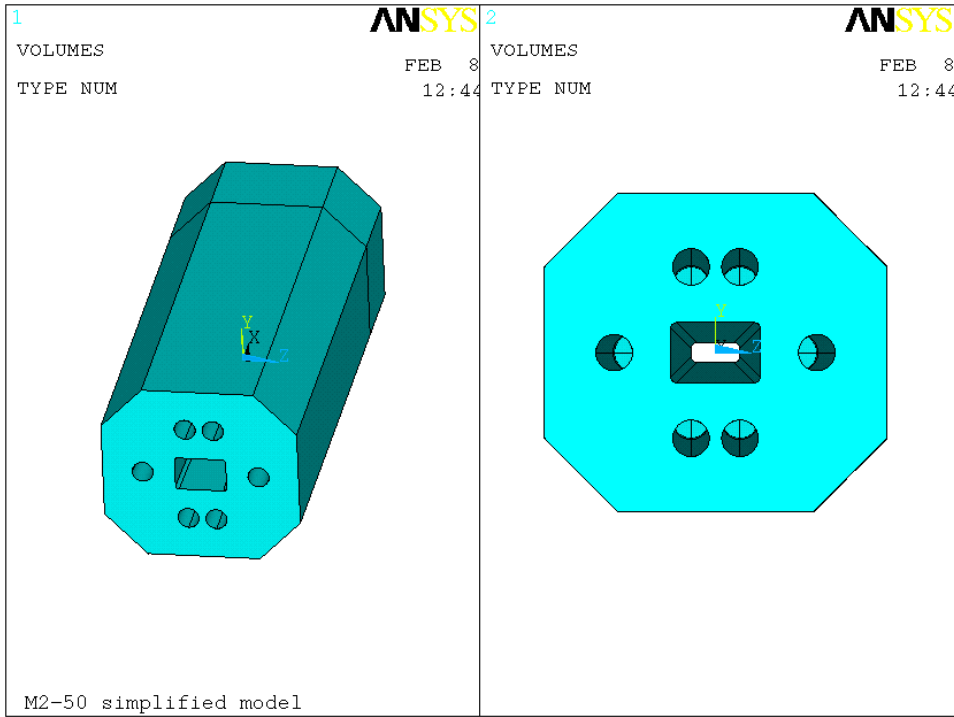


Figure 3.4-3 M2-50 simplified model with external features removed.

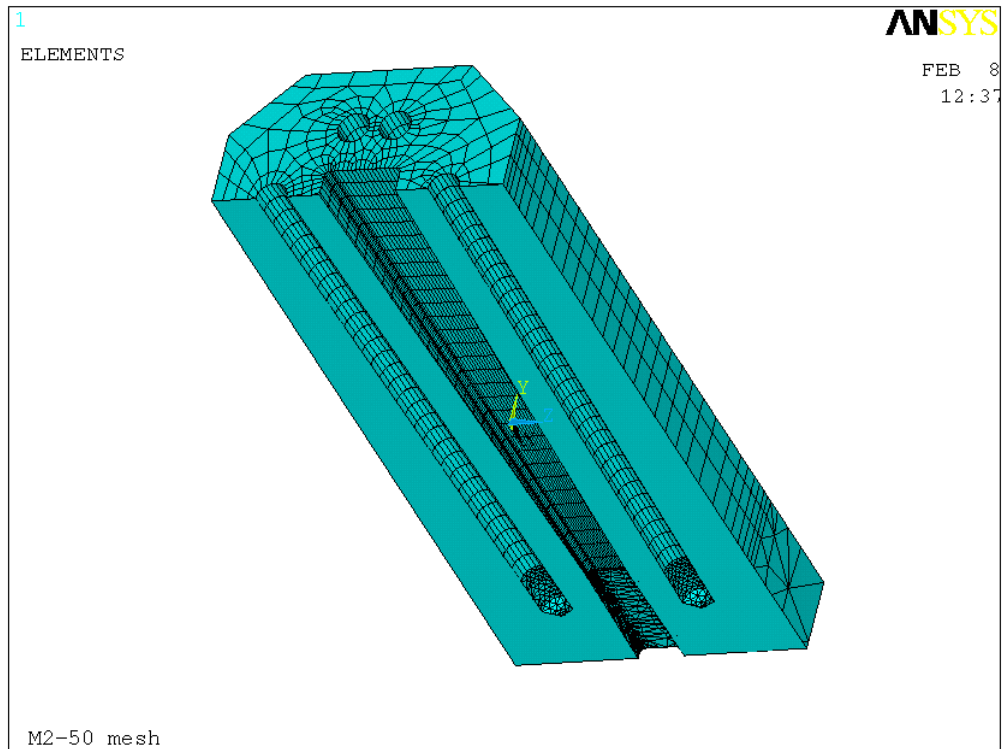


Figure 3.4-4 The cross section of the M2-50 simplified model with brick mesh.

3.4.2. M2-50 Power Calculation

The power of one undulator A at 100 mA and 11 mm gap (k=2.62) at 19.85 m was calculated. The power density distribution and the curve fit are shown in Figure 3.4-5 and Figure 3.4-6, respectively. The fitted formula will be used in ANSYS for the thermal load application.

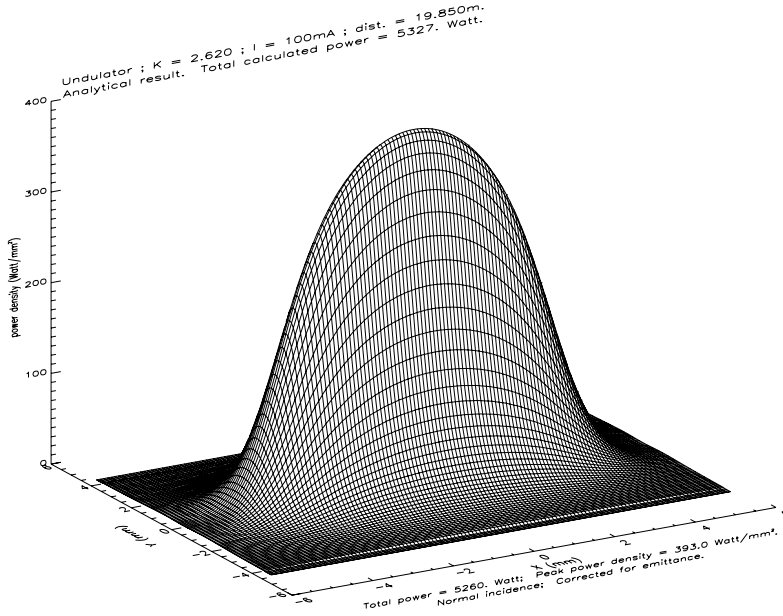


Figure 3.4-5 Undulator A power density distribution at 100 mA, k=2.62 at 19.85 m.

$$\text{Fit} = \exp(5.9737 - 0.030474x^2 - 0.81427y^2 - 0.0045499x^4 + 0.052072y^4 + 0.0052430x^2y^2)$$

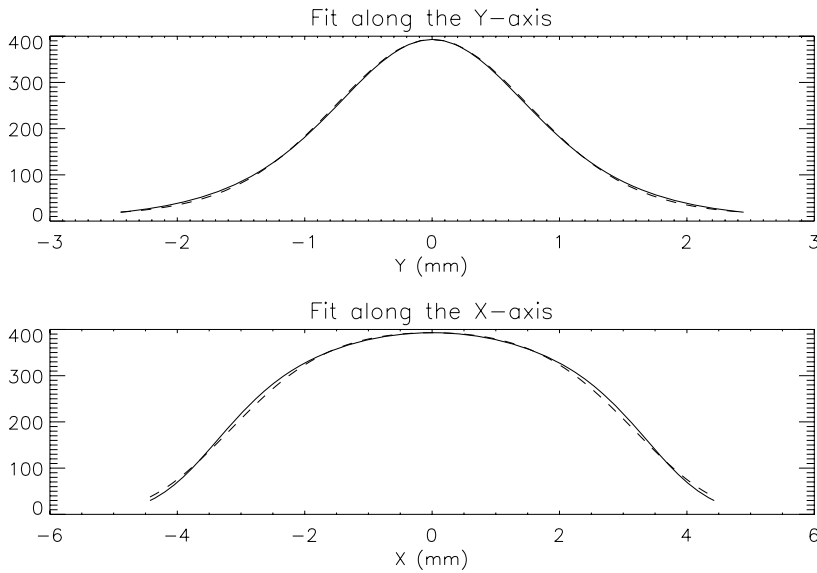


Figure 3.4-6 M2-50 Power density distribution at 19.85 m from the Gaussian fitting formula. The solid line is the calculated data, and the dashed line is the fitted formula.

3.4.3. M2-50 Thermal and Stress Analysis for 100 mA Operation

The temperature distribution of M2-50 for the beam center at the [6, 4.6] mm corner missteering case was calculated for both the exact model (Figure 3.4-1) and the simplified model (Figure 3.4-2). The temperature distribution for the exact model is shown in Figure 3.4-7 and for the simplified model in Figure 3.4-8. The thermal analysis results are also tabulated in Table 3.4-2.

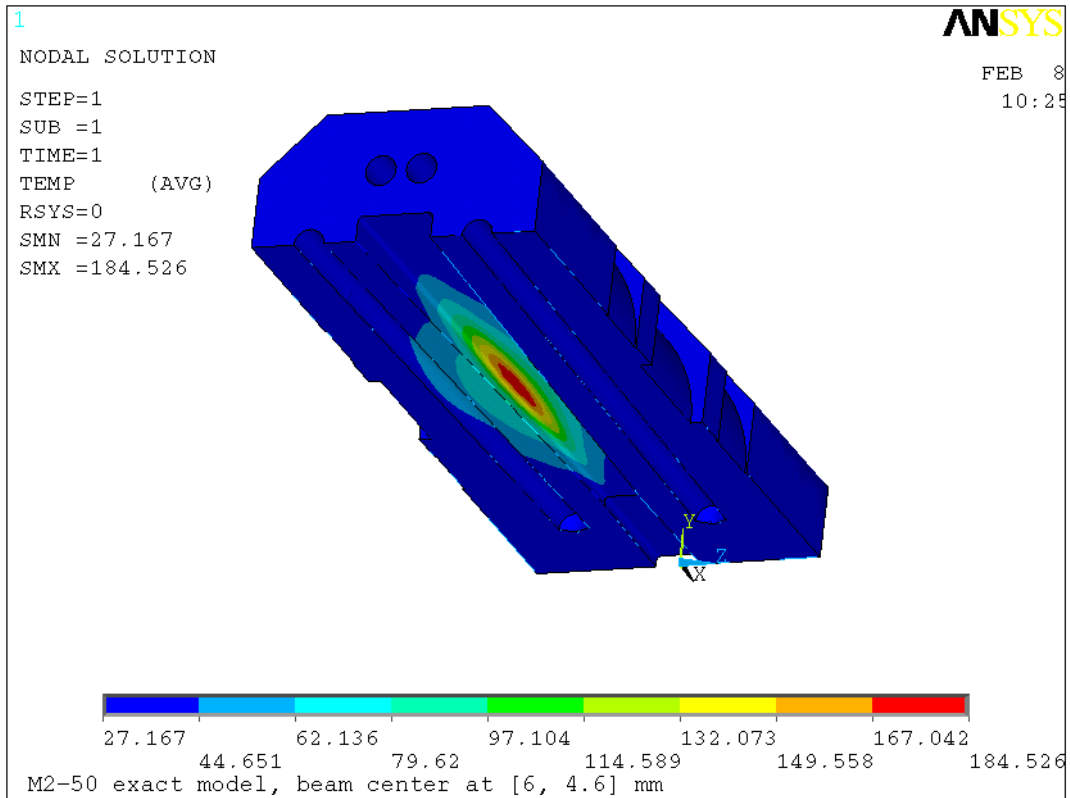


Figure 3.4-7 Temperature distribution (°C) of the M2-50 exact model, beam center [6, 4.6] mm, $h=0.015 \text{ w/mm}^2\text{°C}$, $T_0=25.6\text{°C}$

Table 3.4-2 Thermal analysis comparison of the M2-50 exact model and the simplified model, $h=0.015 \text{ w/mm}^2\text{°C}$, $T_0=25.6\text{°C}$

	M2-50 exact model	M2-50 simplified model with external features suppressed
T_{\max} (°C)	184.5	184.6
T_{wall} (°C)	79.9	79.8

From Table 3.4-2, we see that the difference between the exact model and the simplified model is negligible, so the full aperture case study was done using the simplified model.

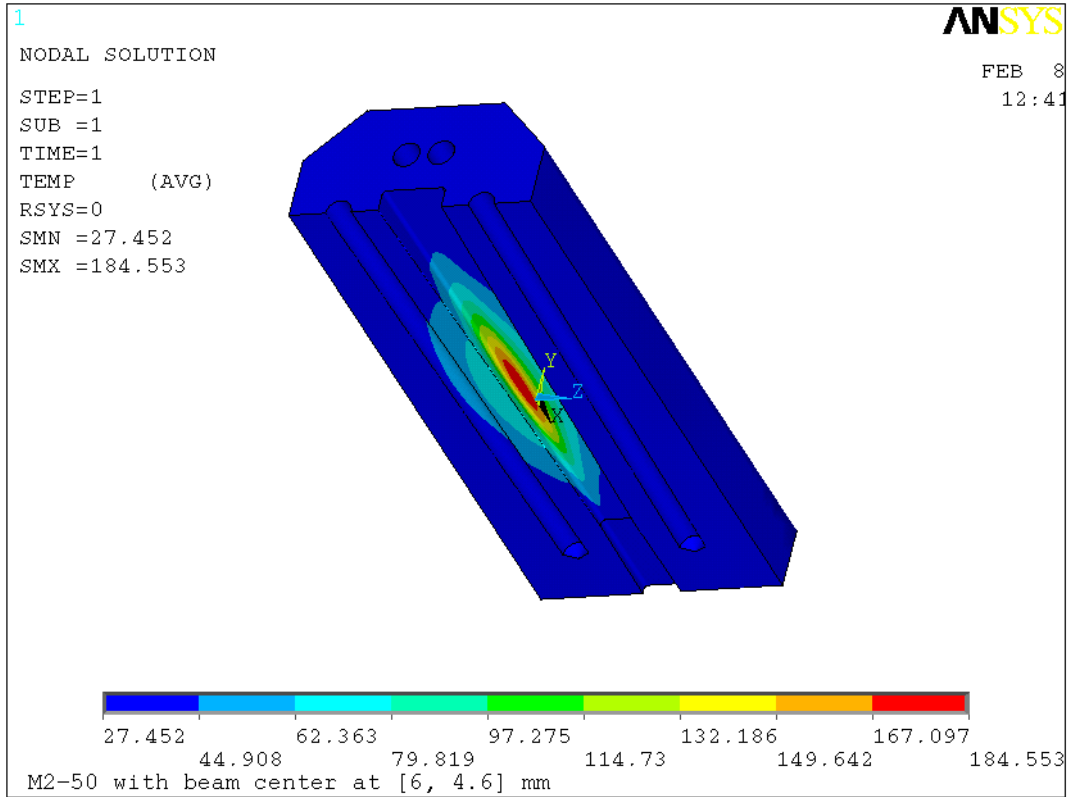


Figure 3.4-8 Temperature distribution ($^{\circ}\text{C}$) for the M2-50 simplified model, beam center [6, 4.6] mm, $h=0.015 \text{ w/mm}^2\text{C}$, $T_0=25.6^{\circ}\text{C}$

The M2-50 mask aperture is very similar to the M2-40 aperture; the M2-50 aperture and beam missteering locations are shown in Figure 3.4-9.

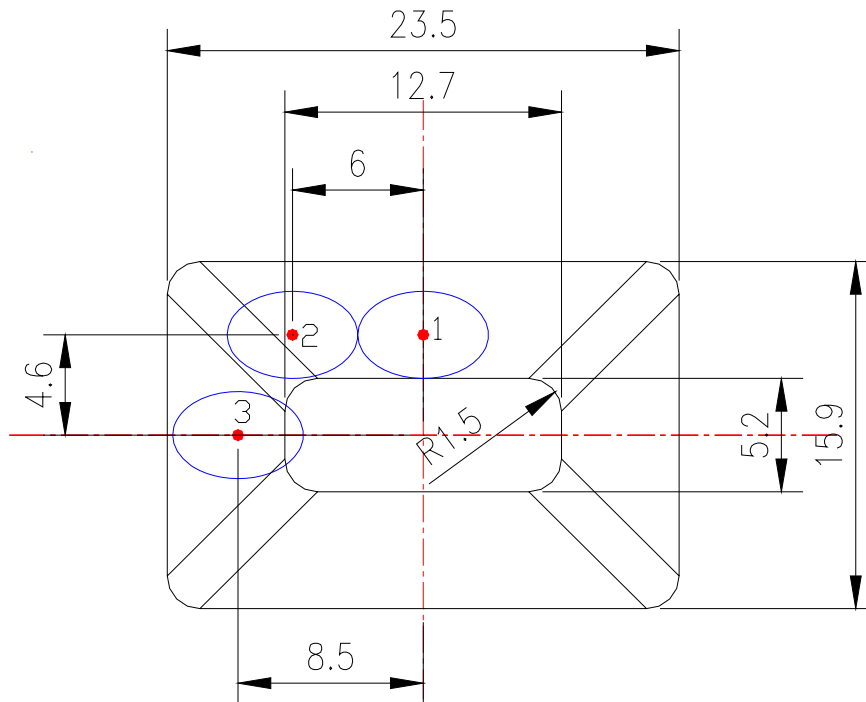


Figure 3.4-9 M2-50 aperture, round dots stand for the beam center, ovals stand for the beam footprint of 6×4 mm.

Temperature and stress data for various locations of the beam are tabulated in Table 3.4-3.

Table 3.4-3 Temperature and stress results for M2-50 with the beam center at various locations (100 mA, $k=2.62$, $h=0.015$ w/mm²°C, $T_0=25.6$ °C)

Beam center position	Beam center coordinates [x,y] mm	Missteering case	T_{\max} (°C)	T_{wall} (°C)	σ_{vm} (MPa)
1	[0, 4.6]	Vertical	201.5 (Figure 3.4-10)	78.3	309.7 (Figure 3.4-11)
2	[6, 4.6]	Near corner	184.6	79.8	308.9
3	[8.5, 0]	Horizontal	107.8	49.6	n/a*

* Temperature is too low to warrant a stress analysis

As predicted, the vertical missteering (position 1) results in the highest temperature, the near corner (position 2) has a lower temperature. The stress value of the vertical missteering is very close to the value at the corner missteering because the corner radius of M2-50 is slightly larger than those of M1-40 and M2-40. The corner stress decreases as the radius increases. The cooling wall temperature is low, which means the cooling channel is positioned far from the heating surface and the temperature will not be sensitive to the film coefficient h . Thus it is not necessary to study the temperature change versus the change of the h value.

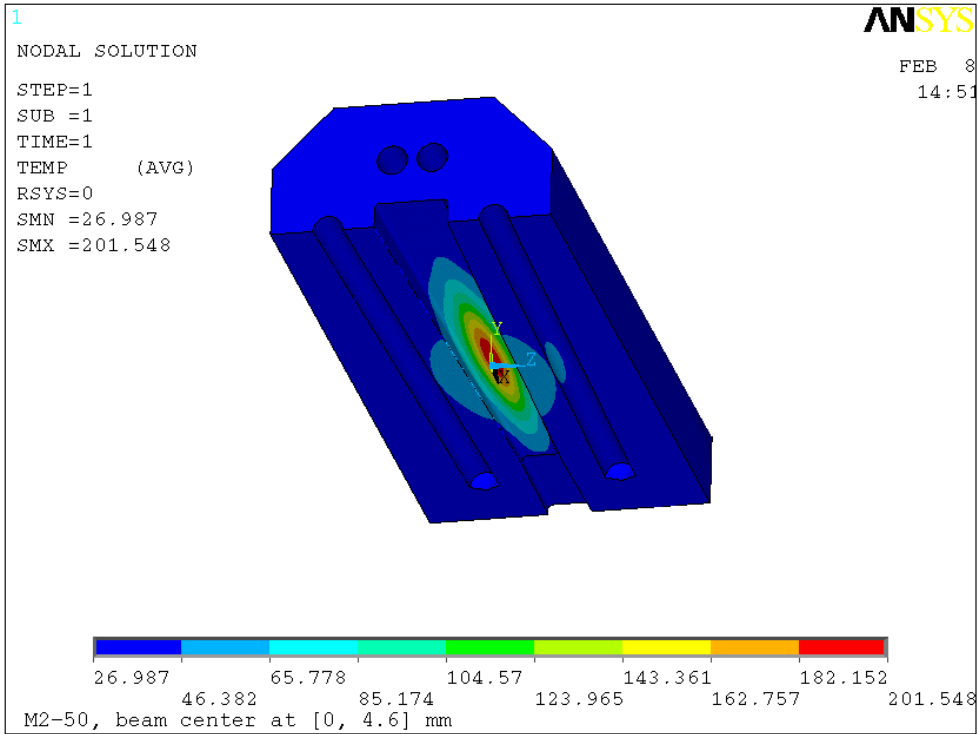


Figure 3.4-10 Temperature distribution ($^{\circ}\text{C}$) for the M2-50 mask, beam center [0, 4.6] mm, $h=0.015 \text{ w/mm}^2\text{C}$, $T_0=25.6^{\circ}\text{C}$.

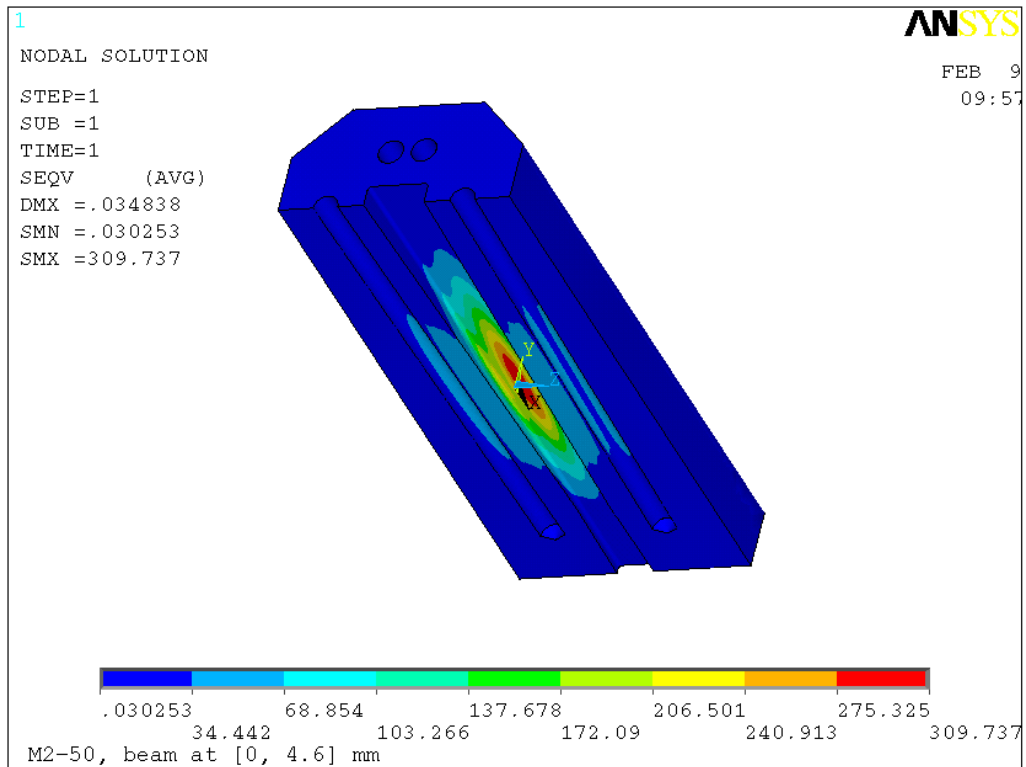


Figure 3.4-11 M2-50 von Mises stress plot (MPa), beam center at [0, 4.6] mm.

3.5. Thermal Analysis of the Photon Shutters P2-30

3.5.1. P2-30 Model and Mesh

The P2-30 photon shutter (PS) is manufactured from two halves of GlidCop forming a “V” shape to intercept the beam. An aperture is machined into the P2-30. When P2-30 is moved up (open), the beam will pass through the aperture. When P2-30 is moved down (closed), the beam will be contained in the “V” block. The P2-30 was modeled in ProE, and the model was read in by ANSYS for analysis. The model and mesh are shown in Figure 3.5-1 and Figure 3.5-2, respectively. The P2-30 is used for both the 1st and 2nd photon shutter (PS1 and PS2, respectively). Because PS1 is located closer to the source than is PS2, with higher power density, the P2-30 analysis will be based on the PS1 location. The key information for P2-30 is shown in Table 3.5-1.

Table 3.5-1 Key dimensions and reference information for P2-30.

Name	P2-30 (1 st Photon Shutter)
Distance to the center of the straight section (m)	18.9
Distance to the center of undulator installed 1.25 m downstream (m)	17.65
Total power (watts)	5327
Peak power density (w/mm ²)	496.4
Inlet aperture H×V (mm×mm)	21.5 × 34
Outlet aperture H×V (mm×mm)	12 × 5.5
Active length (mm)	335
Stroke (mm)	15
Horizontal taper angle	1.68°
Vertical taper angle	N/A
Left and right cooling wall thickness (mm)	10.6 (inlet) ~ 12.2 (outlet)
Reference drawing number	P2-310100-02

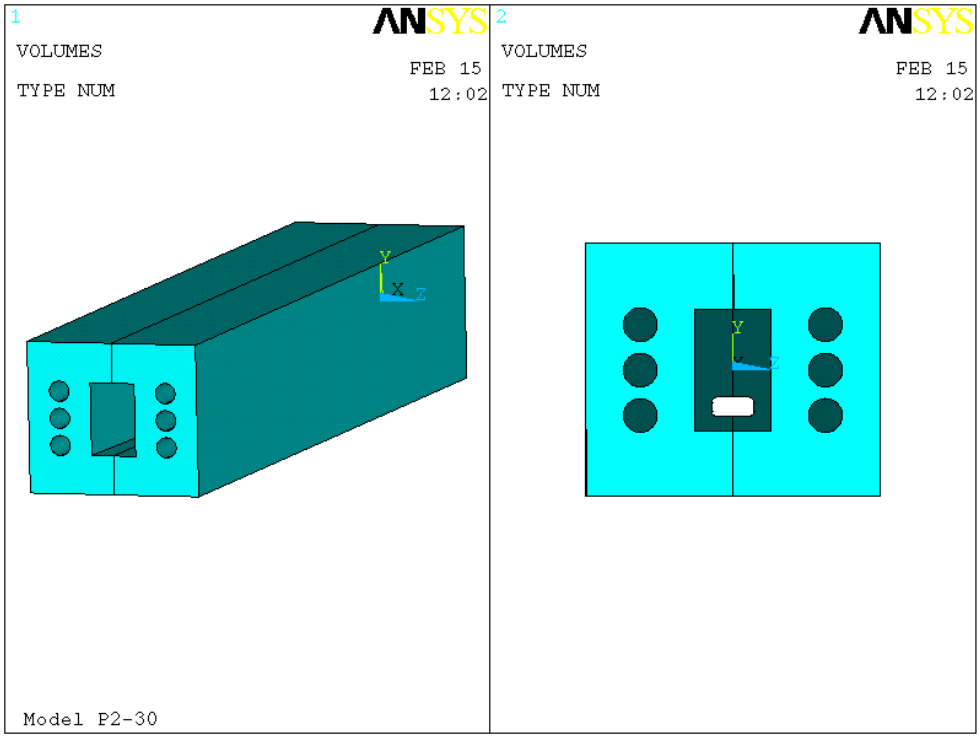


Figure 3.5-1 P2-30 model read in from ProE.

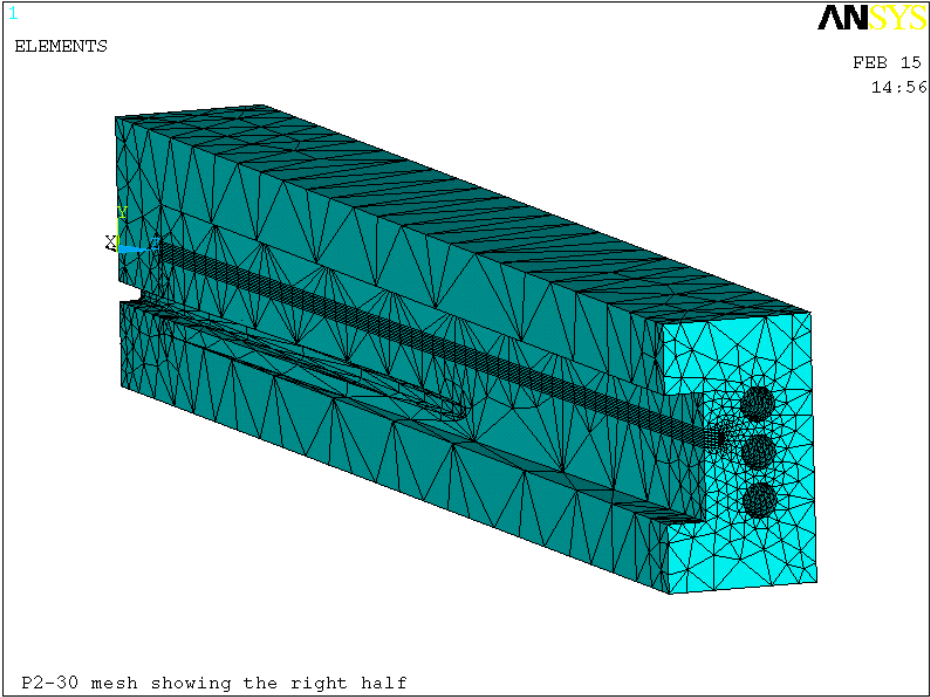


Figure 3.5-2 P2-30 mesh, only the right half is shown.

3.5.2. P2-30 Power Calculation

The power of one undulator A at 100 mA and 11 mm gap ($k=2.62$) at 17.65 m was calculated using SRUFF. The power density distribution and the curve fit are shown in Figure 3.5-3 and Figure 3.5-4, respectively. The fitted formula was used in ANSYS for the thermal load application.

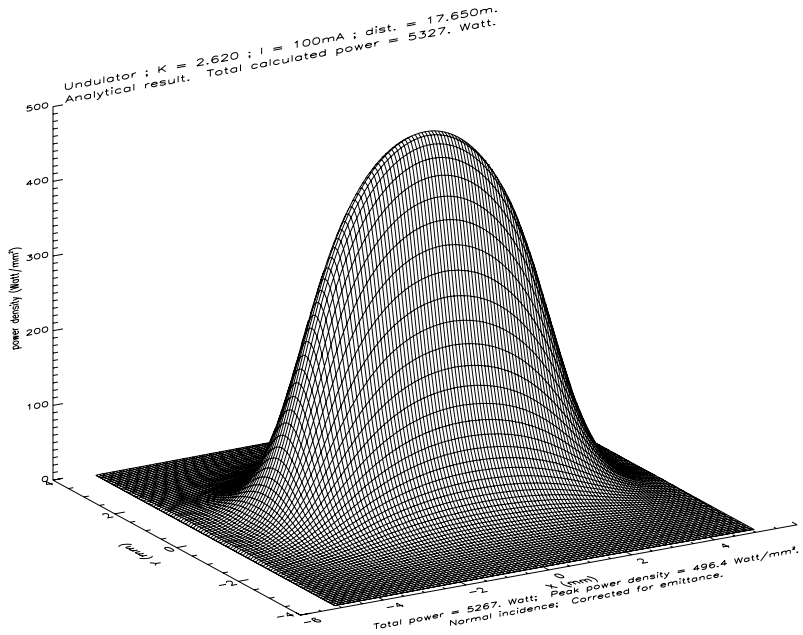


Figure 3.5-3 Undulator A power density distribution at 100 mA, $k=2.62$ at 17.65 m.

$$\text{Fit} = \exp(6.2073 - 0.050023x^2 - 0.94835y^2 - 0.0063703x^4 + 0.055347y^4 + 0.0098197x^2y^2)$$

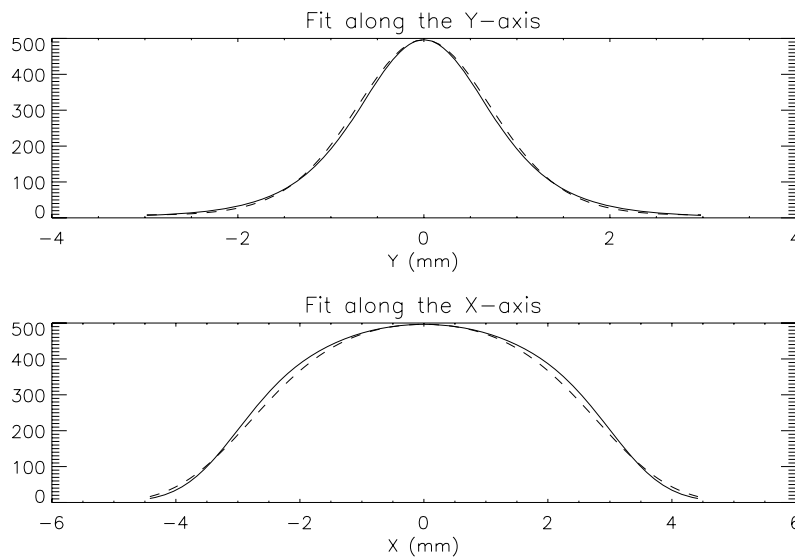


Figure 3.5-4 P2-30 Power density distribution at 17.65 m from the Gaussian fitting formula. The solid line is the calculated data, and the dashed line is the fitted formula.

3.5.3. P2-30 Thermal and Stress Analysis for 100 mA Operation

The analysis was carried out for a shutter at the closed position. Without beam missteering, the beam will be intercepted by both halves of the shutter. If the beam missteers more than 4 mm horizontally, the beam will be intercepted by only one half of the shutter. The results of are tabulated in Table 3.5-2.

Table 3.5-2 Temperature and stress results for P2-30 with two locations for the beam center (100 mA, $k=2.62$, $h=0.015$ w/mm²°C, $T_0=25.6$ °C)

Beam center coordinates [x,y] mm	Missteering case	T _{max} (°C)	T _{wall} (°C)	σ _{vm} (MPa)
[0, 0]	No missteering	135.8	55.8	n/a*
[4, 0]	Horizontal	140.9	59.3	176.2

* Temperature is too low to warrant a stress analysis

The worst case is when one half of the shutter has to take the full beam at horizontal missteering. The cooling wall temperature remains low, which means the cooling channel is positioned far from the heating surface. The temperature will be insensitive to the film coefficient h. Temperature for the case of no missteering is shown in Figure 3.5-5 and the temperature and stress for horizontal missteering are plotted in Figure 3.5-6 and Figure 3.5-7, respectively.

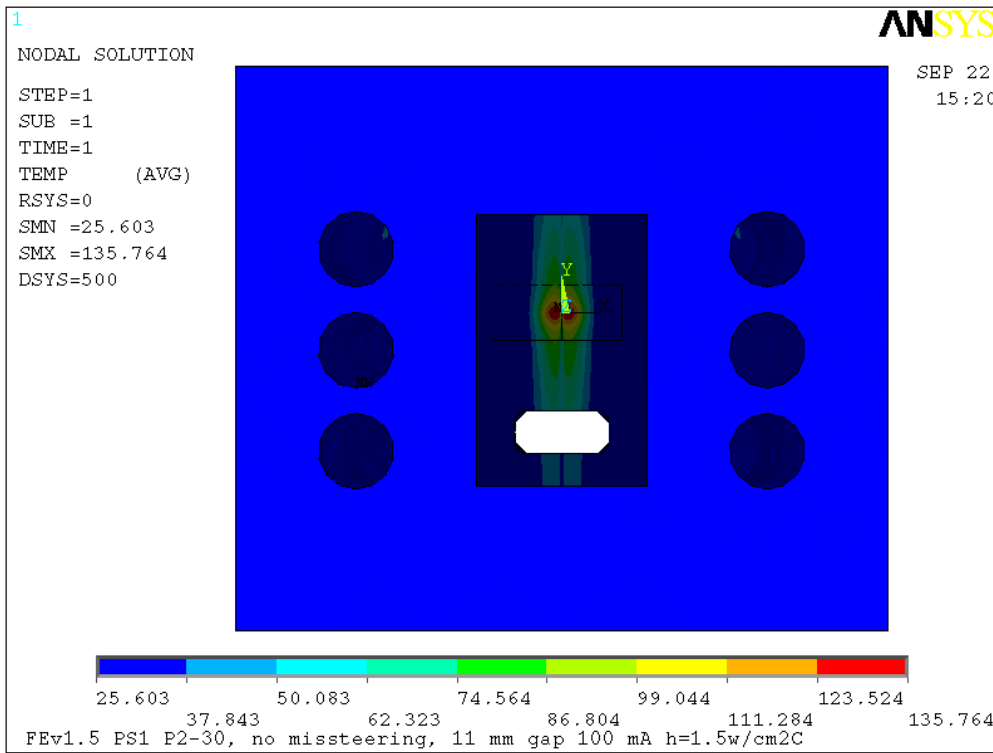


Figure 3.5-5 Temperature plot(°C), no missteering, $h=0.015$ w/mm²°C, $T_0=25.6$ °C.

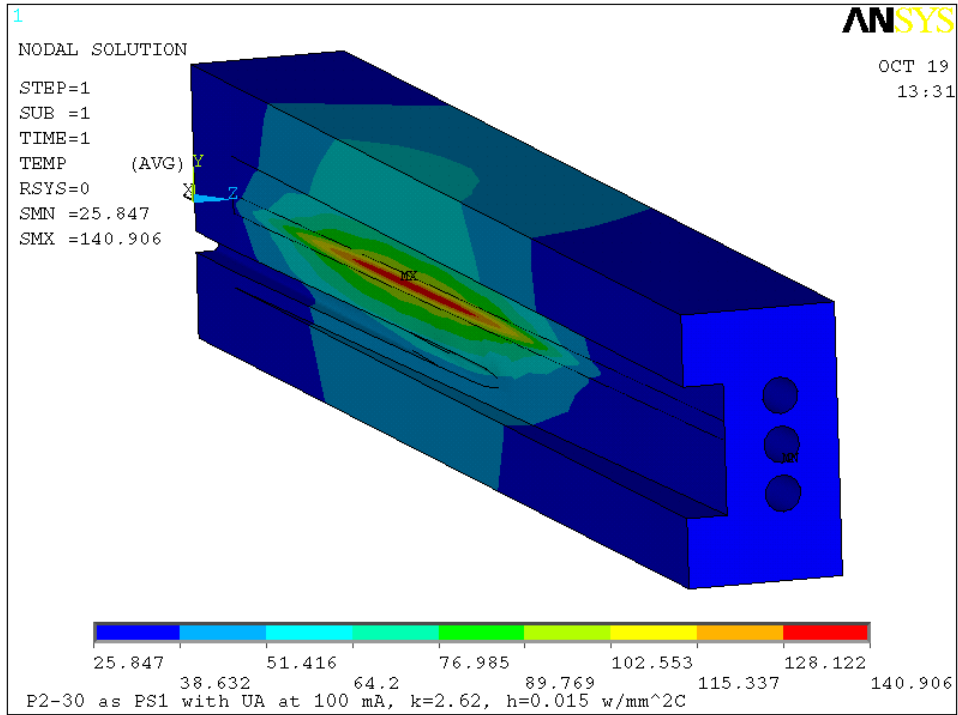


Figure 3.5-6 Temperature distribution (°C) for P2-30 with horizontal missteering, beam center at [4, 0] mm, $h=0.015$ w/mm²C, $T_0=25.6$ °C, showing the right half.

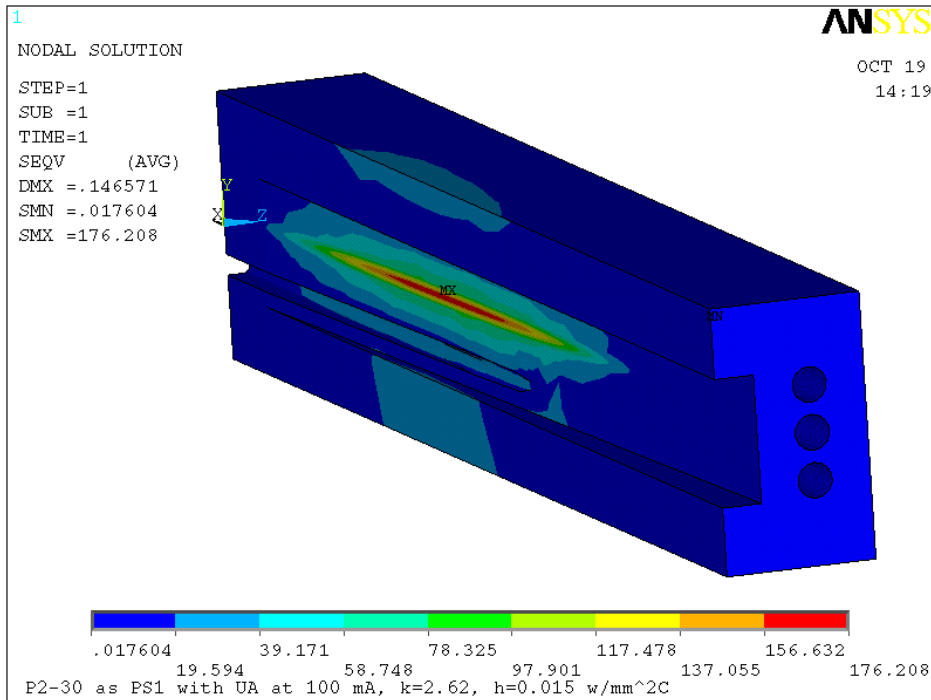


Figure 3.5-7 Von Mises stress plot (MPa) for P2-30, beam center at [4, 0] mm, showing the right half.

3.6. Thermal Analysis of the Exit Mask M4-40

3.6.1. M4-40 Model and Mesh

The M4-40 exit mask is manufactured from a solid round billet of GlidCop. The M4-40 was modeled in ProE, and the model was read in by ANSYS for analysis. Because the model's cross section is not topologically similar, to mesh it with brick mesh would require dividing the model into smaller regions. To avoid too much effort in model manipulation, a tetrahedron mesh was used. To accurately apply heat flux load, the aperture surface area was meshed with 8-nodel quad surface mesh (mesh 200 elements). The model and mesh are shown in Figure 3.6-1 and Figure 3.6-2, respectively. Key information for the M4-40 model is shown in Table 3.6-1.

Table 3.6-1 Key dimensions and reference information for M4-40.

Name	M4-40
Distance to the center of the straight section (m)	25.2
Distance to the center of undulator installed 1.25 m downstream (m)	23.95
Total power (watts)	5327
Peak power density (w/mm ²)	270.3
Inlet aperture H×V (mm×mm)	25.4 × 16.6
Outlet aperture H×V (mm×mm)	3 × 2
Active length (mm)	190
Horizontal taper angle	3.45°
Vertical taper angle	2.24°
Aperture corner radius (mm)	1.0
Top and Bottom cooling wall thickness (mm)	9.0 (inlet) ~ 11.7 (outlet)
Left and right cooling wall thickness (mm)	8.7 (inlet) ~ 14.0 (outlet)
Reference drawing number	4105091004-400001

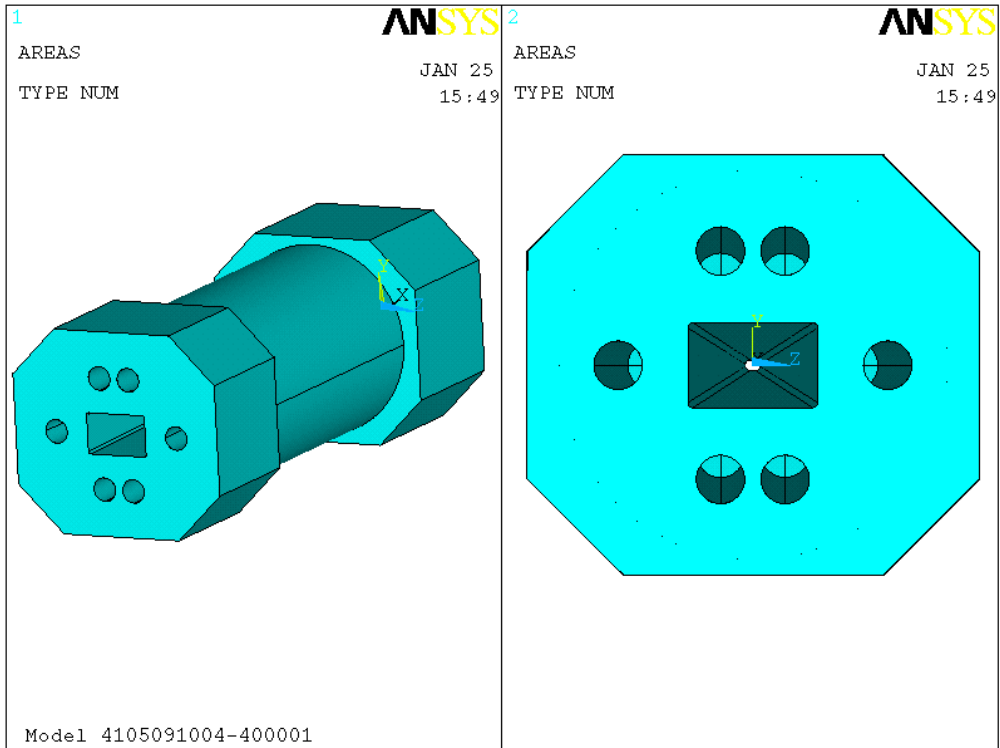


Figure 3.6-1 M4-40 model read in from ProE.

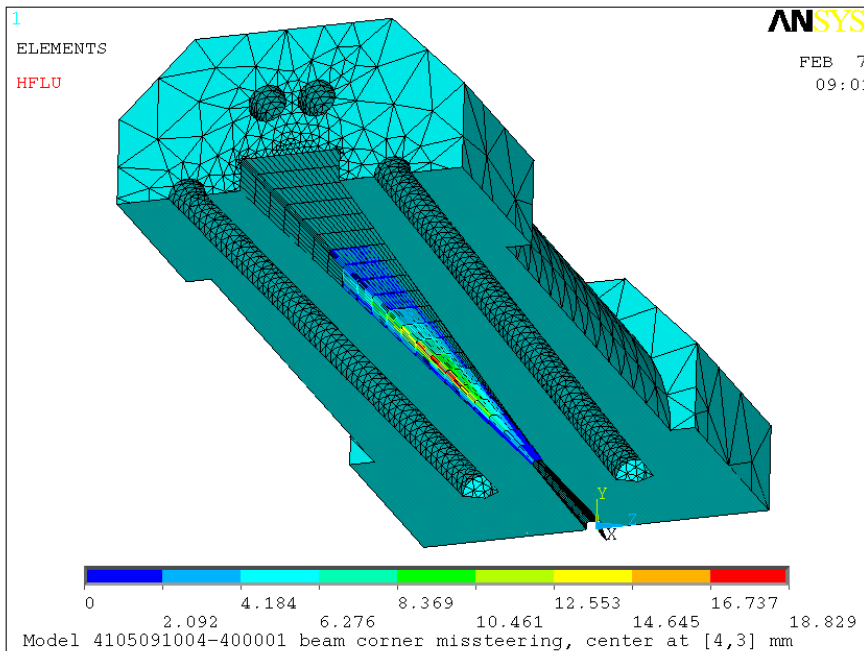


Figure 3.6-2 M4-40 mesh, the cross section is shown to show the aperture, the aperture surface area is mesh with an 8-node quad surface mesh (mesh 200 elements), with the beam center at [4, 3] mm. The heat flux is shown.

3.6.2. M4-40 Power Calculation

The power of one undulator A at 100 mA and 11 mm gap (k=2.62) at 23.95 m was calculated using SRUFF. The power density distribution and the curve fit are shown in Figure 3.6-3 and Figure 3.6-4, respectively. The fitted formula was used in ANSYS for the thermal load application.

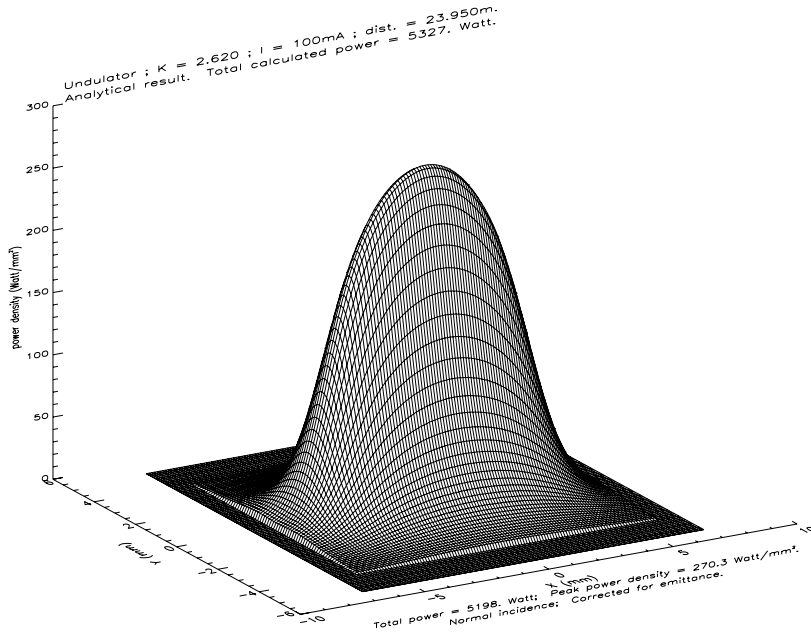


Figure 3.6-3 Undulator A power density distribution at 100 mA, k=2.62 at 23.95 m.

$$\text{Fit} = \exp(5.5997 - 0.019841x^2 - 0.55969y^2 - 0.0021776x^4 + 0.025046y^4 + 0.0017941x^2y^2)$$

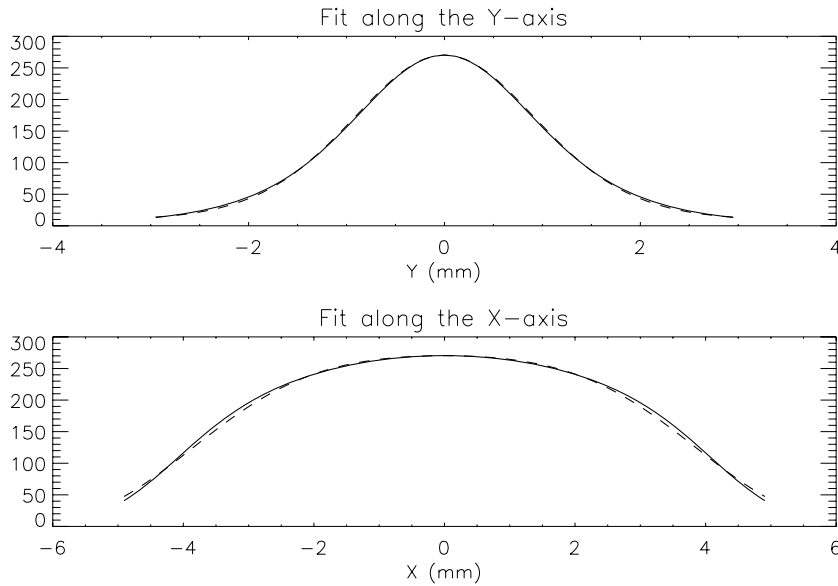


Figure 3.6-4 M4-40 power density distribution Gaussian fitting formula. The solid line is the calculated data, and the dashed line is the fitted formula.

3.6.3. M4-40 Thermal and Stress Analysis for 100 mA Operation

A very detailed beam missteering study of a mask was illustrated in section 3.2.3 with M1-40. As the M1-40 and M4-40 masks are similar, here we calculated fewer points. We covered the vertical, horizontal and one-corner missteering cases. The M4-40 aperture and beam missteering locations are shown in Figure 3.6-5.

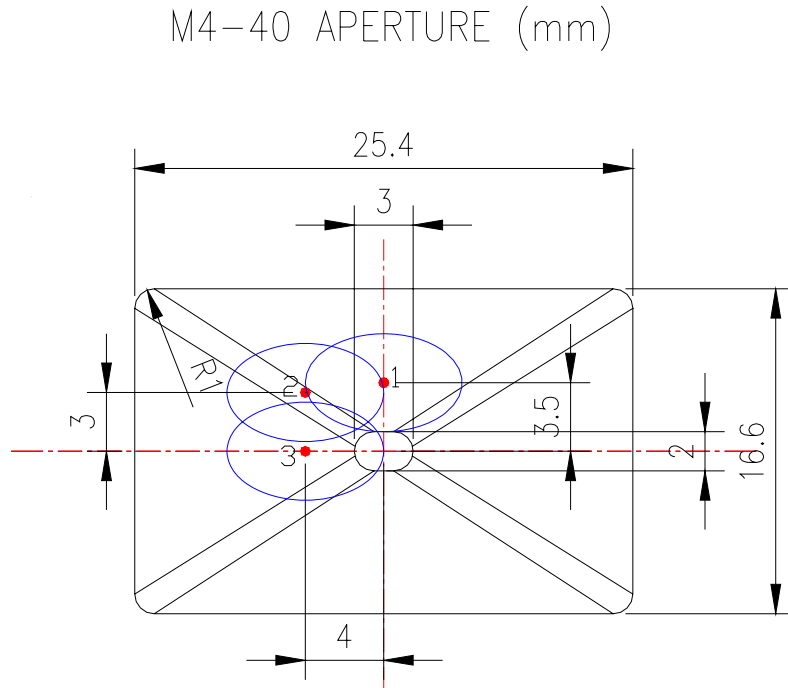


Figure 3.6-5 M4-40 aperture, round dots stand for the beam center, ovals stand for the beam footprint of 8x5 mm.

Temperature and stress data for the beam at three locations are tabulated in Table 3.6-2.

Table 3.6-2 Temperature and stress results for M4-40 with beam center at three locations (100 mA, $k=2.62$, $h=0.015$ w/mm²°C, $T_0=25.6$ °C)

Beam center position	Beam center coordinates [x,y] mm	Missteering case	T_{\max} (°C)	T_{wall} (°C)	σ_{vm} (MPa)
1	[0, 3.5]	Vertical	195.6	74.4	340.2
2	[4, 3]	Corner	171.0	72.2	365.8
3	[4, 0]	Horizontal	142.2	67.3	n/a*

* Temperature is too low to warrant a stress analysis.

As predicted, vertical missteering (position 1) results in the highest temperature, the corner has a lower temperature but higher stress. The cooling wall temperature is low, which means the cooling channels are positioned far from the heating surface, so the temperature will be insensitive to the film coefficient h . Temperature and stress for vertical and corner missteering are plotted in Figure 3.6-6 through Figure 3.6-9.

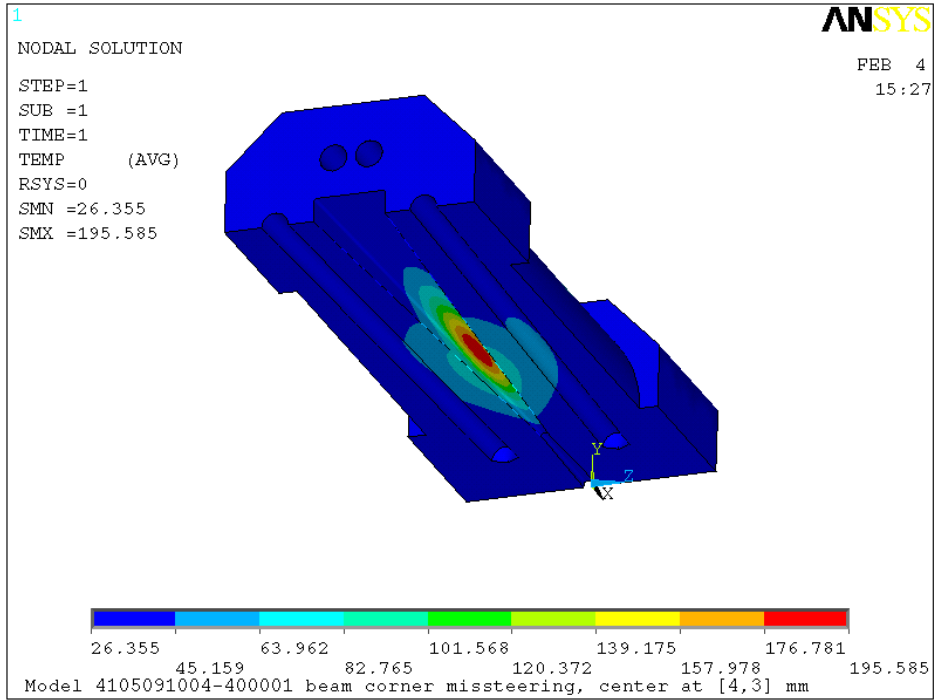


Figure 3.6-6 Temperature plot(°C), vertical missteering, beam center at [0, 3.5] mm.

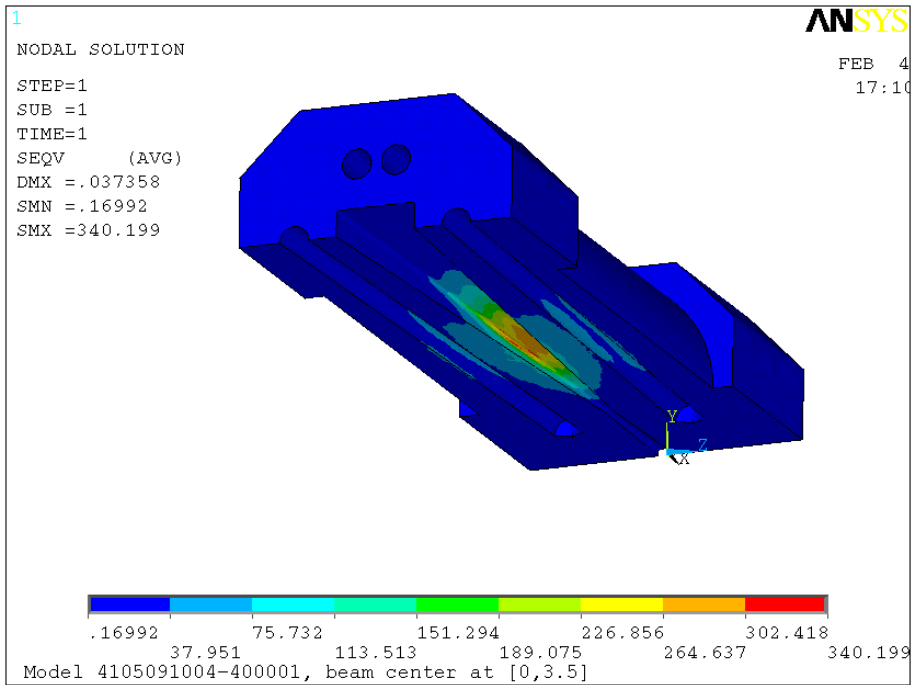


Figure 3.6-7 Von Mises stress plot (MPa), vertical missteering, beam center at [0, 3.5] mm.

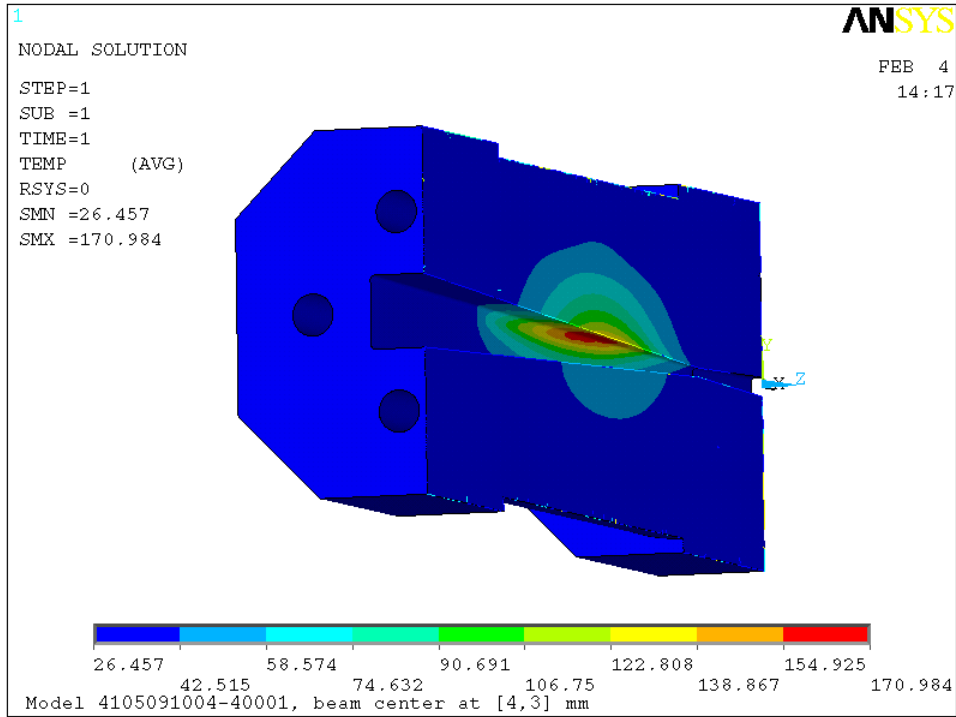


Figure 3.6-8 Temperature plot (°C), corner missteering, beam center at [4, 3] mm.

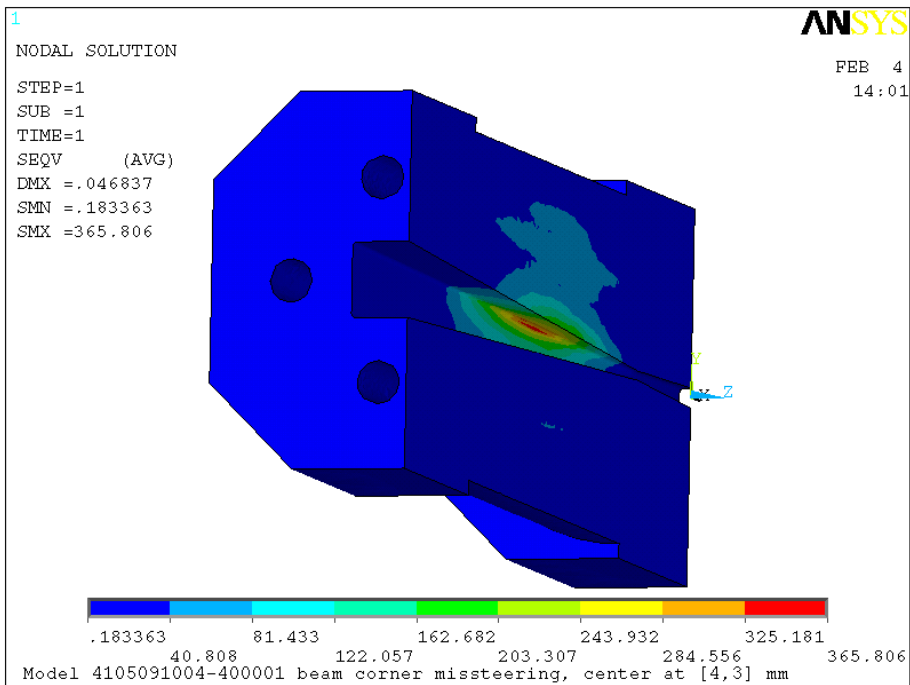


Figure 3.6-9 Von Mises stress plot (MPa), corner missteering, beam center at [4, 3] mm.

3.7. Summary of the Results for Front End v1.5

The maximum temperature and stress of all components of FEv1.5 at 100 mA were calculated. The method shown in section 3.2.4 was used to predict the results for higher beam currents, such as 130 mA. By comparing the maximum temperature and stress results to the failure criteria, the maximum allowed beam current for the front end is derived. The FEv1.5 results are summarized in Table 3.7-1.

Table 3.7-1 FEv1.5 results (one undulator A at $k=2.62$, $h=0.015$ w/mm²°C, $T_0=25.6^\circ\text{C}$)

FEv1.5 Components		M1-40 (FM1)	M2-40 (FM2)	M2-50 (FM3)	P2-30 (PS1)	P2-30 (PS2)	M4-40 (Exit Mask)
Distance to center of straight section (m)		16.75	17.4	21.1	18.9	22.3	25.2
Aperture	Inlet (mm)	38×26	25.8×17.4	23.5×15.9	21.5×34	21.5×34	25.4×16.6
	Outlet (mm)	20×12	11×6	12.7×5.2	12×5.5	12×5.5	3×2
100 mA (vertical missteering on masks, no missteering on P2-30)	T _{max} (°C)	204.8	200.3	201.5	135.8	Same device as PS1, further away from the source	195.6
	T _{wall} (°C)	81.1	78.0	78.3	55.8		74.4
	σ _{vm} (MPa)	319.4	312.0	309.7	n/a*		340.2
100 mA (corner missteering on masks, horizontal missteering on P2-30)	T _{max} (°C)	182.0	191.6	184.6	140.9		171.0
	T _{wall} (°C)	79.0	83.2	79.8	59.3		72.2
	σ _{vm} (MPa)	349.1	326.5	308.9	176.2		365.8
130 mA (linear extrapolated results)	T _{max} (°C)	258.6	252.7	254.3	175.5	246.6	
	T _{wall} (°C)	97.8	100.5	96.1	69.4	89.1	
	σ _{vm} (MPa)	453.8	424.5	402.6	229.1	475.5	
Max. allowed beam current (mA)		130	130	130	225	225	130

Although the FEv1.5 photon shutters can operate at 225 mA with a single undulator A, the stress levels for all masks, especially the exit mask, exceeded the current limits at 130 mA. So overall the FEv1.5 can only operate with one undulator A at 11 mm gap ($k=2.62$) at a maximum beam current of 130 mA. The cooling wall temperature at 130 mA is far below the water boiling temperature due to the thick wall (> 9 mm). The peak temperature is not sensitive to the change of the h value, so the recommended

minimum h value is $0.01 \text{ w/mm}^2\text{°C}$. The cooling water flow trip limit should be set so that the minimum h value is maintained at $0.01 \text{ w/mm}^2\text{°C}$.

4. Thermal Analysis of Components of Front End v1.2u

Among the FEv1.2u components, only the first fixed mask (M1-30) and photon shutters (P1-20 and P2-20) were analyzed over ten years ago, and written reports were published as APS Light Source Notes [4], [5] and in other publications [6]. The models used in the analysis were conceptual design models. Also, when that analysis was performed, the undulator maximum k value was only 2.23, which is much lower than the current value of 2.62. As the power profile depends on the k value and the designs have been modified since the conceptual design, we decided to redo all the analyses using the as-built models and accurate power loads. All components in FEv1.2u except the photon shutters were modeled in ProE. The photon shutters were modeled directly in ANSYS due to the simplicity of the geometry.

4.1. Thermal Analysis of Premasks B7-50 and B7-60

The B7-60 premask is used to protect the first fixed mask M1-30 inlet flange from normal incidence BM radiation from the AM magnet coming down in the same pipe with the undulator beam. The B7-50 is the premask for the wiggler front end to protect the wiggler FE first fixed mask M1-20. The B7-60 is the premask for the undulator only front end to protect the undulator FE first fixed mask M1-30. The B7-60 is essentially a B7-50 plus a GlidCop plate bolted to the B7-50 (shown in Figure 4.1-1). This GlidCop plate reduces the B7-50 inbound horizontal aperture so it can protect the flange of the undulator FE first fixed mask M1-30. Both the B7-50 and the bolt-on plate are manufactured from GlidCop and the BM radiation is normal incidence to the mask. Key information for B7-60 and B7-50 are listed in Table 4.1-1.

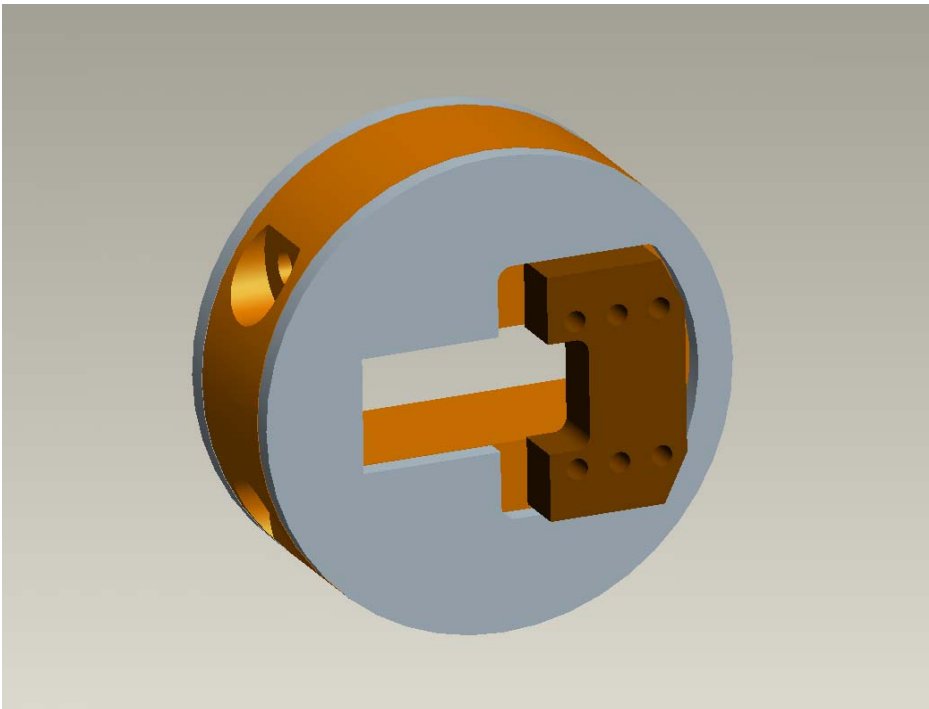


Figure 4.1-1 The B7-60 premask assembly consists of a B7-50 premask plus a bolt-on GlidCop plate.

Table 4.1-1 Key information for pre-masks B7-60 and B7-50.

Name	B7-60	B7-50
Purpose	To protect M1-30	To protect M1-20
Distance to the center of the straight section (m)	16.0	16.0
Distance to the start of the AM magnets (m)	8.27	8.27
Inlet aperture H×V (mm×mm)	(+31/-17.4)× 25	62 × 25
Outlet aperture H×V (mm×mm)	(+31/-17.4)× 25	62 × 25
Total BM fan exit from storage ring exit valve in un-displaced sector	5.5 mrad (refer to drawing 310308-920015-02)	5.5 mrad (refer to drawing 310308-920015-02)
Total BM fan intercept by pre-mask in un-displaced sector	3.5 mrad (inbound)	1.8 mrad (inbound)
Total BM fan exit from storage ring exit valve in displaced sector	4.0 mrad (refer to drawing 310308-920016)	4.0 mrad (refer to drawing 310308-920016)
Total BM fan intercept by pre-mask in displaced sector	3.5 mrad (inbound)	1.8 mrad (inbound)
Reference drawing number	B7-600000-00	4105091407-510001-00

The analysis of B7-50 is not necessary because, due to its large horizontal aperture, it intercepts less BM power than the B7-70 in section 3.1. The B7-60 intercepts the same amount of power as the B7-70. The only difference is B7-70 is internally cooled and B7-60 is contact cooled. For B7-60, the BM power is intercepted by the bolt on plate and cooled via contact to the cooling block of B7-50. At this time, we do not have measured thermal resistance data of GlidCop to GlidCop for B7-60 to perform an accurate thermal analysis involving contact. From the analysis of B7-70, when the ring is operated at 300 mA, B7-70 will reach 208°C. Because B7-60 is contact cooled, the B7-60 peak temperature can be higher. However, even if the bolt-on plate reaches a very high temperature due to poor thermal contact with the cooling block, it will still function as a pre-mask, and it will not fail due to microcracks formed on the surface simply because the microcracks on the bolt-on plate will not propagate to the cooling channels on the B7-50 body. A high temperature on B7-60 will be noticed by a degraded vacuum reading in that region. Thermal contact resistance depends on the surface pressure and roughness. Thermal contact resistance can be reduced by having a silver or indium foil between the bolt-on plate and the B7-50 body. For thermal analysis of a similar pre-mask including the power calculation, refer to section 3.1.

4.2. Thermal Analysis of the First Fixed Mask M1-30

4.2.1. M1-30 Model and Mesh

The M1-30 mask is manufactured from a solid round billet of GlidCop. The M1-30 was modeled in ProE, and the model was read in by ANSYS for analysis. The M1-30 is used for the undulator only front end. For the wiggler front end, the M1-20, which has a larger horizontal aperture, will replace the M1-30. The aperture area of M1-30 was meshed with an 8-node quad area mesh (mesh 200 elements), and the M1-30 volume was meshed with a tetrahedron mesh. The M1-30 model and mesh are shown in Figure 4.2-1 and Figure 4.2-2, respectively. Key information for the M1-30 is shown in Table 4.2-1.

Table 4.2-1 Key dimensions and reference information for M1-30.

Name	M1-30
Distance to the center of the straight section (m)	17.25
Distance to the center of undulator installed 1.25 m downstream (m)	16.0
Total power (watts)	5327
Peak power density (w/mm ²)	615.7
Inlet aperture H×V (mm×mm)	38 × 26
Outlet aperture H×V (mm×mm)	24 × 12
Active length (mm)	267
Horizontal taper angle	1.5°
Vertical taper angle	1.5°
Aperture corner radius (mm)	1.0
Top and bottom cooling wall thickness (mm)	9.9 (outlet), 9.8 (inlet)
Left and right cooling wall thickness (mm)	11.1 (outlet), 10.1 (inlet)
Reference drawing number	4102010101-310001-00

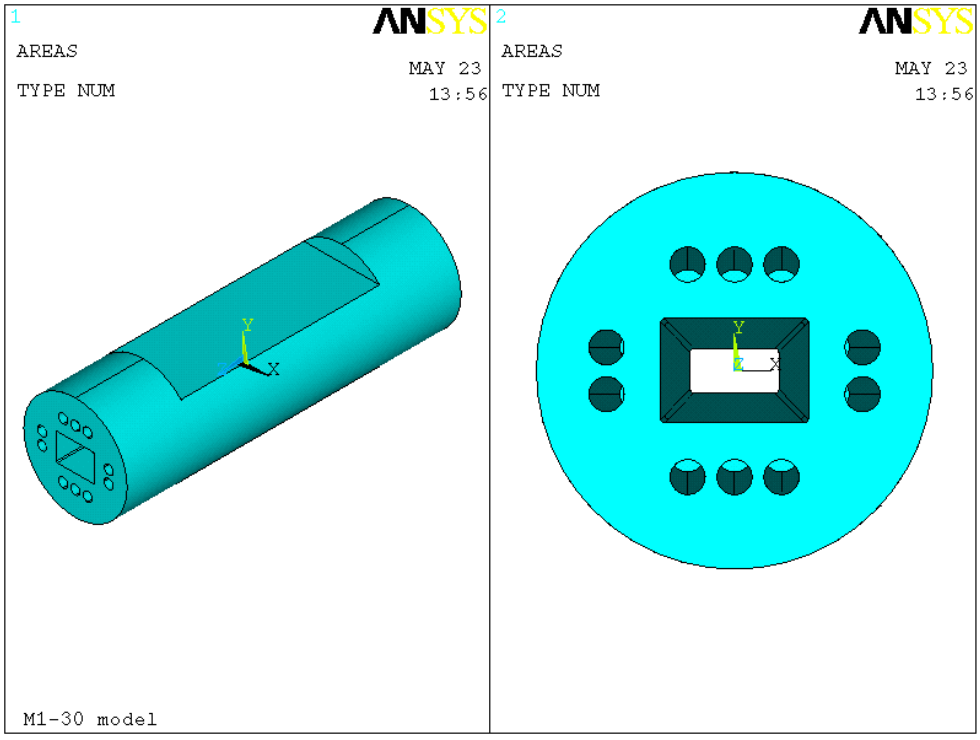


Figure 4.2-1 M1-30 model read in from ProE.

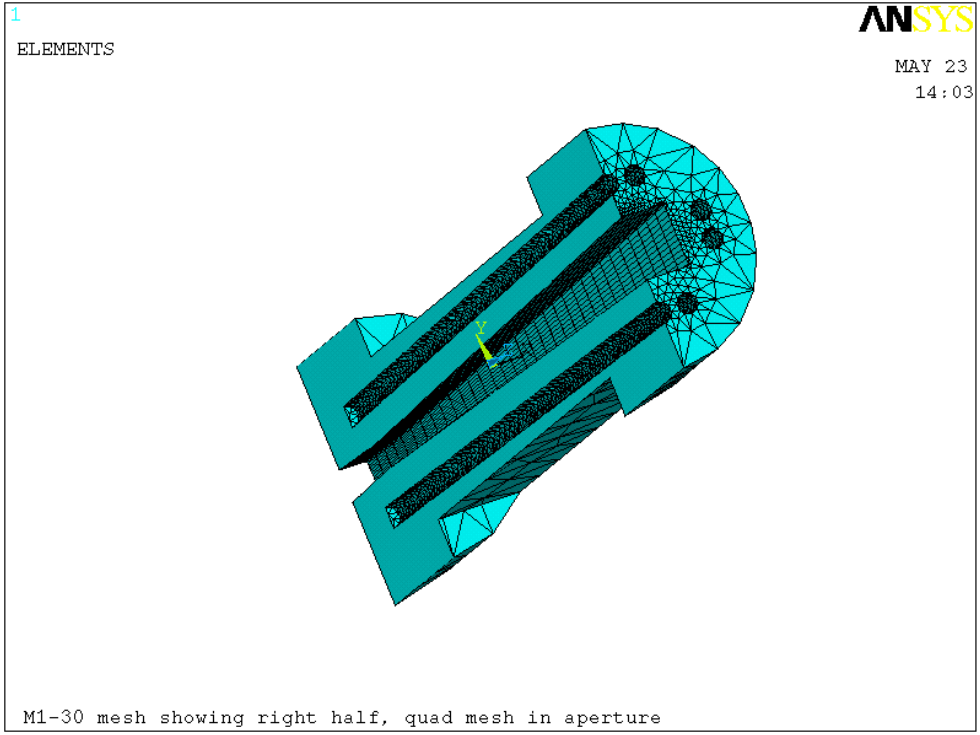


Figure 4.2-2 M1-30 mesh, right half shown, quad mesh in the aperture, tetrahedron mesh for the volume.

4.2.2. M1-30 Power Calculation

The power density distribution from one undulator A at 100 mA and 11 mm gap ($k=2.62$) at 16.0 m was calculated using SRUFF. To be conservative, zero emittance was used. The power density distribution and the curve fitting formula are shown in Figure 4.2-3 and Figure 4.2-4, respectively. The fitted formula was used in ANSYS for the thermal load application.

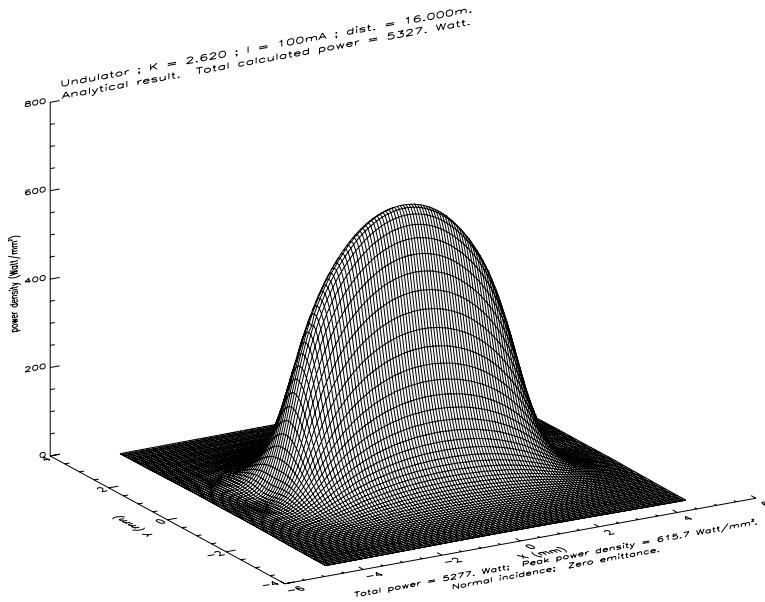


Figure 4.2-3 Undulator A power density distribution at 100 mA, $k=2.62$ at 16 m, zero emittance.

$$\text{Fit} = \exp(6.4228 - 0.016559x^2 - 1.2927y^2 - 0.015842x^4 + 0.13199y^4 + 0.015037x^2y^2)$$

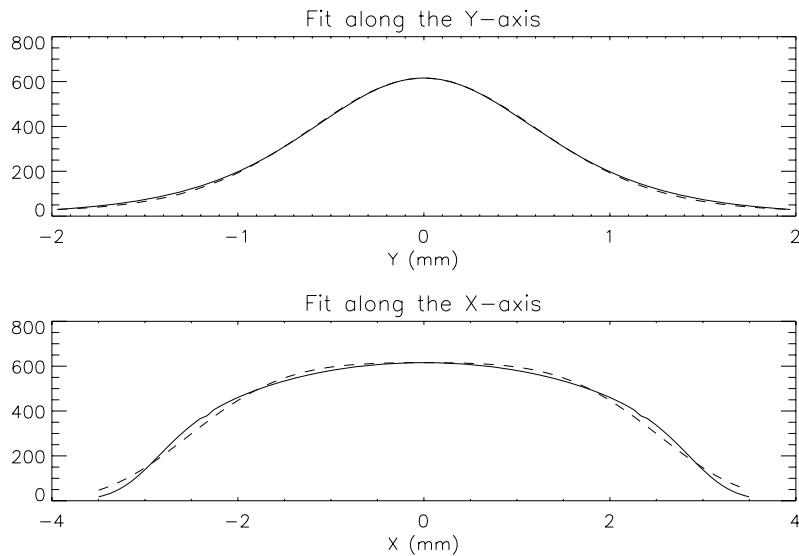


Figure 4.2-4 Power density distribution for M1-30 at 16 m from the Gaussian fitting formula. The solid line is the calculated data, and the dashed line is the fitted formula.

Table 4.2-2 Temperature and stress results for M1-30 with beam center at various locations (100 mA, k=2.62, h=0.02 w/mm²°C, T₀=25.6°C).

Beam center position	Beam center coordinates [x,y] mm	Misstearing case	Max. temperature (°C)	Max. cooling wall temperature (°C)	Max. von Mises stress (MPa)
1	[0,8]	Vertical, full beam on the top surface	247.5 (Figure 4.2-6)	83.0	359.7 (Figure 4.2-7)
2	[11,8]	Vertical, approaching corner, most of beam on the top surface	227.6	75.4	403.6
3	[12,8]	Vertical, approaching corner, partial beam on the corner fillet	216.3 (Figure 4.2-8)	73.7	416.3 (Figure 4.2-9)
4	[13,8]	Corner, beam center on the intersection of the top surface and corner fillet	194.5	68.0	381.6
5	[13.5,7.5]	Corner, beam center on the center of the corner fillet	162.7	59.8	300.2

As predicted, the vertical missteering (position 1) results in the highest temperature. As the beam moves closer to the corner, the temperature decreases because there is more material to conduct heat, while the stress increases due to more constraints at the corner. The highest stress occurs when the beam hits the top surface very close to the intersection of the top and corner fillet. The temperature and stress for the vertical and corner missteering cases are plotted in Figure 4.2-6 through Figure 4.2-9.

Due to the relatively large cooling wall thickness (>9 mm), the results will not be very sensitive to the h value. (Refer to section 3.2.5 for the sensitivity study of the h value.)

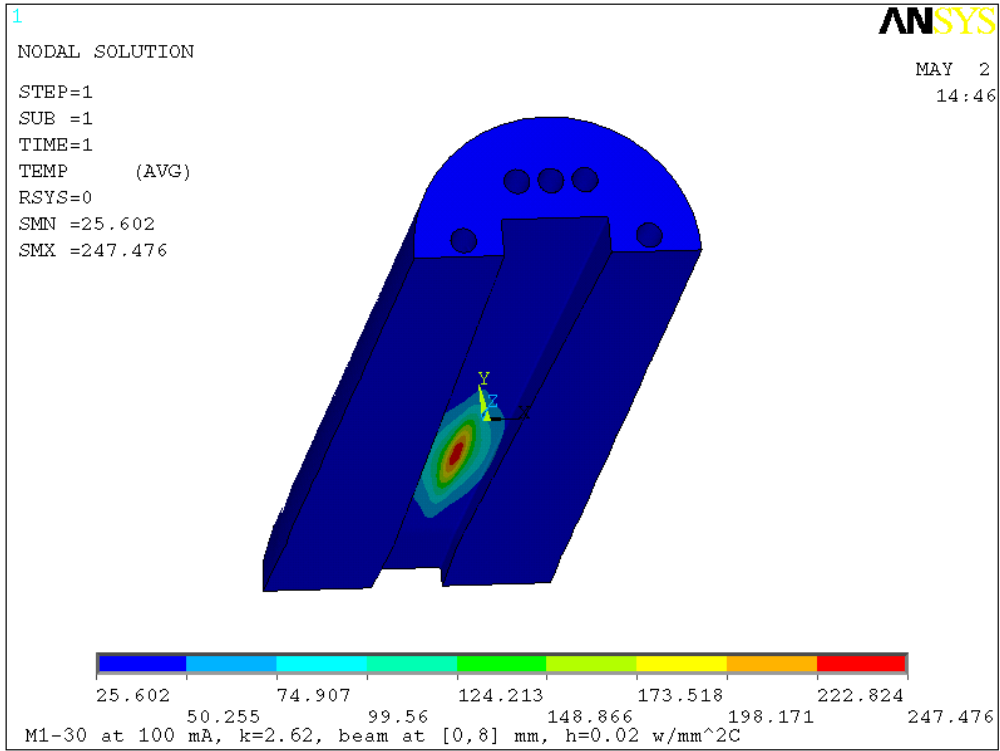


Figure 4.2-6 Temperature plot (°C), vertical missteering, beam center at [0, 8] mm.

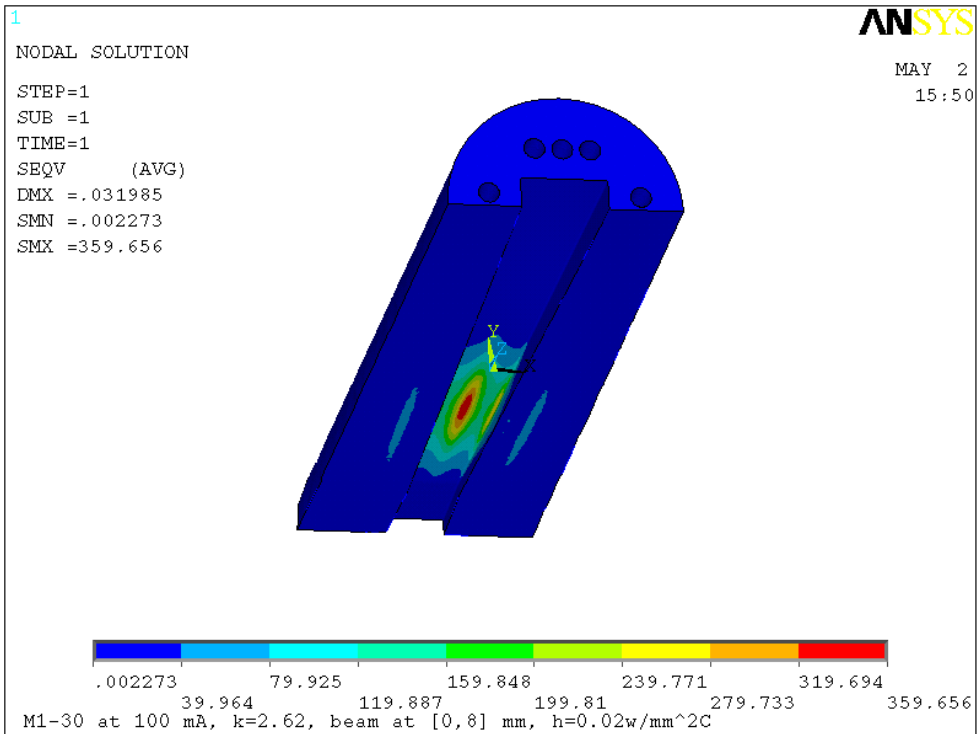


Figure 4.2-7 Von Mises stress plot (MPa), vertical missteering, beam center at [0, 8] mm.

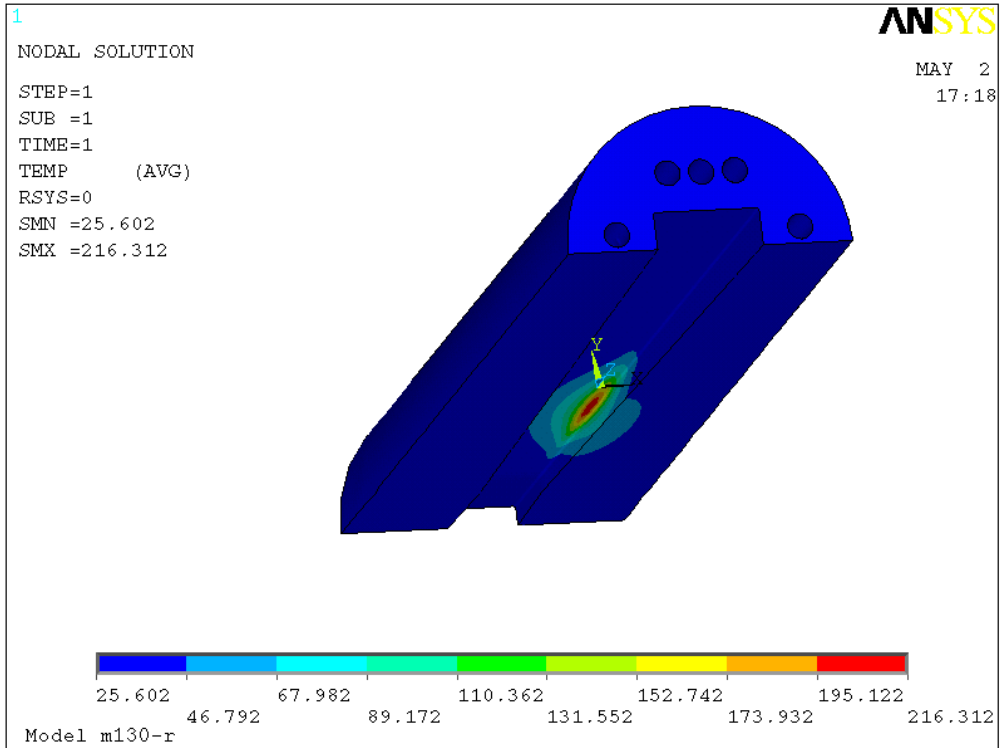


Figure 4.2-8 Temperature plot (°C), near-corner missteering, beam center at [12,8] mm.

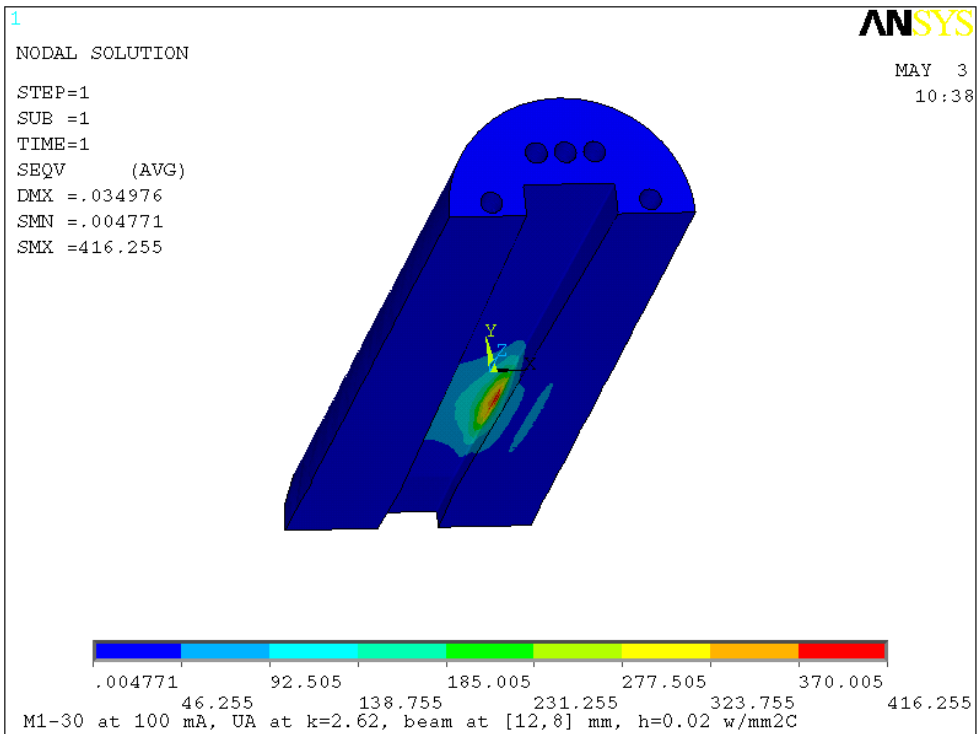


Figure 4.2-9 Von Mises stress plot (MPa), near-corner missteering, beam center at [12, 8] mm.

4.3. Thermal Analysis of the Second Fixed Mask M2-20

4.3.1. M2-20 Model and Mesh

The M2-20 mask is the second fixed mask for the FEv1.2. It is used for both wiggler and undulator front ends. The M2-20 is manufactured from a solid round billet of GlidCop. The M2-20 was modeled in ProE, and the model was read in by ANSYS for analysis. Within ANSYS, the model was divided into three volumes lengthwise.

Volume 1: The middle portion of the mask from the inlet aperture to the outlet aperture (the neck of the mask). This volume can be meshed with a brick mesh because the cross section is topologically similar. Brick mesh is desired when possible because it results in better accuracy and less computation time.

Volume 2 & 3: Volume 2 is from the upstream of the mask to the inlet of the mask, and volume 3 is from the narrowest aperture to the exit end of the mask, these two volumes cannot be meshed with brick mesh and are meshed with tetrahedron mesh. Model and mesh are shown in Figure 4.3-1 and Figure 4.3-2, respectively. Key information for the M2-20 is shown in Table 4.3-1.

Table 4.3-1 Key dimensions and reference information for M2-20

Name	M2-20
Distance to the center of the straight section (m)	20.6
Distance to the center of undulator installed 1.25 m downstream (m)	19.35
Total power (watts)	5327
Peak power density (w/mm ²)	421.0
Inlet aperture H×V (mm×mm)	66 × 18
Outlet aperture H×V (mm×mm)	54 × 6
Active length (mm)	267
Horizontal taper angle	1.5°
Vertical taper angle	1.5°
Aperture corner radius (mm)	1.0
Top and bottom cooling wall thickness (mm)	10
Left and right cooling wall thickness (mm)	6.7
Reference drawing number	4102010105-210001-02

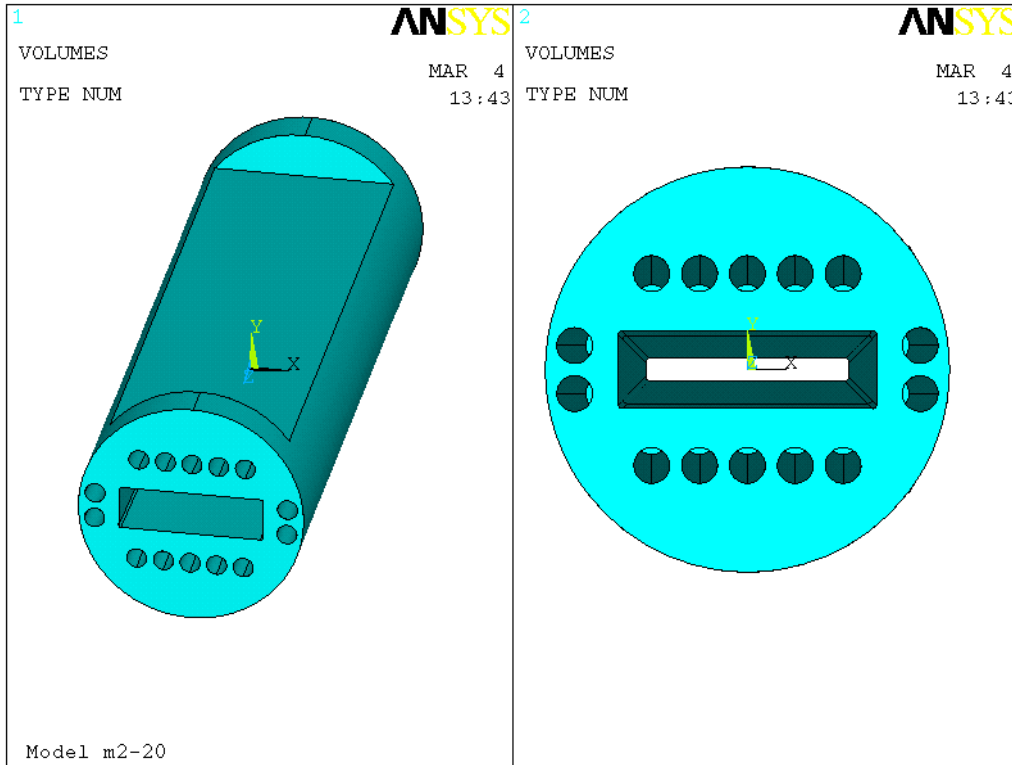


Figure 4.3-1 M2-20 model read in from ProE.

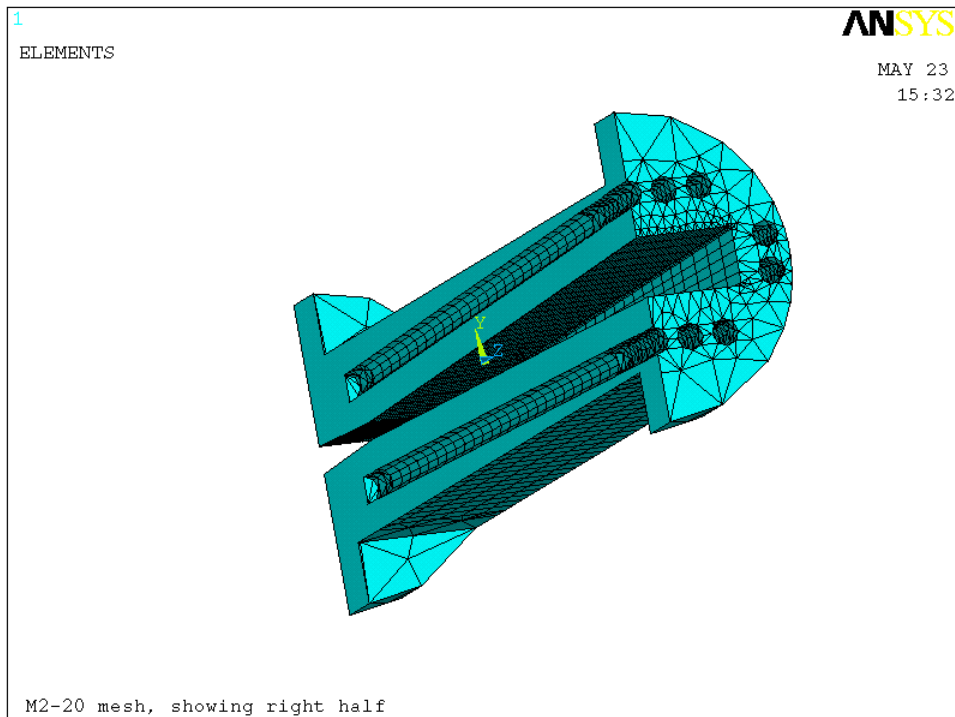


Figure 4.3-2 M2-20 mesh, right half shown, brick mesh for the middle portion from inlet to outlet.

4.3.2. M2-20 Power Calculation

The power density distribution from one undulator A at 100 mA and 11 mm gap ($k=2.62$) at 19.35 m was calculated using SRUFF. To be conservative, zero emittance was used. The power density distribution and the curve fitting formula are shown in Figure 4.3-3 and Figure 4.3-4, respectively. The fitted formula was used in ANSYS for the thermal load application.

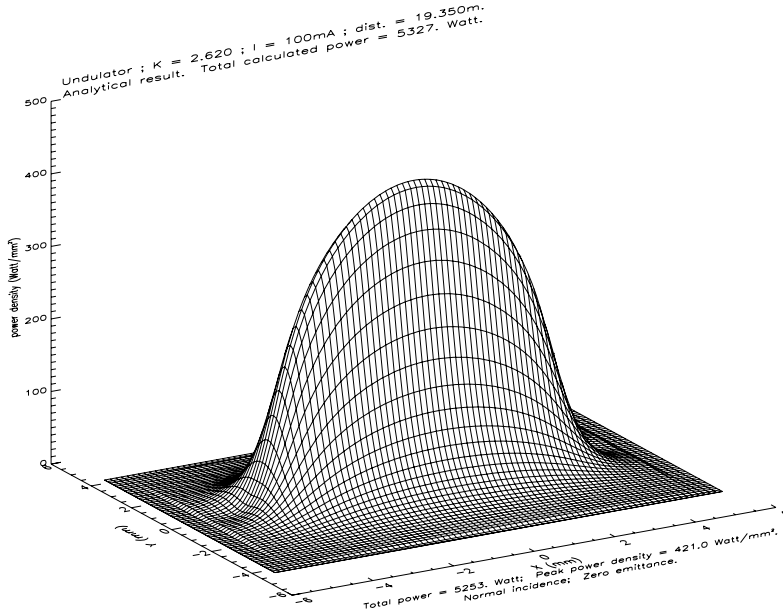


Figure 4.3-3 Undulator A power density distribution at 100 mA, $k=2.62$ at 19.35 m, zero emittance.

$$\text{Fit} = \exp(6.0426 - 0.011485x^2 - 0.88030y^2 - 0.0075361x^4 + 0.059111y^4 + 0.0088099x^2y^2)$$

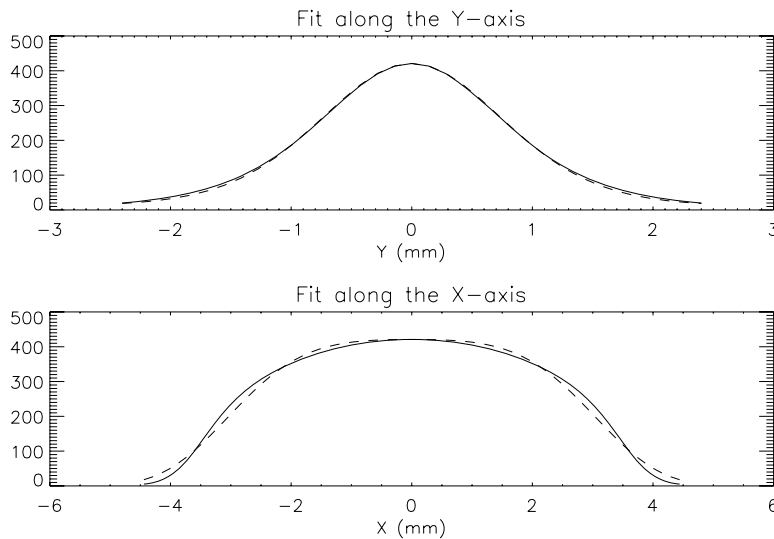


Figure 4.3-4 Power density distribution for M2-20 at 19.35 m from the Gaussian fitting formula. The solid line is the calculated data, and the dashed line is the fitted formula.

4.3.3. M2-20 Thermal and Stress Analysis for 100 mA Operation

The M2-20 horizontal aperture (54 mm exit) is quite large and is shadowed by the upstream M1-30 aperture (24 mm exit). In normal operation with M1-30 at the upstream location, M2-20 will never encounter horizontal or corner missteering. Vertical missteering will be the only load case. However the corner missteering case is still calculated for reference purposes. The M2-20 aperture and beam center locations are shown in Figure 4.3-5. Temperature and stress data for the beam at the vertical and corner missteering cases are tabulated in Table 4.3-2

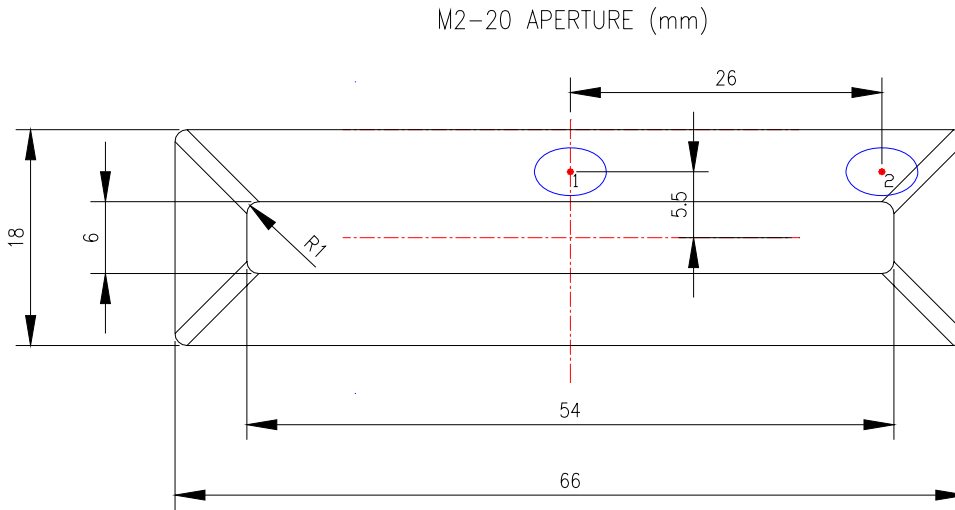


Figure 4.3-5 M2-20 aperture, round dots stand for the beam center, ovals stand for the beam footprint of 6×4 mm.

Table 4.3-2 Temperature and stress results for M2-20 with the beam center at various locations (100 mA, $k=2.62$, $h=0.015$ w/mm²°C, $T_0=25.6$ °C)

Beam center position	Beam center coordinates [x,y] mm	Missteering case	Max. temperature (°C)	Max. cooling wall temperature (°C)	Max. von Mises stress (MPa)
1	[0, 5.5]	Vertical, full beam on the top surface	206.6	89.8	306.2
2	[26, 5.5]	Vertical, approaching corner, partial beam on the corner fillet	190.2	81.3	445.3

As predicted, the vertical missteering (position 1) results in the highest temperature; as the beam moves to the corner, the temperature decreases because more material is there to conduct heat, while the stress increases due to more constraints at the corner. Because the M2-20 horizontal aperture is shadowed by the upstream M1-30 aperture, the corner missteering case will never happen. The temperature and stress for the vertical missteering case are plotted in Figure 4.3-6 and Figure 4.3-7, respectively.

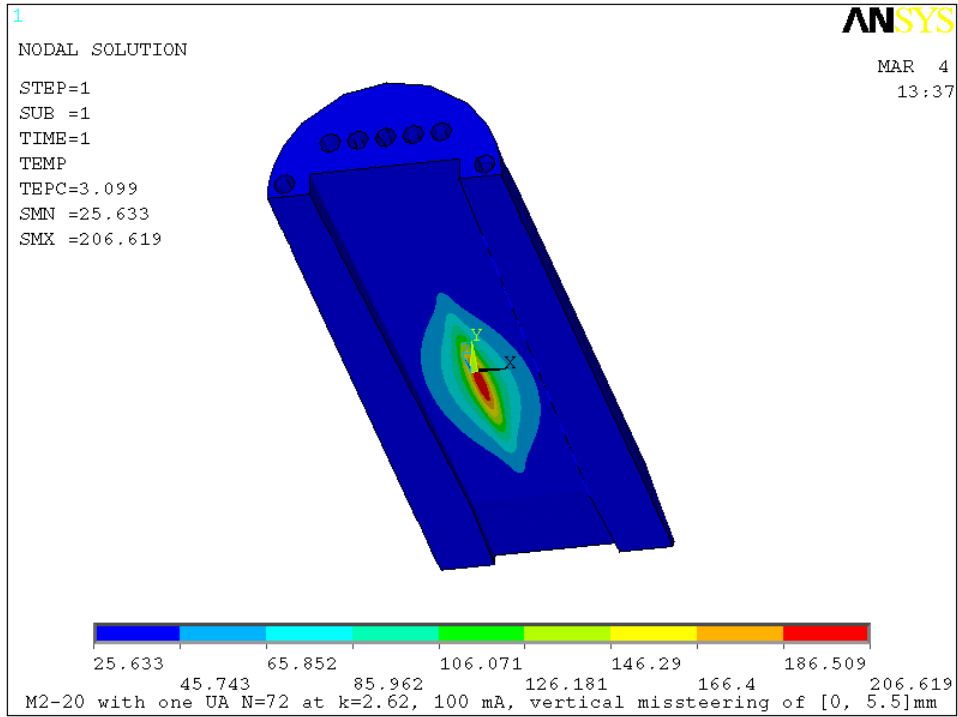


Figure 4.3-6 Temperature plot(°C), vertical missteering, beam center at [0, 5.5] mm.

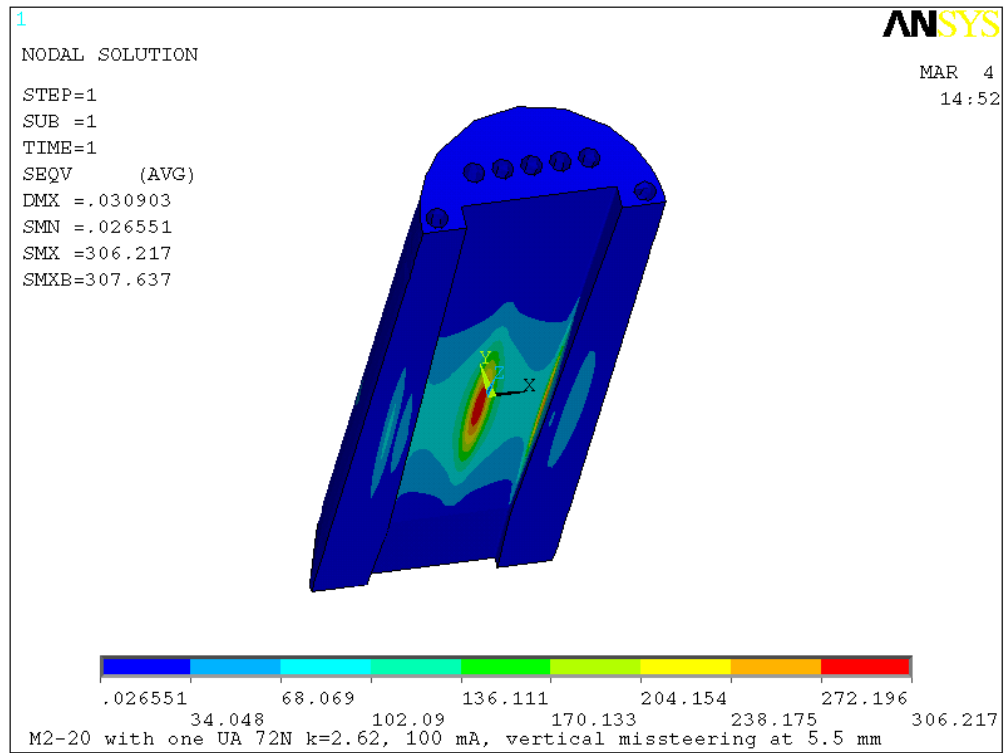


Figure 4.3-7 Von Mises stress plot (MPa), vertical missteering, beam center at [0, 5.5] mm.

4.4. Thermal Analysis of Photon Shutters P1-20 and P2-20

4.4.1. P1-20 and P2-20 Model

Photon shutters P1-20 (PS1) and P2-20 (PS2) have similar designs. They are both hockey-stick-style shutters. The blade is made of a 1/8" thick plate of GlidCop explosion bonded to the OFHC copper base. The PS1 blade is 600 mm long, and the PS2 blade is 300 mm long. The PS1 has a longer blade to accommodate the large vertical exit aperture (12 mm) of the first fixed mask (M1-20 or M1-30) upstream of the PS1, whereas, the aperture of second fixed mask (M2-20) upstream of PS2 has a smaller vertical exit aperture of 6 mm. For finite element analysis (FEA) purposes, the PS1 and PS2 models can be treated as the same. The model was generated directly in ANSYS with a 300 mm length as shown in Figure 4.4-1. Key information for the P1-20 and P2-20 is shown in Table 4.4-1.

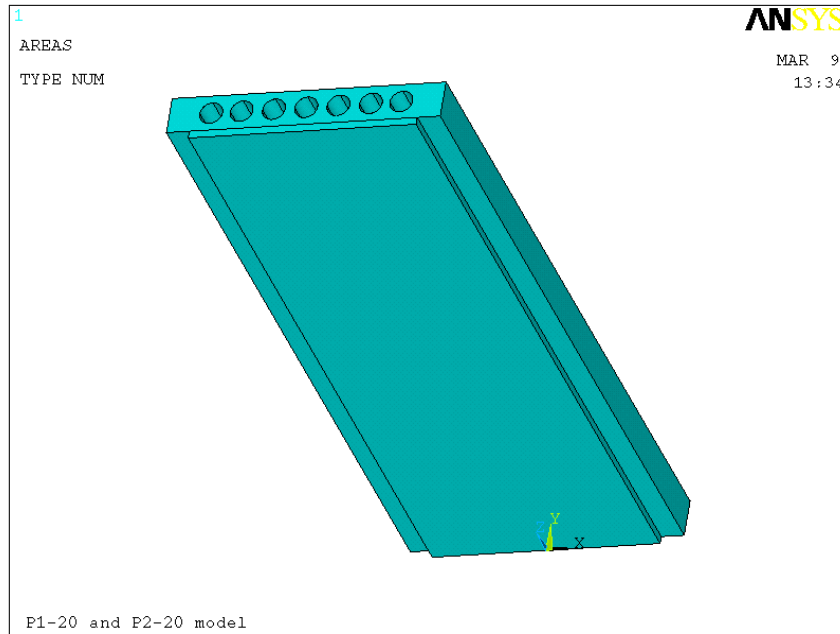


Figure 4.4-1 P1-20 and P2-20 model, blade modeled with 300 mm length.

Table 4.4-1 Key dimensions and reference information for P1-20 and P2-20 at 100 mA, k=2.62.

Name	P1-20 (PS1)	P2-20 (PS2)
Distance to the center of the straight section (m)	18	21.2
Distance to the center of downstream undulator (m)	16.75	19.95
Total power (watts)	5327	5327
Peak power density (w/mm ²)	561.8	396.0
Blade length (mm)	600	300
Beam incident angle (vertical)	1.5°	2.0°
Cooling wall thickness (mm)	6.35	6.35
Reference drawing number	4102010103-210401-02	4102010106-210401-01

4.4.2. P1-20 and P2-20 Power Load

The power density distribution for one 3.3-cm period, 2.4-m-long (72 periods) undulator at 100 mA, 11 mm gap ($k=2.62$) was calculated. To be conservative, zero emittance was used. The power for PS1 and its fitting formula are shown in Figure 4.4-2 and Figure 4.4-3, respectively. The power for PS2 and its fitting formula are shown in Figure 4.4-4 and Figure 4.4-5, respectively.

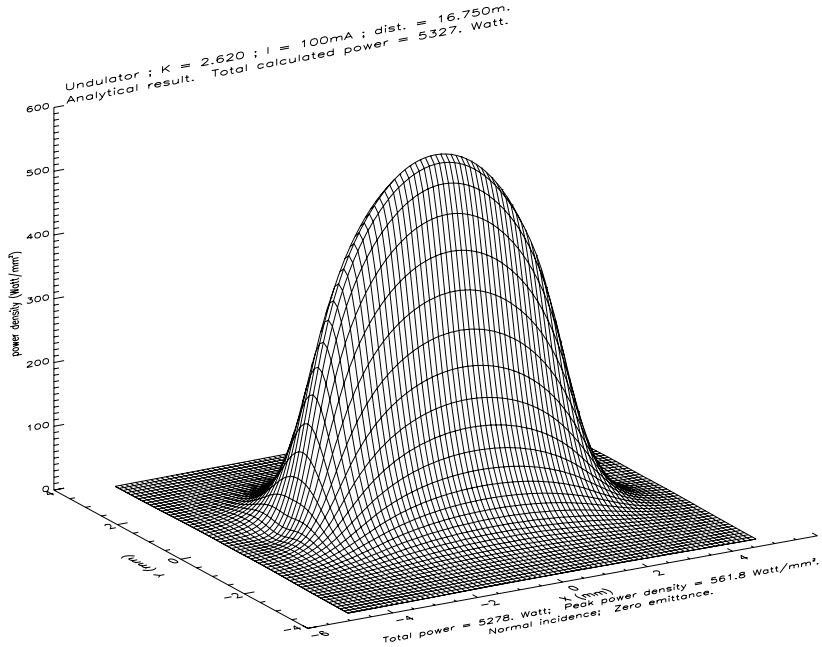


Figure 4.4-2 Undulator power density distribution plot for PS1 at 16.75 m, zero emittance.

$$\text{Fit} = \exp(6.3311 - 0.022998x^2 - 1.1215y^2 - 0.012055x^4 + 0.087897y^4 + 0.0091167x^2y^2)$$

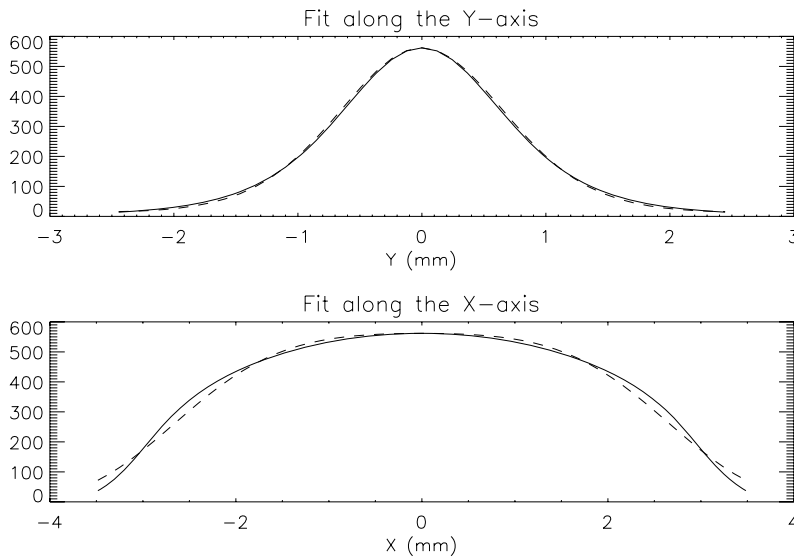


Figure 4.4-3 Undulator power distribution for PS1 at 16.75 m from the Gaussian fitting formula. The solid line is the calculated data, and the dashed line is the fitted formula.

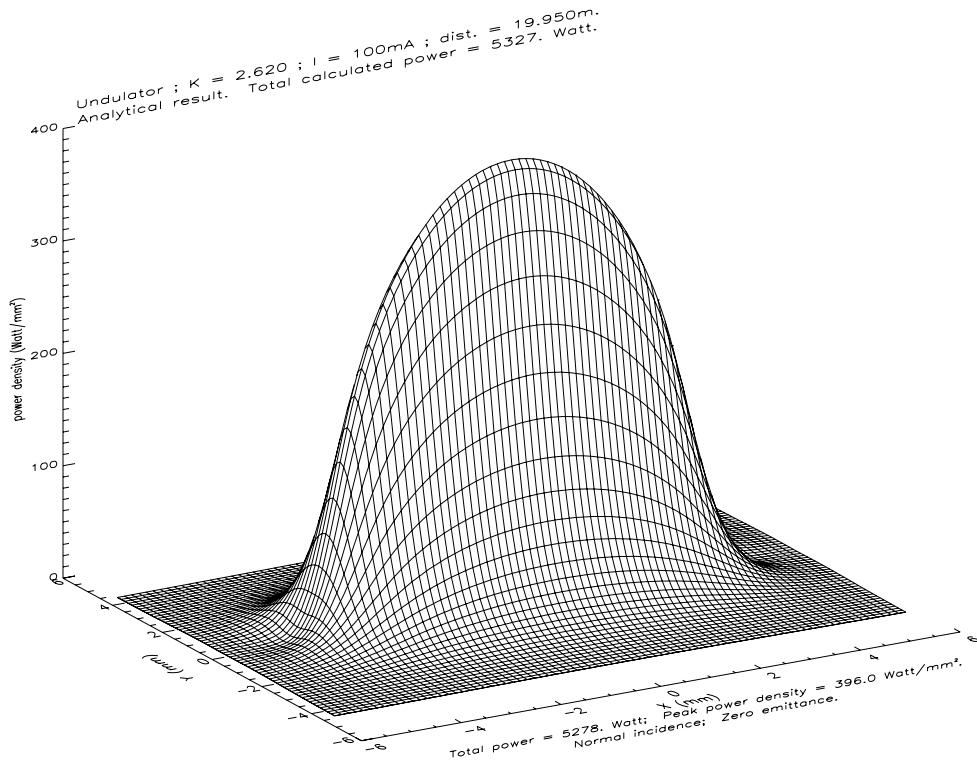


Figure 4.4-4 Undulator power density distribution plot for PS2 at 19.95m, zero emittance.

$$\text{Fit} = \exp(5.9815 - 0.013870x^2 - 0.79251y^2 - 0.0064160x^4 + 0.042904y^4 + 0.0065082x^2y^2)$$

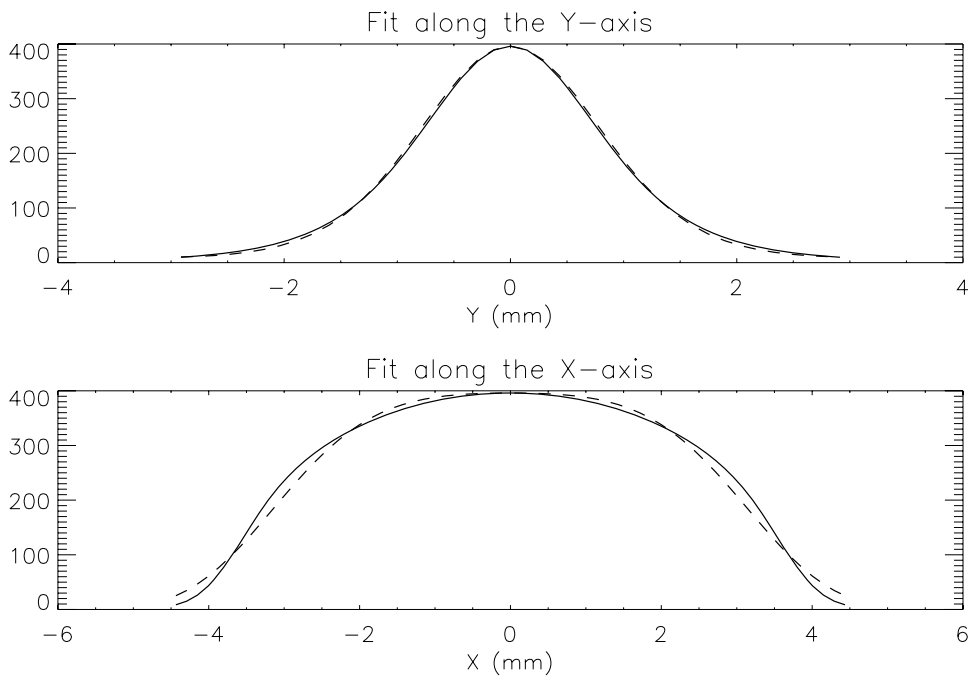


Figure 4.4-5 Undulator power distribution for PS2 at 19.95 m from the Gaussian fitting formula. The solid line is the calculated data, and the dashed line is the fitted formula.

4.4.3. P1-20 and P2-20 Thermal Analysis at 100 mA

Photon shutters PS1 and PS2, with a single 72 period undulator A at 11 mm gap ($k=2.62$) were evaluated. The results are tabulated in Table 4.4-2, and the temperature and stress for PS1 are plotted in Figure 4.4-6 and Figure 4.4-7, respectively. The temperature and stress for PS2 are plotted in Figure 4.4-8 and Figure 4.4-9, respectively.

Table 4.4-2 P1-20 and P2-20 results with 3.3-cm-period, 72-periods undulator at 100 mA, $k=2.62$, $h=0.02$ w/mm²°C, $T_0=25.6$ °C.

Components	Total power (w)	Peak surface power density (w/mm ²)	T _{max} (°C)	T _{wall} (°C)	Max. von Mises stress σ_{vm} (MPa)
PS1	5327	14.7	229.8	115.5	306.1
PS2	5327	13.8	238.7	122.7	305.2

Compared to the masks, PS1 and PS2 have a thinner cooling wall thickness. They will be more sensitive to the film coefficient h . The peak temperature and cooling wall temperature versus the film coefficient are tabulated in Table 4.4-3.

Table 4.4-3 Sensitivity of film coefficient study for PS1 and PS2

Film coefficient h (w/mm ² °C)	Max. temperature (°C)	Max. wall temperature (°C)	% change of peak temperature compare to nominal operating condition	
PS1	$h=0.02$	229.8	115.5	Nominal operating condition
	$h=0.015$	239.5	126.7	4.2% increase
	$h=0.001$	254.9	144.0	10.9% increase
	$h=0.005$	286.9	178.5	24.8% increase
PS2	$h=0.02$	238.7	122.7	Nominal operating condition
	$h=0.015$	249.1	134.7	4.4% increase
	$h=0.001$	265.4	153.1	11.2% increase
	$h=0.005$	299.0	189.4	25.3% increase

Due to the thin-wall design of the photon shutters (6.35 mm cooling wall thickness), the peak temperature is more sensitive to a change in the film coefficient h compared to the fixed masks (see section 3.2.5). To control the peak temperature increase to be less than 5%, the h value should be maintained at a minimum of 0.015 w/mm²°C. The water-flow trip-point setting should ensure that a minimum h of 0.015 w/mm²°C is maintained.

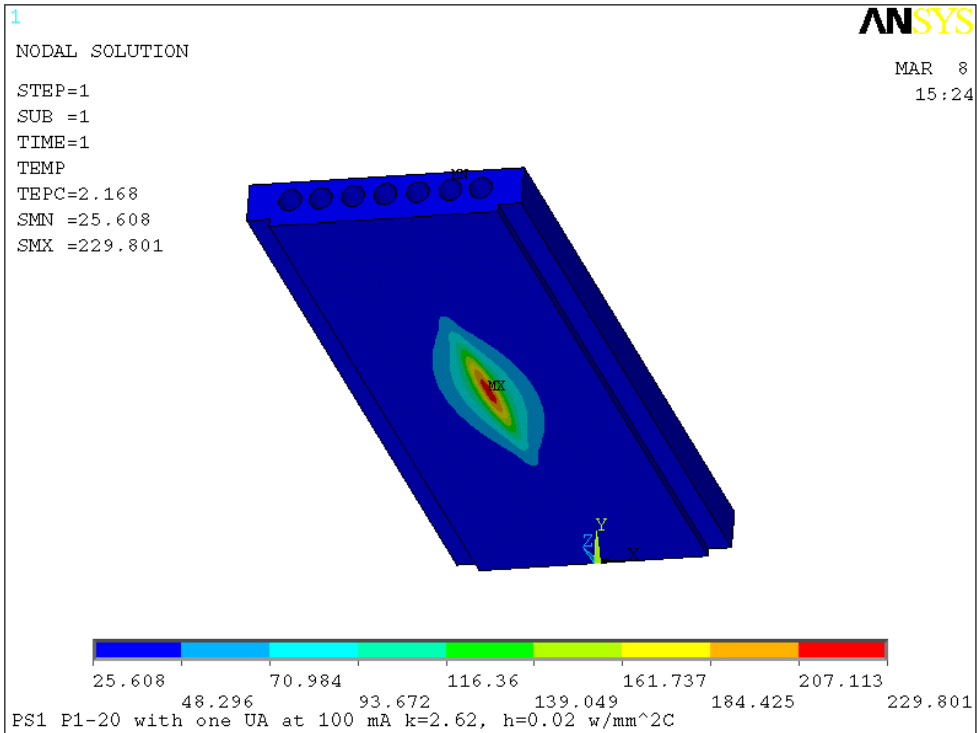


Figure 4.4-6 PS1 temperature plot(°C) with undulator A at 11 mm gap ($k=2.62$), $h=0.02$ w/mm²C.

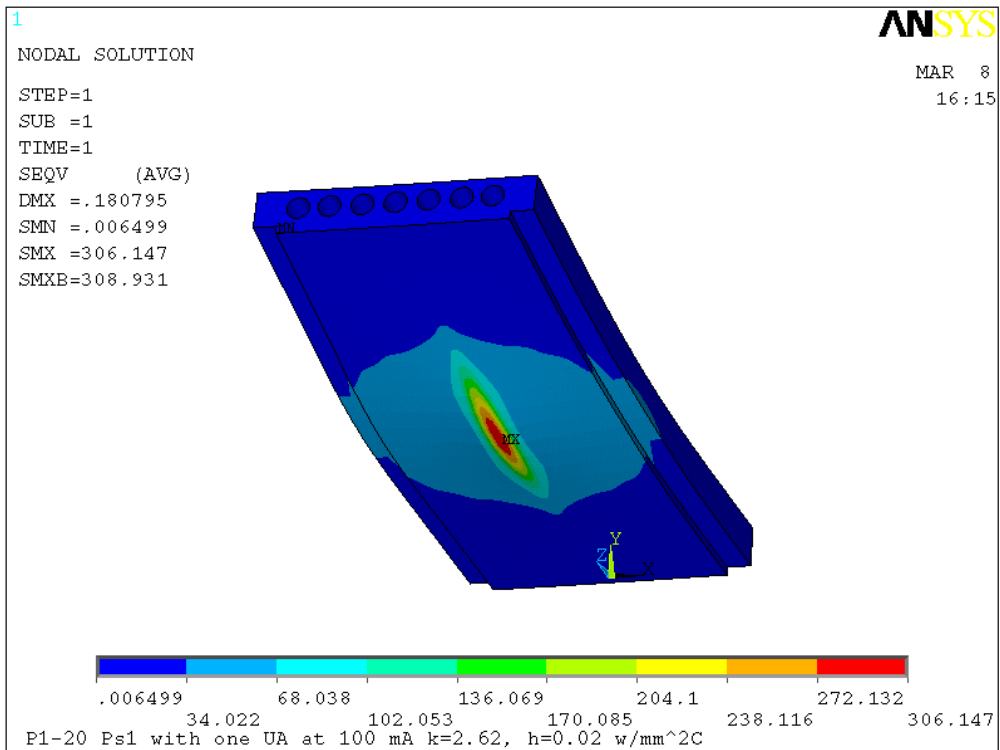


Figure 4.4-7 PS1 von Mises stress plot (MPa), with undulator A $k=2.62$, $h=0.02$ w/mm²C.

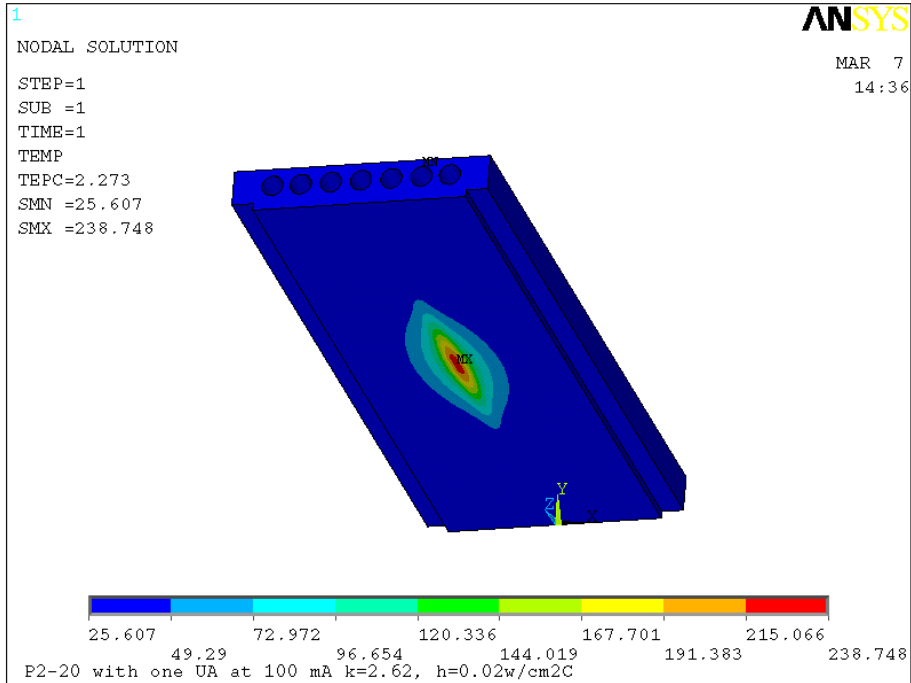


Figure 4.4-8 PS2 temperature plot(°C) with undulator A at 11 mm gap (k=2.62), h=0.02 w/mm²C.

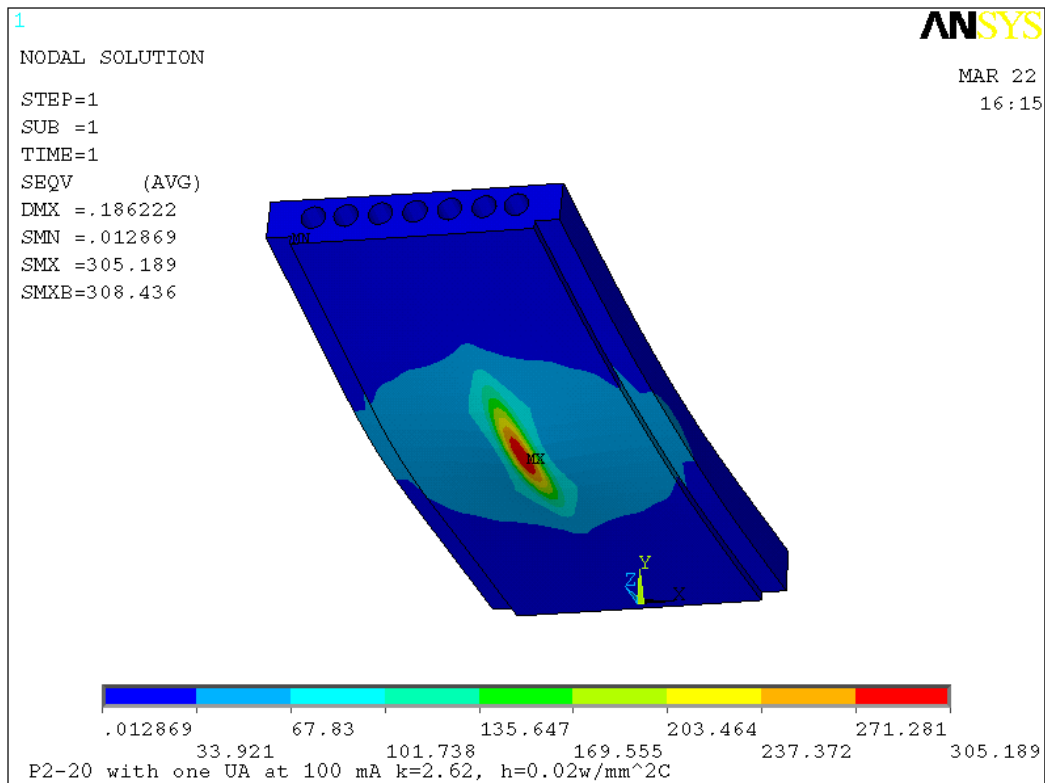


Figure 4.4-9 PS2 von Mises stress plot (MPa), with undulator A k=2.62, h=0.02 w/mm²C.

4.5. Thermal Analysis of the Exit Mask L5-83

4.5.1. L5-83 Model and Mesh

The exit mask of the FEv1.2 front end is L5-83 and is installed just outside the ratchet wall. The exit aperture of L5-83 is 4.5×4.5 mm. Mask L5-83 is manufactured from a solid round billet of GlidCop. There are total of four cooling channels along the beam direction in L5-83. These cooling channels have copper mesh in them to enhance the heat transfer coefficient. The L5-83 was modeled in ProE, and the model was read in by ANSYS for analysis. The aperture area used an 8-node quad mesh (mesh 200 element), and the rest of the model used a tetrahedron mesh. The model and mesh are shown in Figure 4.5-1 and Figure 4.5-2, respectively. Key information for L5-83 is shown in Table 4.5-1.

Table 4.5-1 Key dimensions and reference information for L5-83.

Name	L5-83
Distance to the center of the straight section (m)	25.0
Distance to the center of undulator installed 1.25 m downstream (m)	23.75
Total power (watts)	5327
Peak power density (w/mm ²)	279.4
Inlet aperture H×V (mm×mm)	41 × 24
Outlet aperture H×V (mm×mm)	4.5 × 4.5
Body length (mm)	279
Horizontal taper angle	4.0°
Vertical taper angle	2.0°
Aperture corner radius (mm)	1.5
Top and bottom cooling wall thickness (mm)	9.4
Left and right cooling wall thickness (mm)	9.0
Reference drawing number	4105091505-830001-01

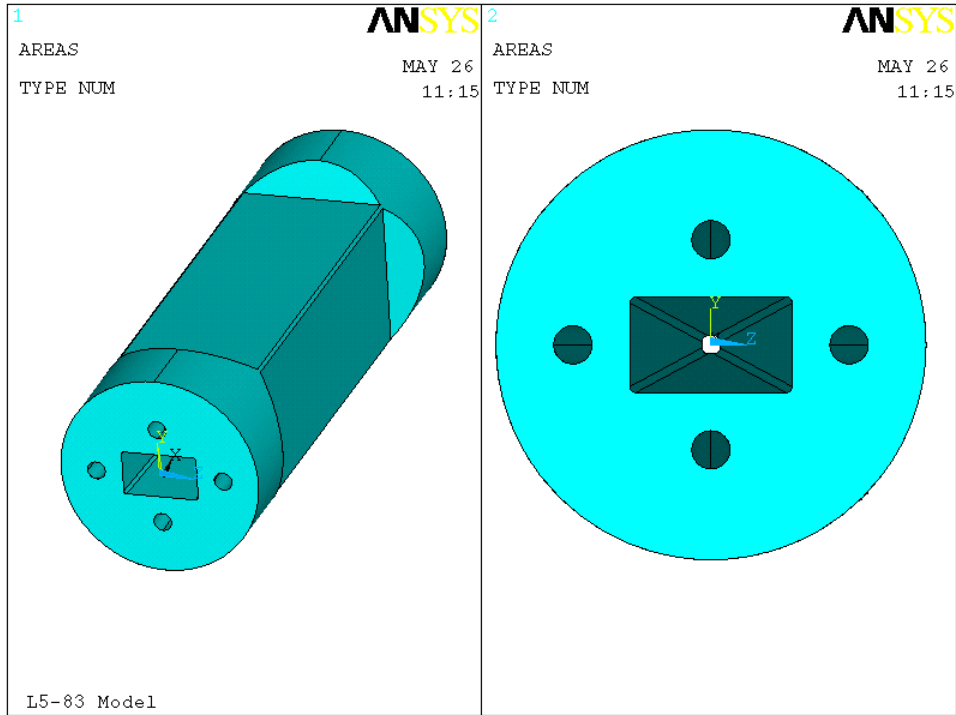


Figure 4.5-1 L5-83 model read in from ProE.

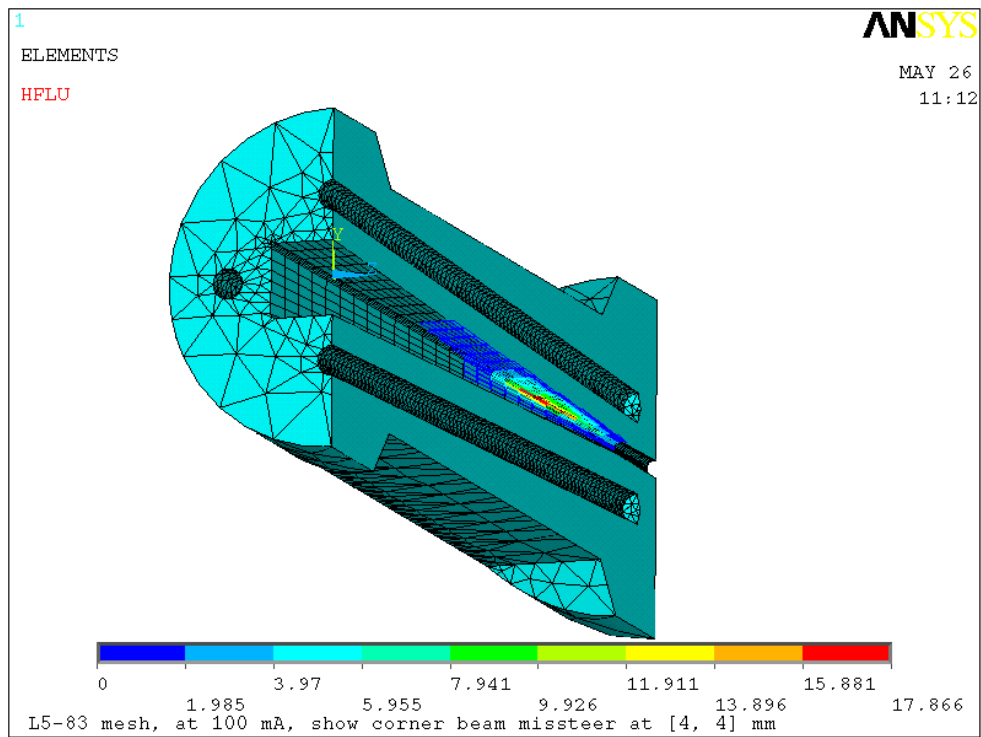


Figure 4.5-2 L5-83 mesh showing the beam with corner missteering.

4.5.2. L5-83 Power Calculation

The power density distribution from one undulator A at 100 mA and 11 mm gap ($k=2.62$) at 23.75 m (distance of L5-83 to the center of the undulator) was calculated. Zero emittance was used. The power density distribution and the curve fitting formula are shown in Figure 4.5-3 and Figure 4.5-4, respectively.

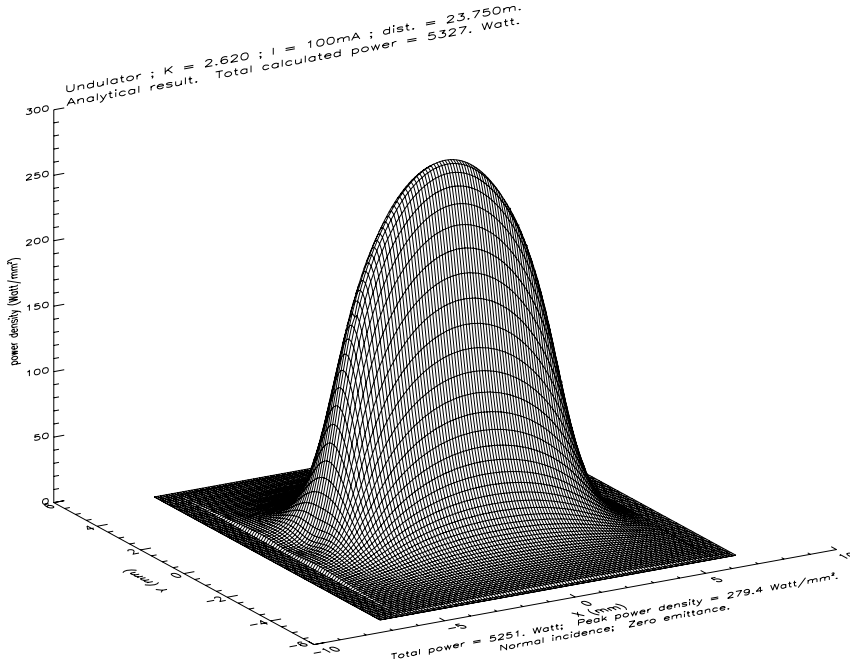


Figure 4.5-3 Undulator A power density distribution at 100 mA, $k=2.62$ at 23.75 m, zero emittance.

$$\text{Fit} = \exp(5.6328 - 0.0087302x^2 - 0.58394y^2 - 0.0031280x^4 + 0.027063y^4 + 0.0024776x^2y^2)$$

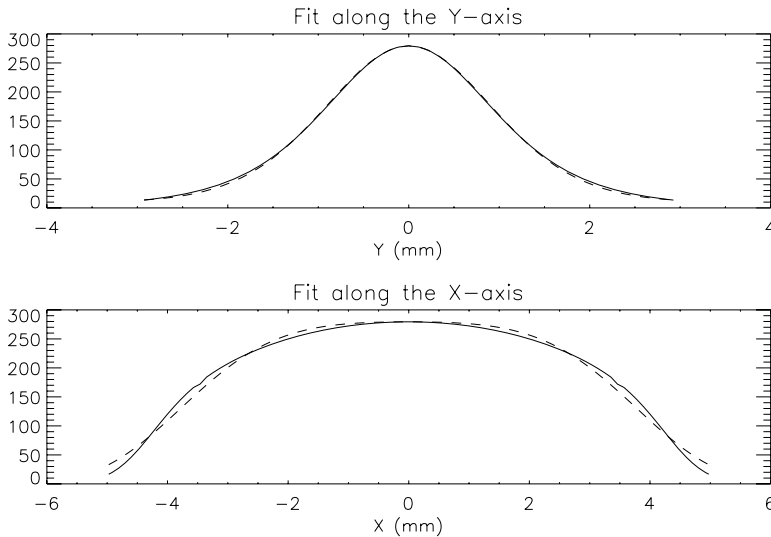


Figure 4.5-4 L5-83 power density distribution Gaussian fitting formula at 23.75 m. The solid line is the calculated data, and the dashed line is the fitted formula.

4.5.3. L5-83 Thermal and Stress Analysis for 100 mA Operation

The cases of beam vertical, horizontal and corner missteering were studied. The L5-83 aperture and beam center locations are shown in Figure 4.5-5.

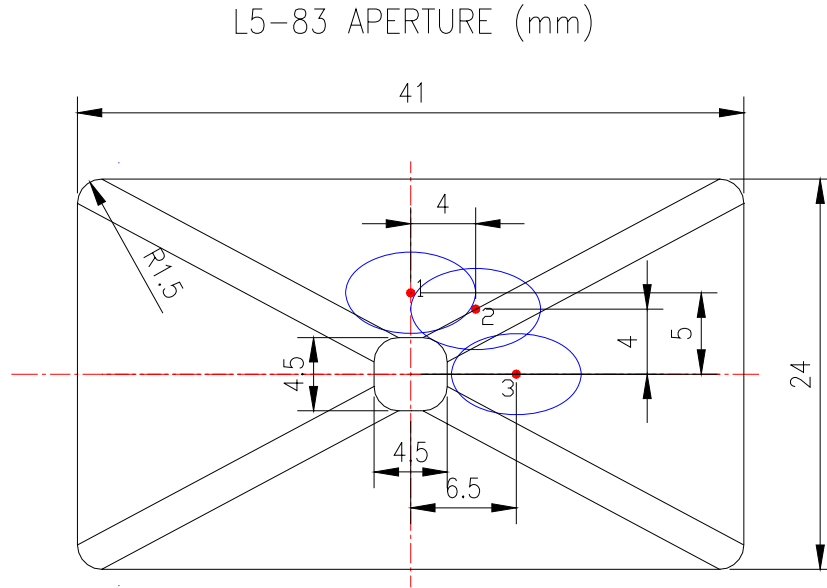


Figure 4.5-5 L5-83 aperture, round dots stand for the beam center, ellipses stand for the beam size of 8x5 mm.

Temperature and stress data for the beam at various locations are tabulated in Table 4.5-2.

Table 4.5-2 Temperature and stress results for L5-83 with beam center at various locations (100 mA, $k=2.62$, $h=0.015$ w/mm²°C, $T_0=25.6$ °C)

Beam center position	Beam center coordinates [x,y] mm	Missteering case	T_{max} (°C)	T_{wall} (°C)	σ_{vm} (MPa)
1	[0, 5]	Vertical	190.6	91.3	309.1
2	[4, 4]	Corner	179.7	85.0	389.4
4	[6.5, 0]	Horizontal	168.3	77.3	253.7

As predicted, the vertical missteering (position 1) results in the highest temperature, and the corner missteering results in the highest stress. The cooling wall temperature is low, which means the cooling channels are positioned far enough from the heating surface, so the temperature will be insensitive to the film coefficient h . Temperature and stress for vertical and corner missteering are plotted in Figure 4.5-6 through Figure 4.5-9.

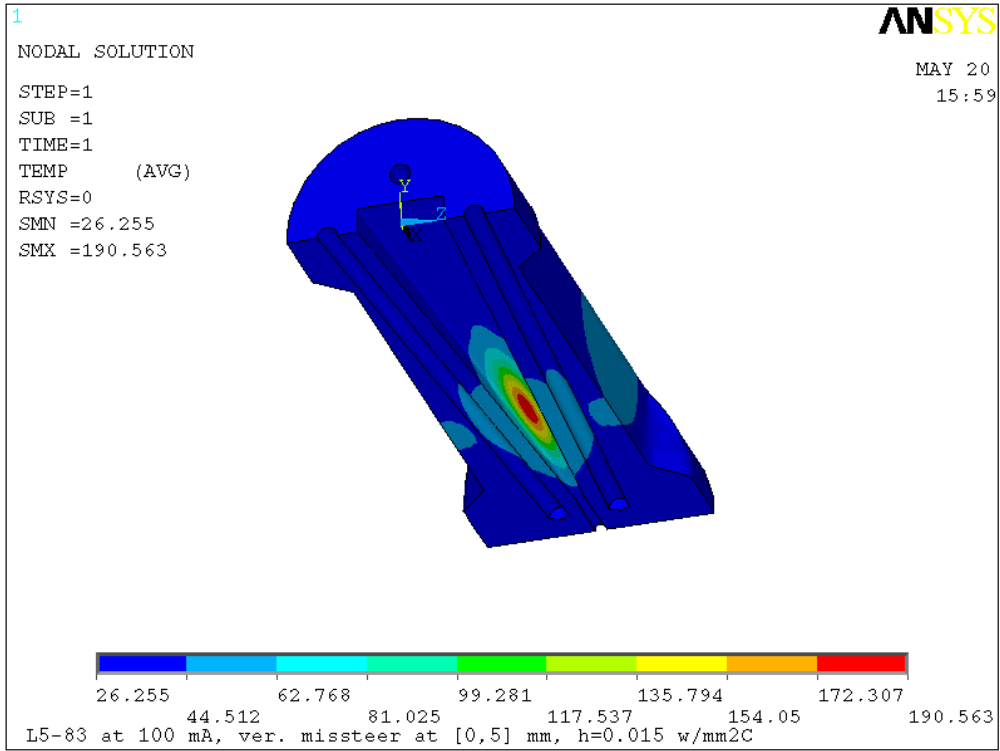


Figure 4.5-6 L5-83 temperature plot (°C), vertical missteering, beam center at [0, 5] mm.

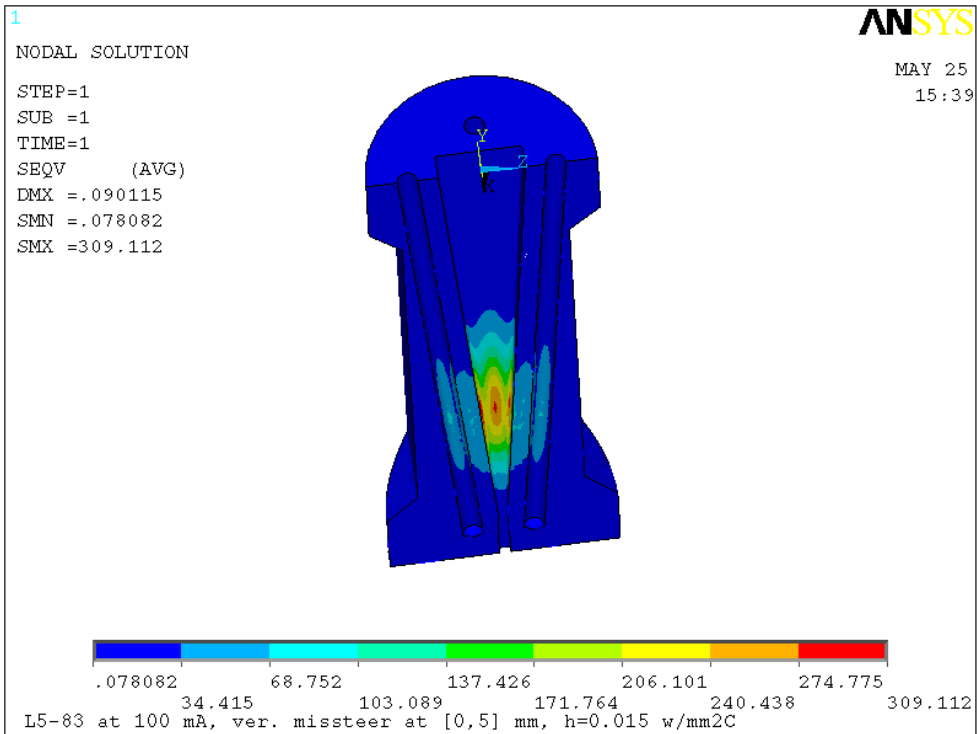


Figure 4.5-7 L5-83 von Mises stress plot (MPa), vertical missteering, beam center at [0, 5] mm.

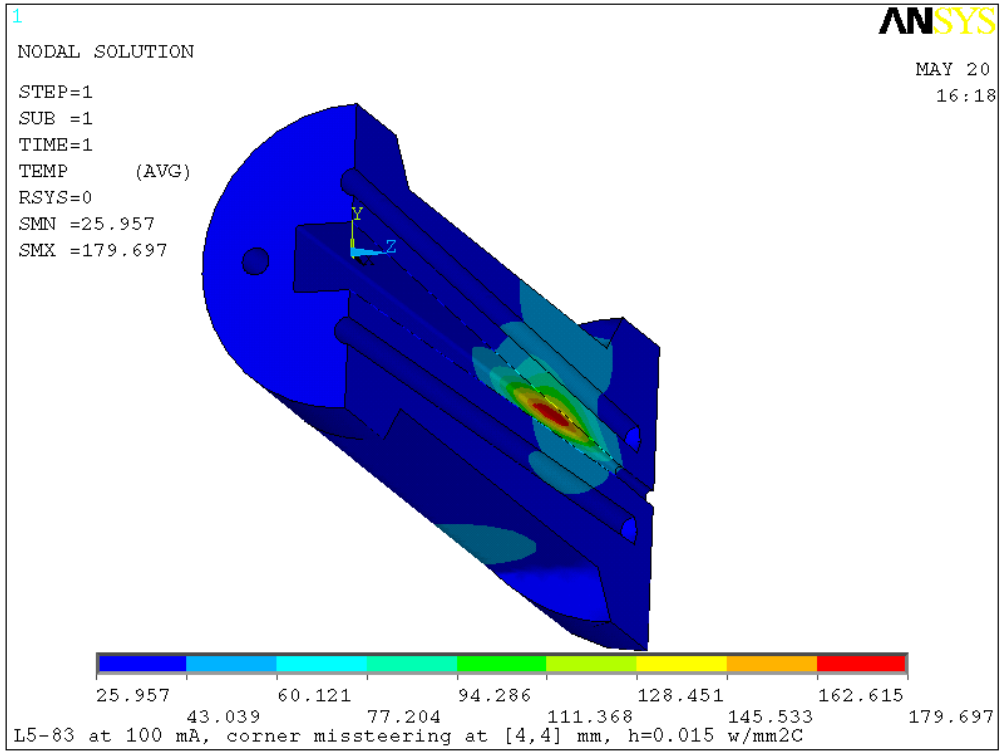


Figure 4.5-8 L5-83 temperature plot (°C), corner missteering, beam center at [4, 4] mm.

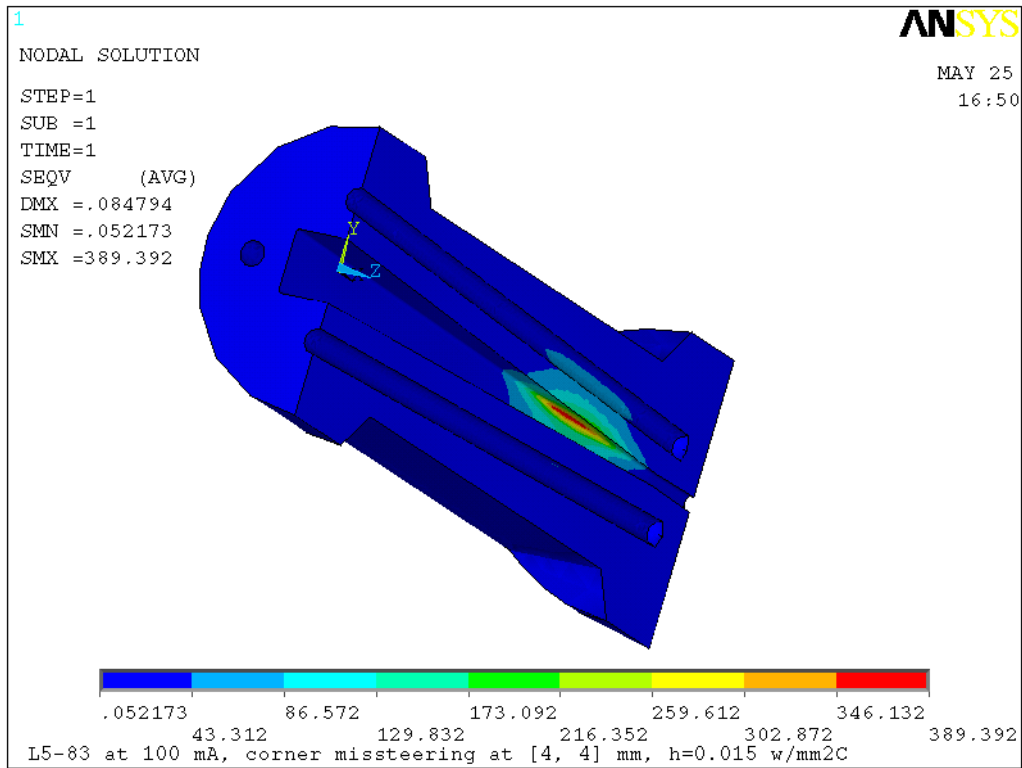


Figure 4.5-9 L5-83 von Mises stress plot (MPa), corner missteering, beam at [4, 4] mm.

4.6. Thermal Analysis of the Exit Mask M4-30

4.6.1. M4-30 Model and Mesh

The M4-30 mask is used in some FEv1.2 front ends and is installed just downstream of exit mask L5-83 to reduce the exit aperture from 4.5×4.5 mm to 3×2 mm; M4-30 is installed in front ends 1-ID, 7-ID and 10-ID. The M4-30 mask is manufactured from a solid round billet of GlidCop. The mask has a total of 14 horizontal cooling channels perpendicular to the beam for the top and bottom surfaces of the aperture. These cooling channels have copper mesh in them to enhance the heat transfer coefficient. The mask has a total of seven vertical cooling channels perpendicular to the beam for the left and right surfaces of the aperture. These cooling channels are clear and without copper mesh. The M4-40 was modeled in ProE, and the model was read in by ANSYS for analysis. Because the cooling holes are perpendicular to the beam direction, it was not possible to use a brick mesh in the model. Instead, a tetrahedron mesh was used. The aperture surface area is meshed with an 8-node quad mesh (mesh 200 element). The volume was meshed with a tetrahedron mesh. The model and mesh are shown in Figure 4.6-1 and Figure 4.6-2, respectively. Key information for the M4-30 mask is shown in Table 4.6-1.

Table 4.6-1 Key dimensions and reference information for M4-30.

Name	M4-30
Distance to the center of the straight section (m)	25.4
Distance to the center of undulator installed 1.25 m downstream (m)	24.15
Total power (watts), note only the power pass through L5-83 aperture will reach M4-30	2887
Peak power density (w/mm ²)	267.7
Inlet aperture H×V (mm×mm)	10.35 × 9.35
Outlet aperture H×V (mm×mm)	3 × 2
Body length (mm)	143
Horizontal taper angle	1.5°
Vertical taper angle	1.5°
Aperture corner radius (mm)	1.0 (half circle)
Top and Bottom cooling hole diameter (mm)	9.53
Left and right cooling hole diameter (mm)	6.35
Top and bottom cooling wall thickness (mm)	7.5 (inlet) ~ 7.4 (outlet)
Left and right cooling wall thickness (mm)	12.9 (inlet) ~ 15.8 (outlet)
Reference drawing number	4105091004-300001-00

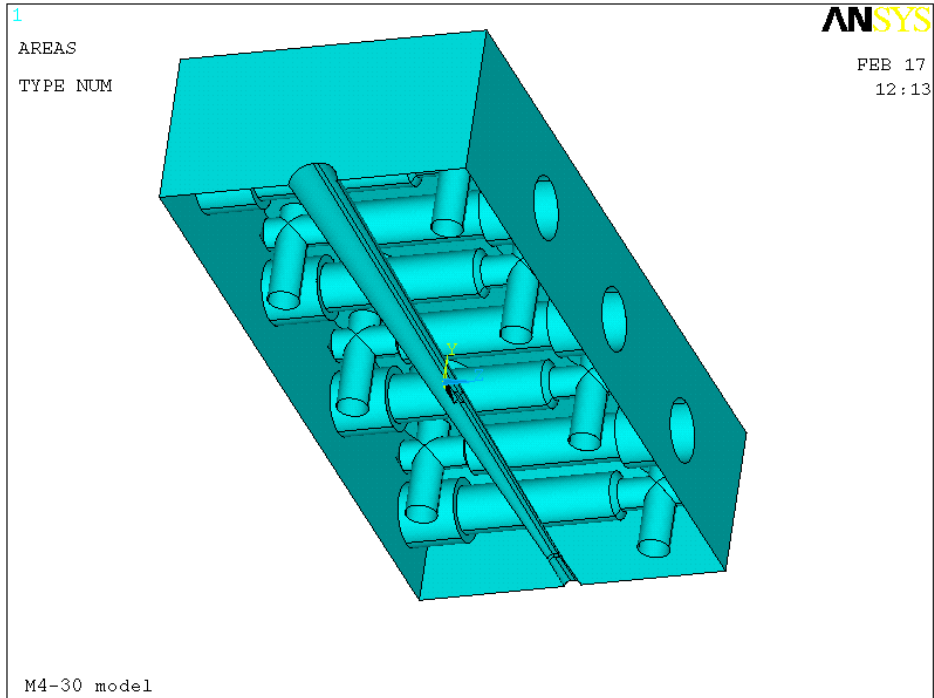


Figure 4.6-1 M4-30 model upper half shows the aperture and cooling channels. The horizontal cooling channels have copper mesh inserts and the vertical cooling channels have no inserts.

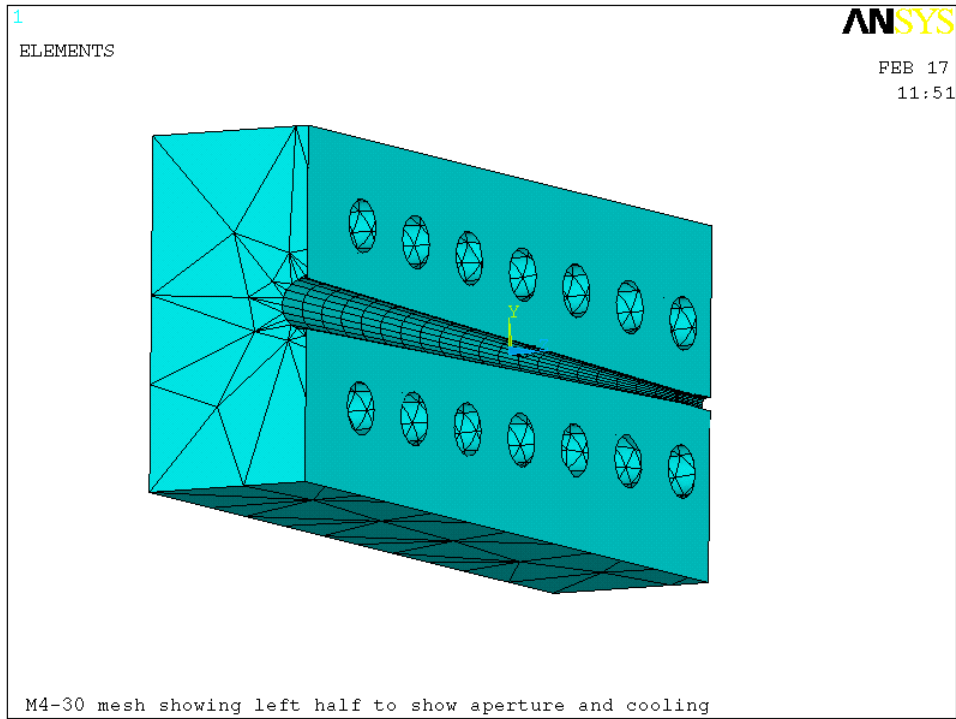


Figure 4.6-2 M4-30 mesh left half shows the aperture and cooling channel.

4.6.2. M4-30 Power Calculation

The power density distribution from one undulator A at 100 mA and 11 mm gap ($k=2.62$) for mask M4-30 at 24.15 m was calculated. Because exit mask L5-83 at 25.0 m is installed upstream of M4-30, its aperture of 4.5×4.5 mm at 25.0 m is taken into account in the power calculation. Only the power passing through the aperture of L5-83 will be seen by M4-30. The power density distribution and the curve fitting formula are shown in Figure 4.6-3 and Figure 4.6-4, respectively.

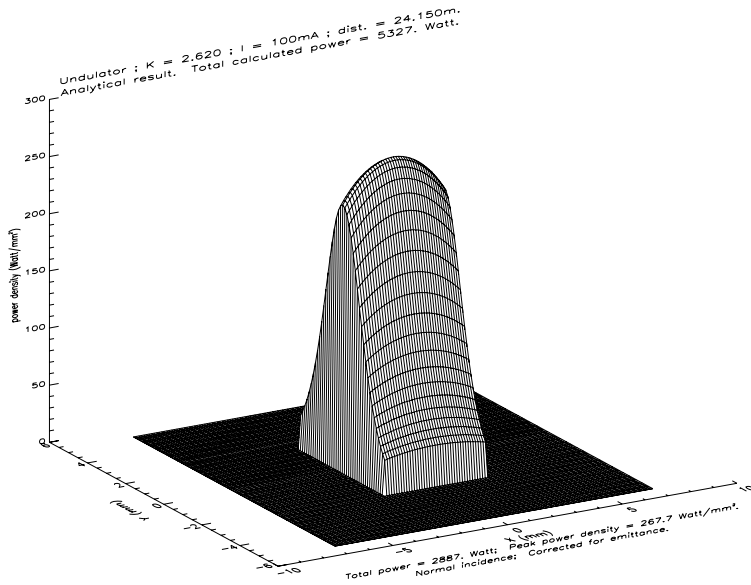


Figure 4.6-3 Undulator A power density distribution at 100 mA, $k=2.62$ at 24.15 m, taking into account the L5-83 aperture upstream.

$$\text{Fit} = \exp(5.5897 - 0.026386x^2 - 0.56682y^2 - 0.00051578x^4 + 0.031534y^4 - 0.00084072x^2y^2)$$

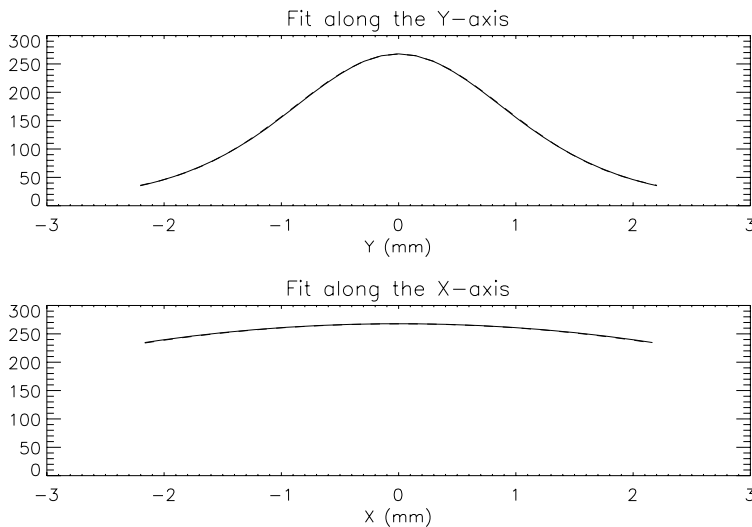


Figure 4.6-4 Power density distribution Gaussian fitting formula for M4-30 at 24.15 m. The solid line is the calculated data, and the dashed line is the fitted formula.

4.6.3. M4-30 Thermal and Stress Analyses for 100 mA Operation

The detail for the M4-30 aperture is shown in Figure 4.6-5. Due to the immediate upstream aperture of 4.5×4.5 mm in mask L5-83, and accounting for the beam divergence, the beam can only move within the 4.6×4.6 mm aperture region of M4-30. This is called the missteering envelope. The beam that passes through the L5-83 mask will not be fully absorbed by M4-30. A portion of the beam will pass through the aperture of M4-30. We will study the cases of beam missteering that represent the maximum amount of power absorbed in M4-30. The M4-30 aperture and beam center locations are shown in Figure 4.6-5.

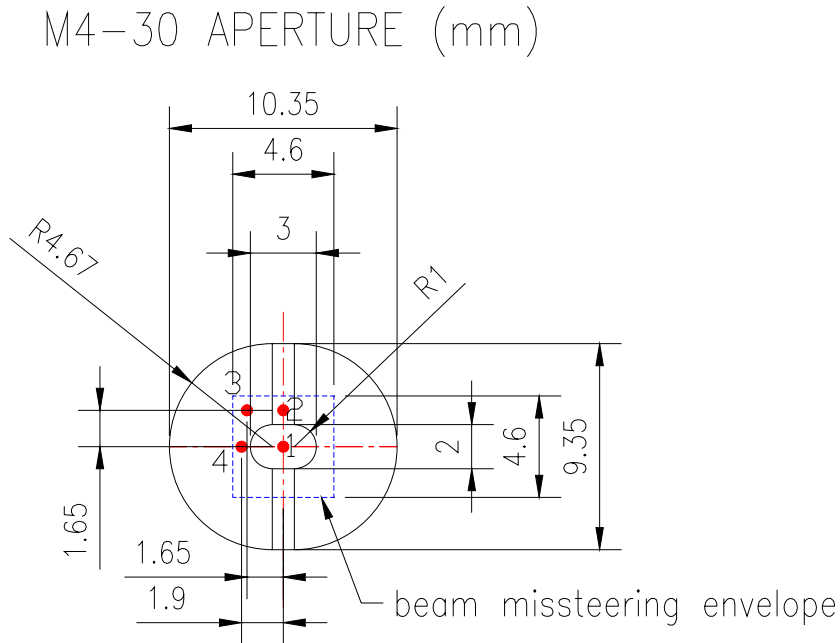


Figure 4.6-5 M4-30 aperture, round dots stand for the beam center, dashed lines stand for the beam missteering envelope.

Temperature and stress data for the beam at various locations are tabulated in Table 4.6-2.

Table 4.6-2 Temperature and stress results for M4-30 with beam center at various locations (100 mA, $k=2.62$, $h=0.015$ w/mm²°C for horizontal cooling channels with mesh and $h=0.01$ w/mm²°C for clear vertical cooling channels, $T_0=25.6$ °C)

Beam center position	Beam center coordinates [x,y] mm	Missteering case	T _{max} (°C)	T _{wall} (°C)	σ _{vm} (MPa)
1	[0, 0]	No missteering	84.9	53.5	n/a*
2	[0, 1.65]	Vertical	103.1	58.3	161.3
3	[1.65, 1.65]	Corner	89.5	51.3	135.1
4	[1.9, 0]	Horizontal	77.2	44.3	n/a*

* Temperature is too low to warrant a stress analysis

As predicted, the vertical missteering (position 2) results in the highest temperature. For this mask, due to the large radius of a half circle corner, the corner does not have high stress. The maximum stress is also at vertical missteering. The cooling wall temperature is low, which means that the cooling channels are positioned far enough from the heating surface, and the calculated values of temperatures and stresses will be insensitive to the film coefficient. Temperature and stress for vertical and corner missteering are plotted in Figure 4.6-6 through Figure 4.6-9.

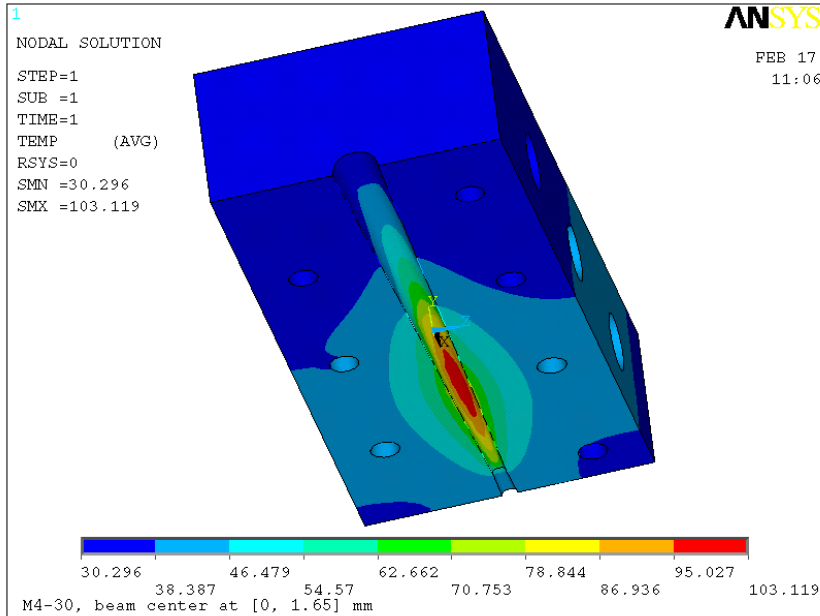


Figure 4.6-6 Temperature plot(°C), vertical missteering, beam center at [0, 1.65] mm.

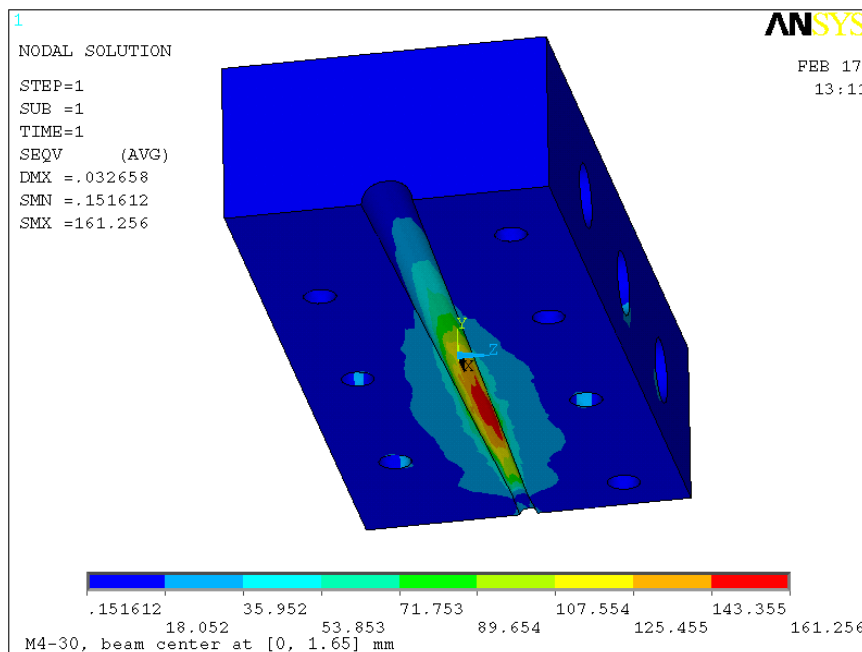


Figure 4.6-7 Von Mises stress plot (MPa), vertical missteering, beam center at [0, 1.65] mm.

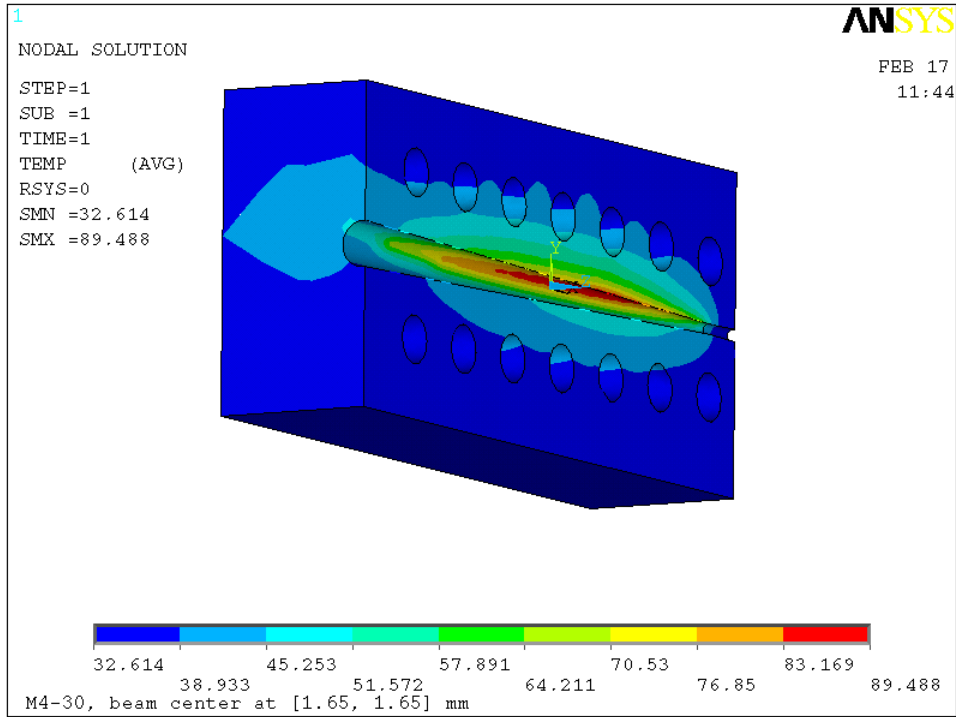


Figure 4.6-8 Temperature plot (°C), corner missteering, beam center at [1.65, 1.65] mm.

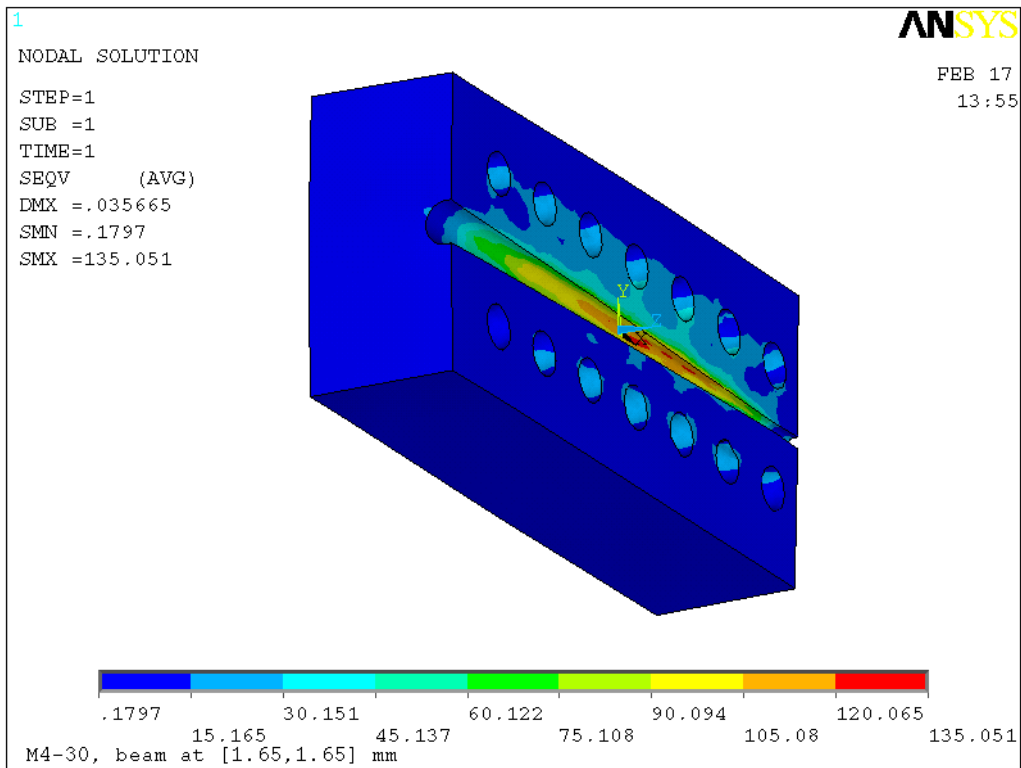


Figure 4.6-9 Von Mises stress plot (MPa), corner missteering, beam center at [1.65, 1.65] mm.

4.7. Summary of the Results for Front End v1.2u

The maximum temperature and stress of all components of FEv1.2u at 100 mA were calculated. The method shown in section 3.2.4 was used to predict the results for higher beam currents, such as 130 mA. By comparing the maximum temperature and stress results to the failure criteria, the maximum allowed beam current for the front end is derived. FEv1.2u results are summarized in Table 4.7-1.

Table 4.7-1 FEv1.2u results (one undulator A at $k=2.62$, $T_0=25.6^\circ\text{C}$).

FEv1.2u Components		M1-30 (FM1)	M2-20 (FM2)	P1-20 (PS1)	P2-20 (PS2)	L5-83 (Exit Mask)	M4-30 (2 nd Exit Mask)
Distance to center of the straight section (m)		17.25	20.6	18.0	21.2	25.0	25.4
Aperture	Inlet (mm)	38×26	66×18	n/a*	n/a	41×24	10.4×9.4
	Outlet (mm)	24×12	54×6	n/a	n/a	4.5×4.5	3×2
Incidence angle	Hori.	1.5°	1.5°	n/a	n/a	4.0°	1.5°
	Ver.	1.5°	1.5°	1.5°	2.0°	2.0°	1.5°
h (w/mm ² °C)		0.02	0.015	0.02	0.02	0.015	0.015
100 mA (vertical missteering on masks)	T _{max} (°C)	247.5	206.6	229.8	238.7	190.6	103.1
	T _{wall} (°C)	83.0	89.8	115.5	122.7	91.3	58.3
	σ _{vm} (MPa)	359.7	306.2	306.1	305.2	309.1	161.3
100 mA (corner missteering on masks)	T _{max} (°C)	216.3	Case does not exist due to large hori. aperture	n/a	n/a	179.7	89.5
	T _{wall} (°C)	73.7				85.0	51.3
	σ _{vm} (MPa)	416.3				389.4	135.1
130 mA (linear extrapolated results)	T _{max} (°C)	314.1	260.9	291.1	302.6	240.1	126.4
	T _{wall} (°C)	100.2	109.1	142.5	151.8	111.0	68.1
	σ _{vm} (MPa)	541.2	398.1	397.9	396.8	506.2	209.7
Max. allowed beam current (mA)		130	130	130	130	130	250

* n/a stands for not applicable.

At 130 mA beam current, PS2 reached the maximum allowed temperature of 300 °C. Both PS1 and PS2 almost reached the maximum allowed von Mises stress limit of

400 MPa. The PS2 cooling wall temperature also nearly reached the water boiling temperature of 153°C at 60 psig. So the maximum allowed beam current is limited to 130 mA just by PS1 and PS2 alone. The first fixed mask and the exit mask also experience high stress at beam corner missteering. Because beam corner missteering is rare, the maximum allowable beam current for the front end should be based on the performance of the photon shutters. So overall the FEv1.2u can operate with one undulator A at 11 mm gap ($k=2.62$) at a maximum beam current of 130 mA. For all masks, the cooling wall temperature is far below the water boiling temperature due to the thick-wall (> 9 mm) design. However, because the first fixed mask and the exit mask experience high stress with beam corner missteering and a normal film coefficient h , further reduction of the h value will result in a higher stress value. So the minimum h value for the first fixed mask and the exit mask should be $0.015 \text{ w/mm}^2\text{°C}$. The minimum h value for the rest of the masks should be maintained at $0.01 \text{ w/mm}^2\text{°C}$. The photon shutters have a thin-wall design (6.35 mm), they are more sensitive to a change in the film coefficient. In order to limit the peak temperature change to 5% from the normal operation, the minimum film coefficient h for the photon shutters should be maintained at $0.015 \text{ w/mm}^2\text{°C}$ (see section 4.4.3). The cooling water flow trip limit should be set according to the above recommendations.

5. Special Case: 3-ID Front End

Beamline 3-ID has the same FEv1.2u front-end components as other beamlines with FEv1.2u. However the source is quite different, it has two in-line 2.7-cm-period undulators. One undulator used to be a 2.4-m-long 88-period device, and another undulator used to be a 2.0-m-long 74-period device. At the May 2005 shutdown, the 2.0-m-long undulator was replaced by a 2.4-m-long undulator. Now both undulators are 2.4 m long. Before the May 2005 shutdown, the maximum k that could be achieved by the undulators was 1.655. At the May 2005 shutdown, 3-ID users requested the initial gap to be set smaller to allow the maximum k to be 1.697 (up from 1.655 previously). Although users will still use k of 1.655 for experiments, this smaller gap setting is to allow users to further close the gap to correct the degraded magnetic field due to radiation damage of the undulators magnets. The increase of the undulator length plus the increased k value will cause the total power emitted by the undulators to increase by 14%. As the masks only see the beam when beam is missteered while the photon shutters are exposed to the full beam at normal operation, it is necessary to take a close look at the photon shutters in 3-ID front end as it is now configured.

5.1. Thermal Analysis of the 3-ID Photon Shutters

To accurately calculate the source power profile, the current source emittance data is used.

$$\sigma_x = 271.2 \text{ } \mu\text{m}$$

$$\sigma_y = 8.6 \text{ } \mu\text{m}$$

$$\sigma_x' = 11.4 \text{ } \mu\text{rad}$$

$$\sigma_y' = 2.9 \text{ } \mu\text{rad}$$

One undulator is installed in the upstream bay and another undulator is installed in the downstream bay, so the center of the undulators will be the center of the straight section. The two U2.7 88-period undulators will be considered as one U2.7 176-period undulator.

$$\text{PS1 location: } 18.0 \text{ m}$$

$$\text{PS2 location: } 21.2 \text{ m}$$

The thermal and stress analyses for PS1 and PS2 at 100 mA with U2.7-N176 at $k=1.655$ and $k=1.697$ were both calculated and compared to the previous condition of one U2.7-N88 plus a U2.7-N74 and also compared to the one undulator A at 130 mA. The results are tabulated in Table 5.1-1.

Table 5.1-1 Thermal and stress results of 3-ID PS1 and PS2 with two 2.4-m-long U2.7 compared to several other operating conditions (h=0.02 w/mm²°C)

Load cases		Previous operating condition	Current operating condition	Current worst possible K	A normal undulator A at 130 mA
Configuration and beam current		U2.7-N74 US plus U2.7-N88 DS, k=1.655, 100 mA	U2.7-N176 K=1.655, 100 mA	U2.7-N176 K=1.697, 100 mA	U3.3-N72 K=2.62, 130 mA
PS1 (1.5° angle)	Total power (w)	5845	6350	6676	6925
	Peak power density (w/mm ²)	820.8	890.4	914.6	730.3
	Max. temperature (°C)	246	271	282	291
	Max. cooling wall temperature (°C)	111	125	130	142
	Max. von Mises stress (MPa)	359	387	404	398
PS2 (2.0° angle)	Total power (w)	5845	6350	6676	6925
	Peak power density (w/mm ²)	591.2	643.4	660.8	514.8
	Max. temperature (°C)	261	289.0	301	303
	Max. wall temperature (°C)	121	135	145	152
	Max. von Mises stress (MPa)	370	399	416	397
Notes	Cooling water temperature used	20° C.	25.6° C to match ASD cooling water supply spec.		
	Emittance data used	Standard: $\sigma_x=352 \mu\text{m}$, $\sigma_y=18 \mu\text{m}$, $\sigma_x'=22 \mu\text{rad}$, $\sigma_y'=4.2 \mu\text{rad}$,	Current: $\sigma_x=271.2 \mu\text{m}$, $\sigma_y=8.6 \mu\text{m}$, $\sigma_x'=11.4 \mu\text{rad}$, $\sigma_y'=2.9 \mu\text{rad}$,		zero
	Date calculated	03/2002	04/2005		03/2005

As a general note, because the calculations were done at different times, different emittance data were used. Total power in a specific aperture and the peak power density depend slightly on the emittance data. The smaller the emittance, the higher the peak power density will be. The standard emittance data was used several years ago and is still the default data on the source calculation programs, such as SRUFF and XOP. Standard emittance data are now outdated. The current emittance data are the low-emittance data, and have been used for the last couple of years. Zero emittance gives the highest peak power density and results in the most conservative calculation.

3-ID Results, Discussion and Conclusion

As we see, PS2 has both the higher temperature and higher stress due to the larger incidence angle to the beam. At $k=1.697$, both the maximum temperature limit of $300\text{ }^{\circ}\text{C}$ and the von Mises stress limit have been reached. So the maximum beam current that 3-ID can run is 100 mA . At a higher current run, gap restrictions should be exercised. The power profile for PS2 is shown in Figure 5.1-1, and the temperature and stress for PS2 are shown in Figure 5.1-2 and Figure 5.1-3, respectively.

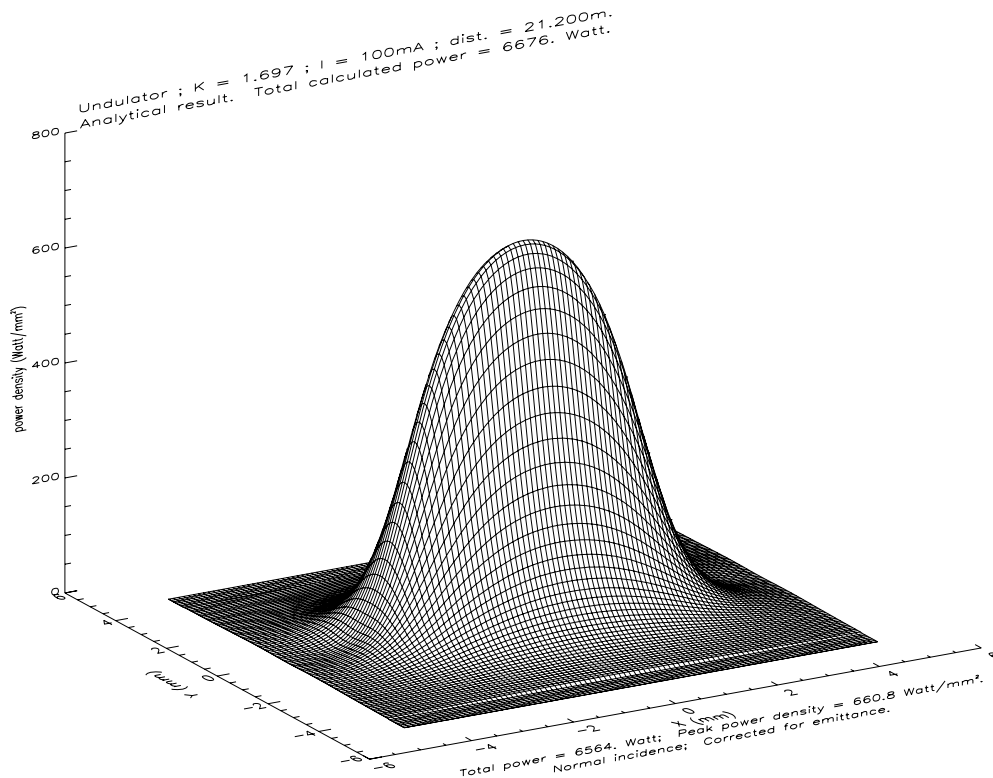


Figure 5.1-1 Power distribution of the U2.7 N=176 undulator at 100 mA $k=1.697$ for the 3-ID PS2.

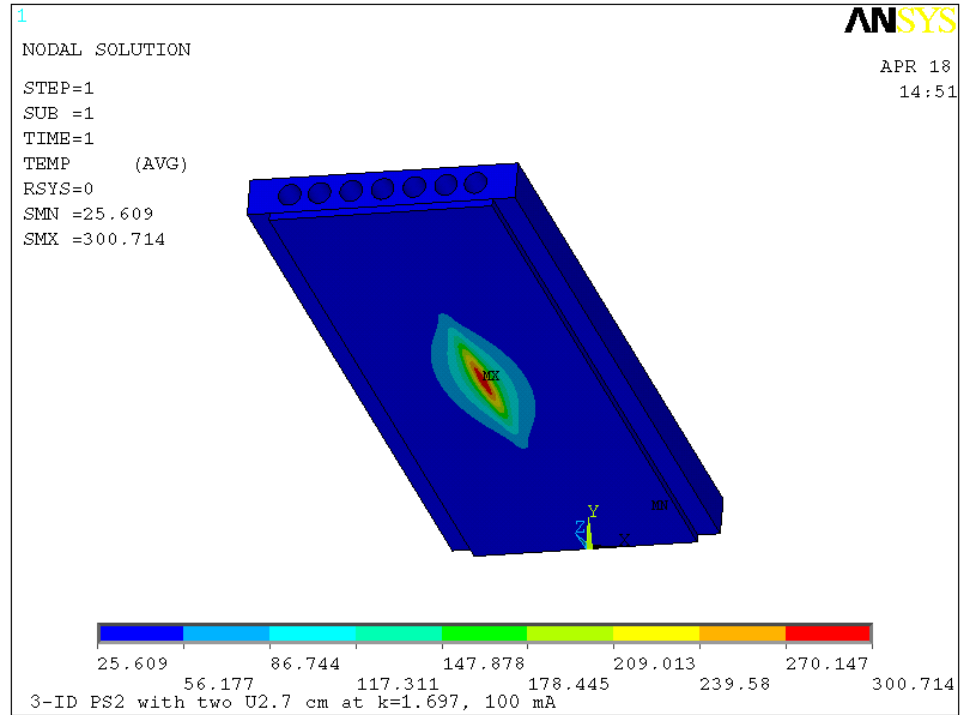


Figure 5.1-2 3-ID PS2 temperature plot (°C) with U2.7 N=176 at 100 mA k=1.697, h=0.02 w/mm²C.

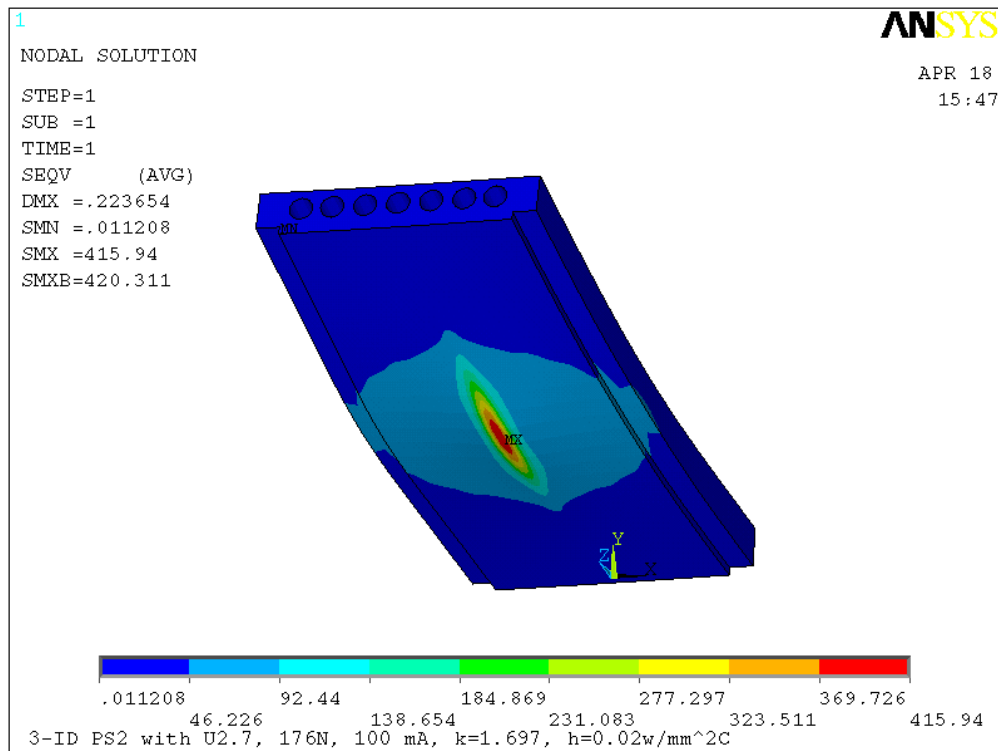


Figure 5.1-3 3-ID PS2 von Mises stress plot (MPa) with U2.7 N=176 at 100 mA, k=1.697.

6. Special Case: 4-ID Front End

6.1. 4-ID General Information

The beamline 4-ID front end has a mixture of FEv1.2 and FEv1.5 components: FEv1.2-type photon shutters (P1-20 and P2-20) and FEv1.5-type fixed masks (M1-40, M2-40 and M2-50). It also has a special exit mask (M7-20) to accommodate the canted beam configuration. There are two insertion devices installed in 4-ID. One is an undulator A with a minimum gap of 9.5 mm installed in the downstream bay of the straight section, and the other is a circular polarized undulator (CPU) installed in the upstream bay of the straight section. The beams from the two undulators have a 0.27 mrad horizontal separation. The parameters of the two devices are listed in Table 6.1-1.

Table 6.1-1 4-ID Undulator A and CPU parameters

100 mA beam current	Undulator A	CPU
Period length	3.3 cm	12.8 cm
Number of periods	72	34
Maximum K (at 9.5 mm gap)	3.175	2.75
Total power	7822 w	714 w
Peak power density	189 kw/mrad ²	19.9 kw/mrad ²

As the photon shutters intercept the full beam routinely and the fixed masks only see the beam when the beam is missteered, the limit of the beamline will be determined by the photon shutters. The exit mask in 4-ID is a unique component. So the photon shutters and the exit mask will be analyzed under these sources.

6.2. Thermal Analysis of the 4-ID P1-20 and P2-20

Key information for the PS1 (P1-20) and PS2 (P2-20) for 4-ID front end, as well as the power data, are shown in Table 6.2-1.

Table 6.2-1 Parameter of PS1 and PS2 relevant to thermal analysis

100 mA beam current	PS1	PS2
Distance to the center of straight section (m)	18.5	21.9
Distance to the undulator A (m)	17.25	20.65
Distance to the CPU	19.75	23.15
Distance of two beam horizontal separation (mm)	5.0	5.9
Beam incident angle	1.5°	2.0°
Peak power density at normal incidence with UA only at 9.5 mm gap (w/mm ²)	634.6	443.4
Peak incidental power density (UA) only at 9.5 mm gap, k=3.175 (w/mm ²)	16.6	15.5
Film coefficient h (w/cm ² °C)	2.0	2.0
Bulk water temperature (°C)	20	20
Emittance data used: standard	$\sigma_x=352 \mu\text{m}$, $\sigma_y=18 \mu\text{m}$, $\sigma_x'=22 \mu\text{rad}$, $\sigma_y'=4.2 \mu\text{rad}$,	

Several cases are analyzed and the temperature and stress results are tabulated in Table 6.2-2.

Table 6.2-2 Maximum temperature and von Mises stress of PS1 and PS2 in several cases.

Load Case #	Temperature and stress results	PS1 (P1-20)	PS2 (P2-20)
Case #1 100 mA, CPU off UA only at 9.5 mm gap (k=3.175) $P_{total_UA} = 7822$ w $P_{peak_UA} = 189$ kw/mrad ²	T_{max} (°C)	285	296
	T_{wall} (°C)	138	149
	Max. von Mises stress (MPa)	N/A*	N/A*
Case #2 100 mA UA at 9.5 mm gap (k=3.175) plus CPU at k=2.75, $P_{total_UA} = 7822$ w $P_{peak_UA} = 189$ kw/mrad ² $P_{total_CPU} = 714.4$ w $P_{peak_CPU} = 19.9$ kw/mrad ²	T_{max} (°C)	297	308
	T_{wall} (°C)	147	158
	Max. von Mises stress (MPa)	410	403
Case #3 100 mA UA at k=3.07 (sulphur edge) with CPU at k=2.75 $P_{total_UA} = 7314$ w $P_{peak} = 183$ kw/mrad ² (UA)	T_{max} (°C)	284	293
	T_{wall} (°C)	141	150
	Max. von Mises stress (MPa)	N/A*	N/A*
Case #4 130 mA UA at k=2.62 (Pd L-edge) with CPU at k=2.75 $P_{total_UA} = 6925$ w $P_{peak_UA} = 201$ kw/mrad ² (UA)	T_{max} (°C)	284	294
	T_{wall} (°C)	137	147
	Max. von Mises stress (MPa)	395	393

*N/A means the stress data is not calculated since the stress data for UA at k=3.175 with the CPU is calculated.

The power distribution for undulator A at k=3.175 at the PS2 location is shown in Figure 6.2-1, and the power distribution for the CPU at the PS2 location is shown in Figure 6.2-2. The maximum temperature and von Mises stress for PS2 with undulator A at k=3.175 and the CPU are shown in Figure 6.2-3 and Figure 6.2-4, respectively.

Results, Discussion and Conclusion

- 1) With undulator A at the minimum gap of 9.5 mm (k=3.175) and the CPU at k=2.75, the maximum current allowed for 4-ID is 100 mA.
- 2) For the 11 mm gap (Pd L-edge, E1=3.173, k=2.624), 4-ID is allowed to run with the CPU at k=2.75 at 130 mA.

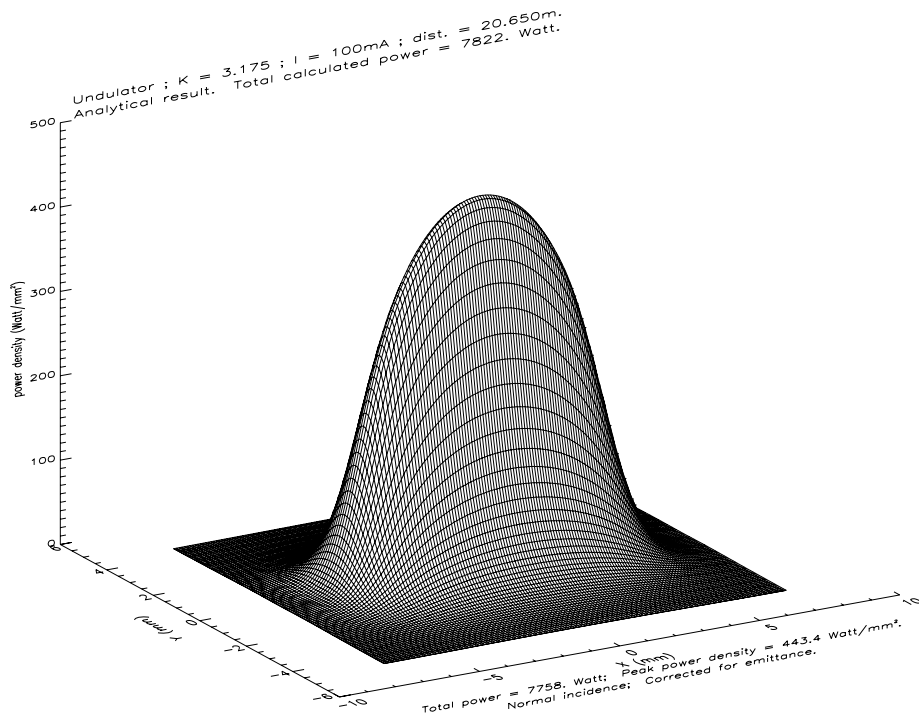


Figure 6.2-1 Undulator A power distribution at $k=3.175$ at PS2 location for 4-ID front end, standard emittance.

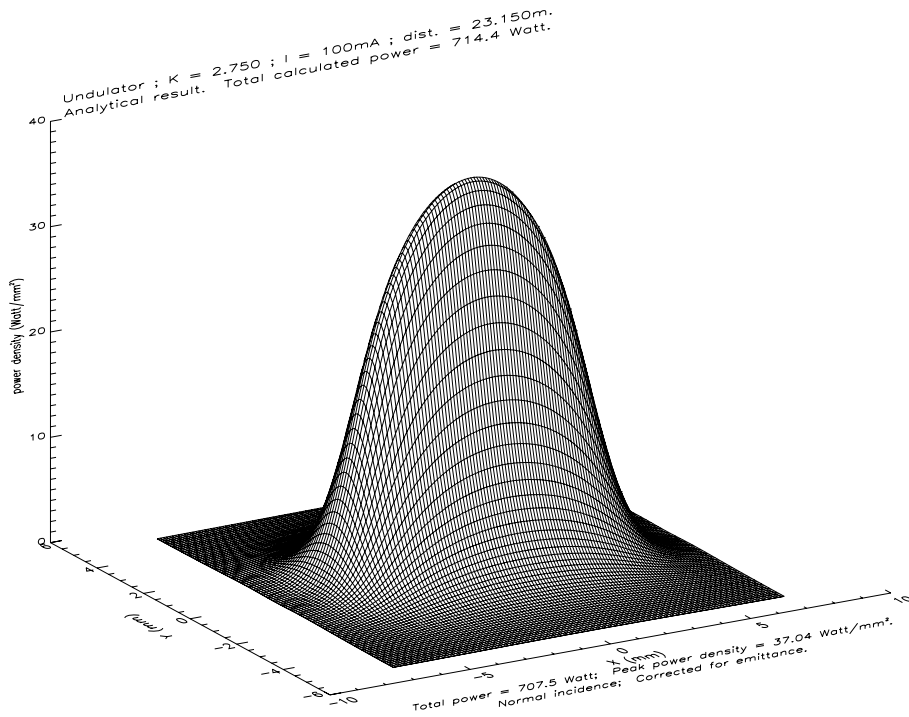
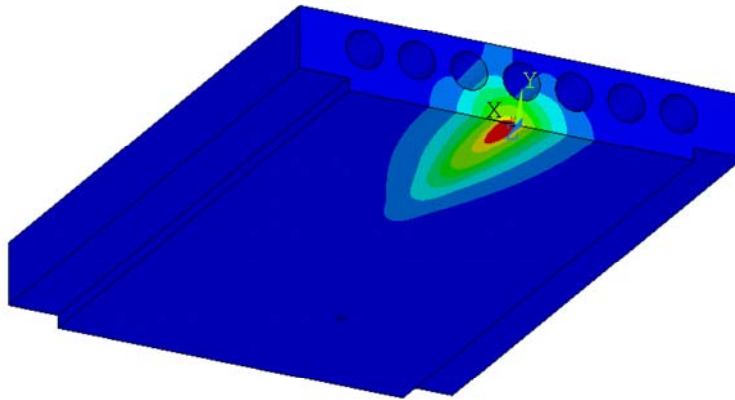


Figure 6.2-2 CPU power distribution at $k=2.75$ at PS2 location for 4-ID front end, standard emittance.

1



```

ANSYS 6.1
SEP 16 2002
16:16:46
PLOT NO. 1
NODAL SOLUTION
STEP=1
SUB =1
TIME=1
TEMP
TEPC=4.202
SMN =20.009
SMX =307.574

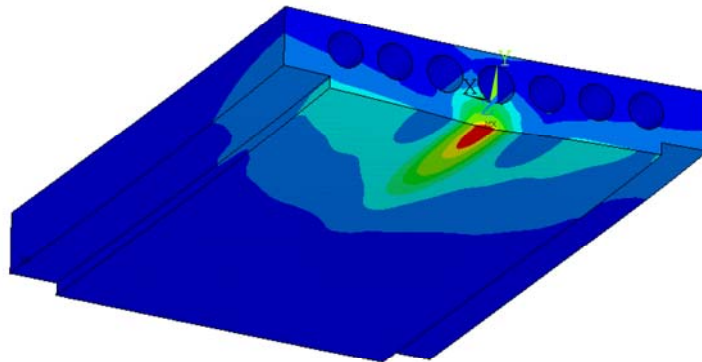
```

Blue	20.009
Light Blue	51.961
Cyan	83.913
Green	115.864
Light Green	147.816
Yellow-Green	179.767
Yellow	211.719
Orange	243.671
Red-Orange	275.622
Red	307.574

4-ID PS2 UA33 at 9.5 mm gap with CPU at k=2.75 at 100 mA

Figure 6.2-3 4-ID PS2 temperature plot (°C) with UA at k=3.175 plus CPU at k=2.75 at 100 mA.

1



```

ANSYS 6.1
SEP 18 2002
15:11:03
PLOT NO. 1
NODAL SOLUTION
STEP=1
SUB =1
TIME=1
SEQV (AVG)
DMX =.292866
SMN =.018006
SMX =402.95
SMXB=407.001

```

Blue	.018006
Light Blue	44.788
Cyan	89.559
Green	134.329
Light Green	179.099
Yellow-Green	223.869
Yellow	268.64
Orange	313.41
Red-Orange	358.18
Red	402.95

4-ID PS2 UA33 at 9.5 mm gap with CPU at k=2.75 at 100 mA

Figure 6.2-4 4-ID PS2 von Mises stress (MPa) with UA at k=3.175 plus CPU at k=2.75 at 100 mA.

6.3. Thermal Analysis of the 4-ID Exit Mask M7-20

6.3.1. M7-20 Model and Mesh

The M7-20 mask is the exit mask of 4-ID front end and is installed just outside the ratchet wall. The exit aperture of the L7-20 is 11.4×4.5 mm. The wider horizontal aperture is to accommodate the two canted beams. The M7-20 is manufactured from a solid round billet of GlidCop. There are total of six cooling channels along the beam direction in M7-20. These cooling channels have copper mesh in them to enhance the heat transfer coefficient. The M7-20 was modeled in ProE, and the model was read in by ANSYS for analysis. The model for the aperture area used an 8-node quad mesh (mesh 200 element), and the rest of the model used a tetrahedron mesh. The model and mesh are shown in Figure 6.3-1 and Figure 6.3-2, respectively. Key information for M7-20 is shown in Table 6.3-1.

Table 6.3-1 Key dimensions and reference information for M7-20.

Name	M7-20
Distance to the center of the straight section (m)	25.0
Distance to the center of undulator installed 1.25 m downstream (m)	23.75
Total power at 100 mA (watts)	7822 (UA) +714 (CPU)
Peak power density at 100 mA (w/mm ²)	339.9 (UA) 29.3 (CPU)
Inlet aperture H×V (mm×mm)	24.2 × 13.2
Outlet aperture H×V (mm×mm)	11.4 × 4.5
Body length (mm)	133
Horizontal taper angle	2.78°
Vertical taper angle	1.88°
Aperture corner radius (mm)	1.5
Top and bottom cooling wall thickness (mm)	9.5
Left and right cooling wall thickness (mm)	10.0
Reference drawing number	M7-200001-02-2

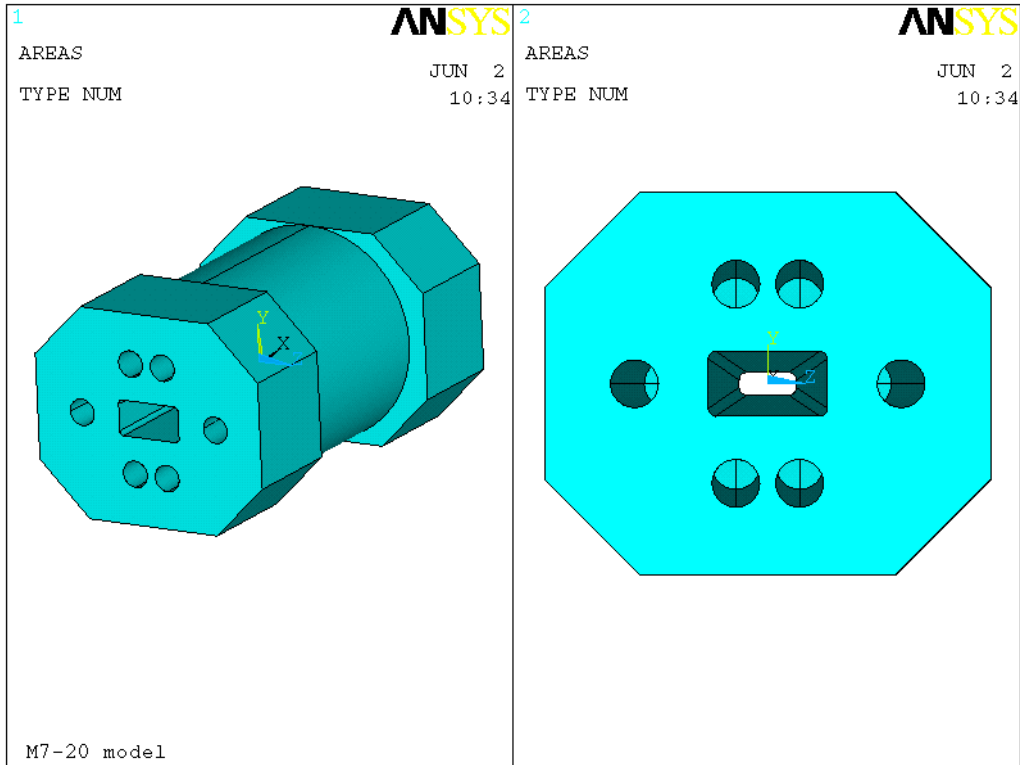


Figure 6.3-1 M7-20 model read in from ProE.

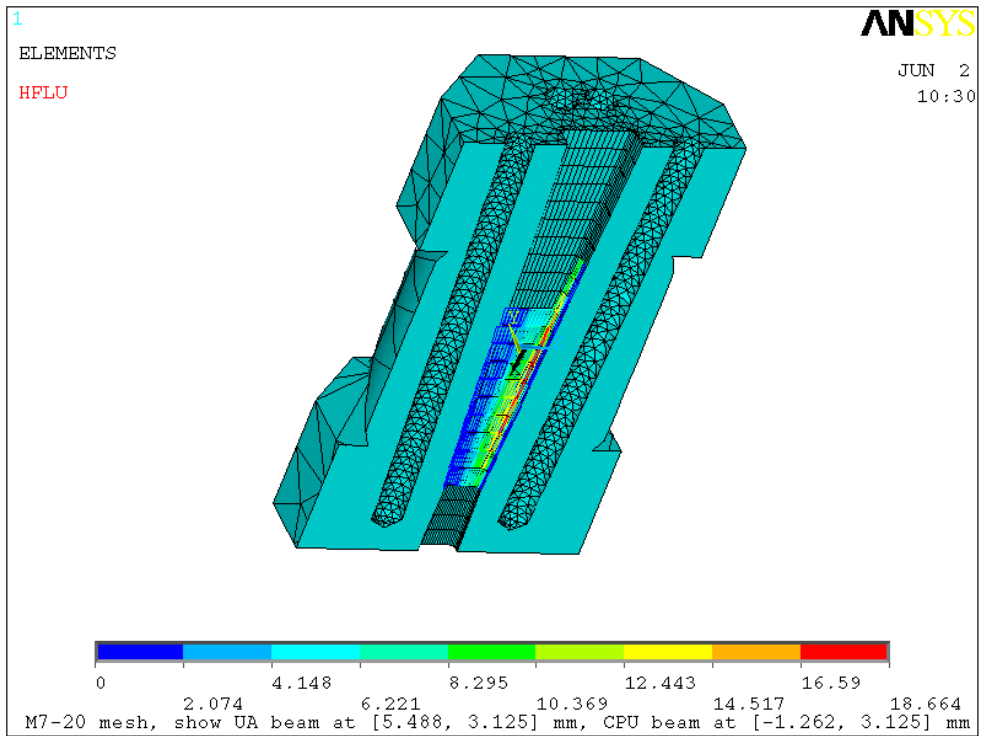


Figure 6.3-2 M7-20 mesh showing the undulator A beam with corner missteering and the CPU beam.

6.3.2. M7-20 Power Calculation

The power density distribution of the undulator A at 100 mA and 9.5 mm gap ($k=3.175$) at 23.75 m (downstream bay of the straight section) and the CPU ($k=2.75$) at 26.25 m (upstream bay of the straight section) were calculated. Zero emittance was used. The power density distribution and the curve fitting for undulator A are shown in Figure 6.3-3 and Figure 6.3-4, respectively. The power density and curve fitting for the CPU are shown in Figure 6.3-5 and Figure 6.3-6, respectively.

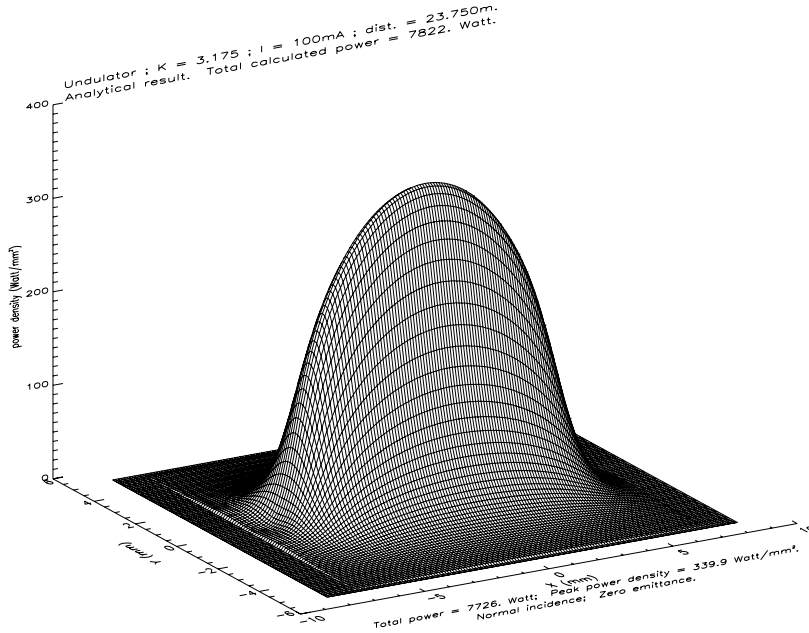


Figure 6.3-3 Undulator A power distribution at 100 mA, $k=3.175$, $N=72$ at 23.75 m, zero emittance.

$$\text{Fit} = \exp(5.8285 - 0.0030279x^2 - 0.58177y^2 - 0.0015909x^4 + 0.027372y^4 + 0.0013742x^2y^2)$$

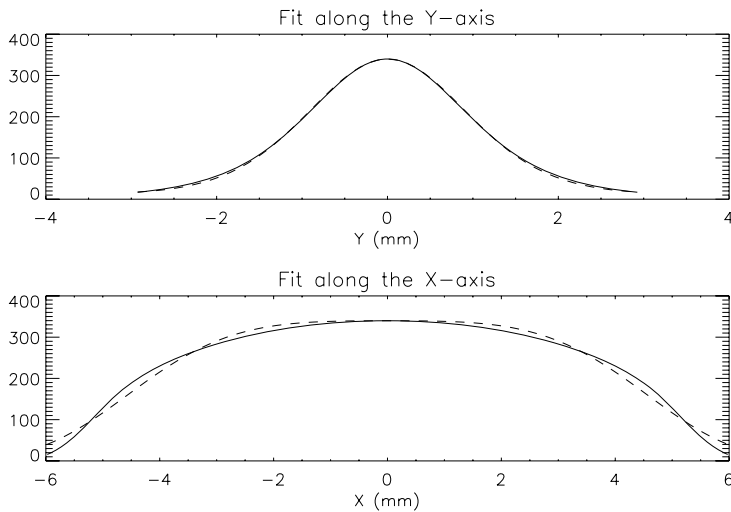


Figure 6.3-4 Undulator A power density Gaussian fitting formula for M7-20 at 23.75 m. The solid line is the calculated power, and the dashed line is the fitted formula.

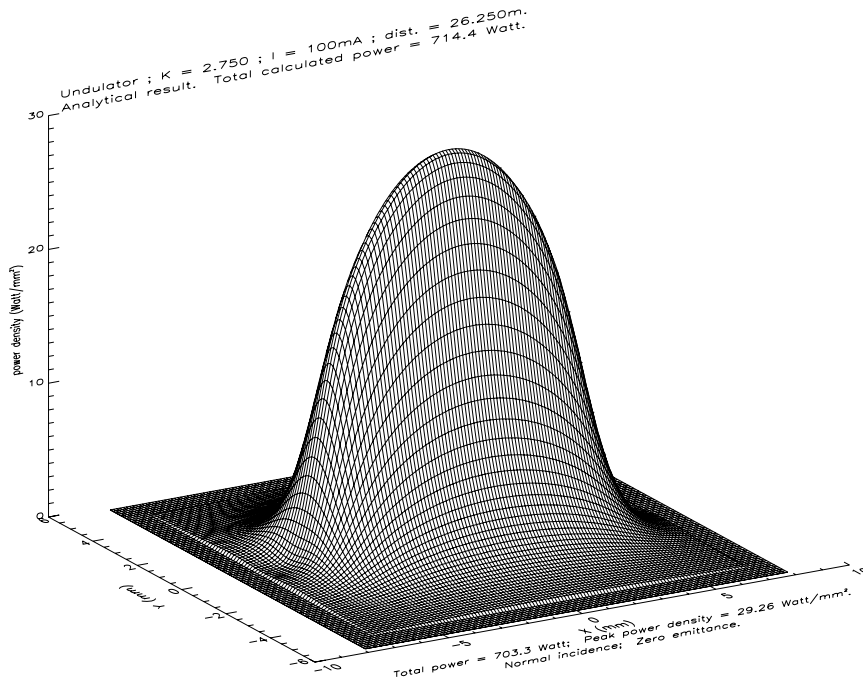


Figure 6.3-5 M7-20 CPU power distribution at 100 mA, k=2.75, N=34 at 26.25 m, zero emittance.

$$\text{Fit} = \exp(3.3762 - 0.0069089x^2 - 0.48493y^2 - 0.0016392x^4 + 0.020368y^4 + 0.00093213x^2y^2)$$

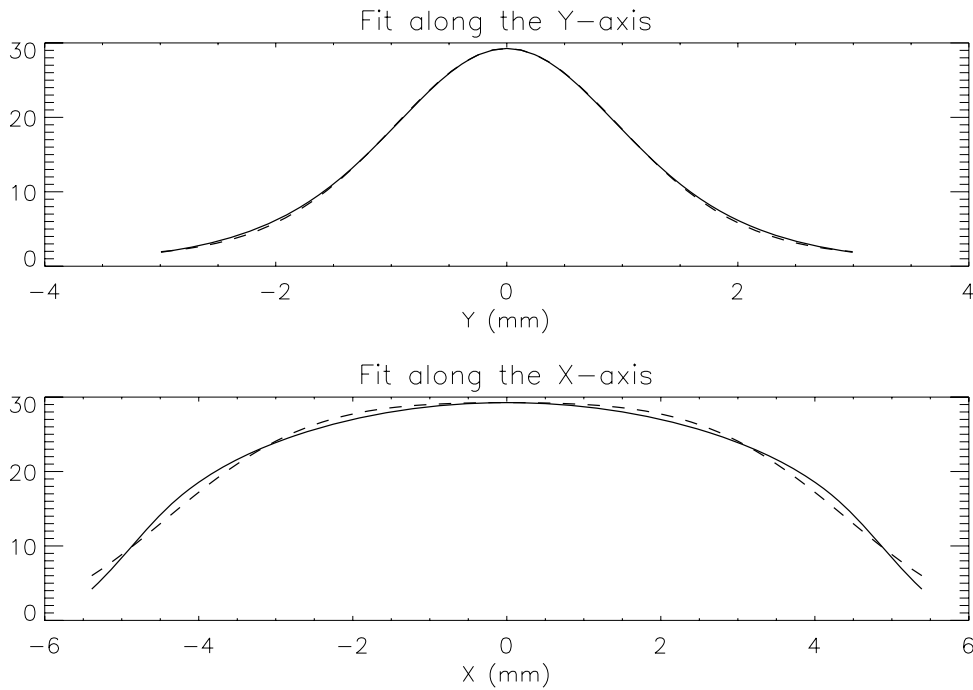


Figure 6.3-6 M7-20 CPU power density distribution Gaussian fitting formula at 26.25 m. The solid line is the calculated power, and the dashed line is the fitted formula.

6.3.3. M7-20 Thermal and Stress Analysis for 100 mA Operation

The detail for the M7-20 aperture is shown in Figure 6.3-7. Because the upstream mask M2-50 at 21.1 m has an aperture of 12.7×5.2 mm, the beam missteering will be restricted within an 18×8 mm region on M7-20 located at 25 m. This is called the missteering envelope. The beam that passes through the M2-50 mask will not be fully absorbed by M7-20. A portion of the beam will pass through the aperture of M7-20. We will study the cases of beam missteering that cause the maximum amount of power to be absorbed in M7-20. Temperature and stress data for the beam at various locations are tabulated in Table 6.3-2.

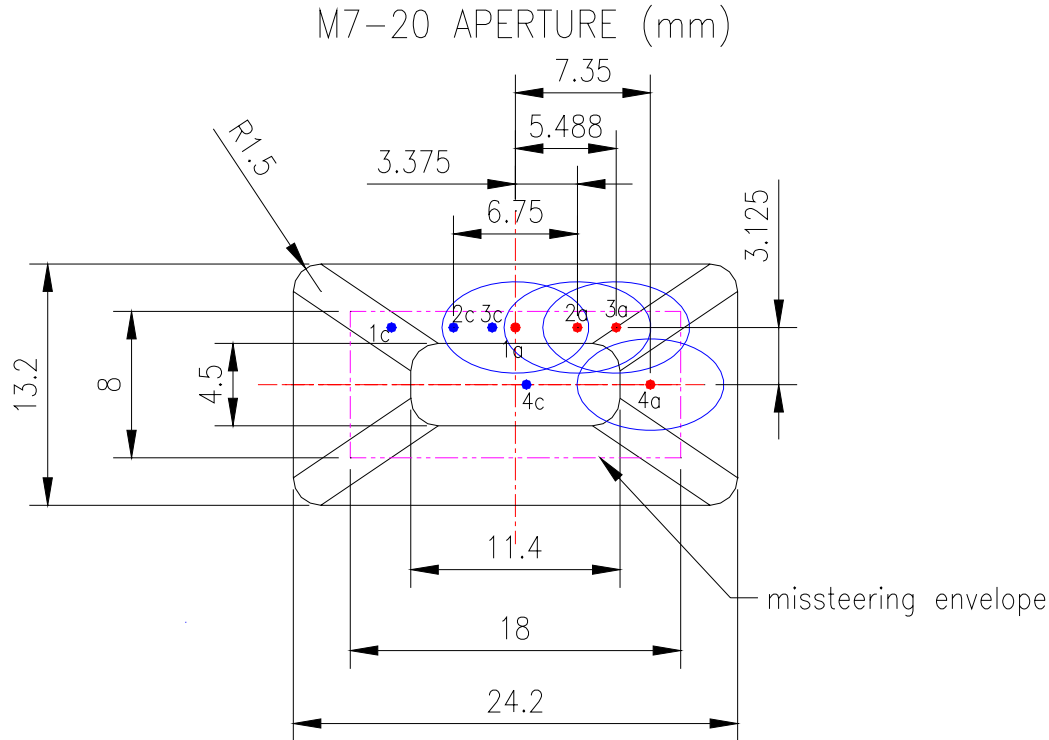


Figure 6.3-7 M7-20 aperture, round dots stand for the beam center, ellipses stand for the beam size of 8×5 mm, 1a stands for undulator A at position 1, 1c stands for the CPU at position 1. The horizontal separation between the UA and the CPU is 6.75 mm.

Table 6.3-2 Temperature and stress results for M7-20 with the beam center at various locations (100 mA, UA k=3.175, CPU k=2.75, h=0.015 w/mm²°C, T₀=25.6°C).

UA beam center position	UA beam center coordinates [x,y] mm	Missteering case	T _{max} (°C)	T _{wall} (°C)	σ _{vm} (MPa)
1a	[0, 3.125]	Vertical	247.0	103.5	472.9
2a	[3.375, 3.125]	Near corner	245.2	110.7	516.9
3a	[5.488, 3.125]	Corner	221.3	102.3	484.8
4a	[7.35, 0]	Horizontal	153.2	62.3	233.4

As predicted, the vertical missteering (position 1) results in the highest temperature, and the near-corner missteering (position 2) results in the highest stress. The

temperature decrease from position 1 to position 2 is not obvious because more power is absorbed in the mask at position 2 compared to at position 1. The beam profile outside the missteering envelope is not absorbed into the mask. The cooling channels are positioned far enough from the heating surface, so that the cooling wall temperature is low and insensitive to the film coefficient. Temperature and stress for near-corner missteering are plotted in Figure 6.3-8 and Figure 6.3-9, respectively.

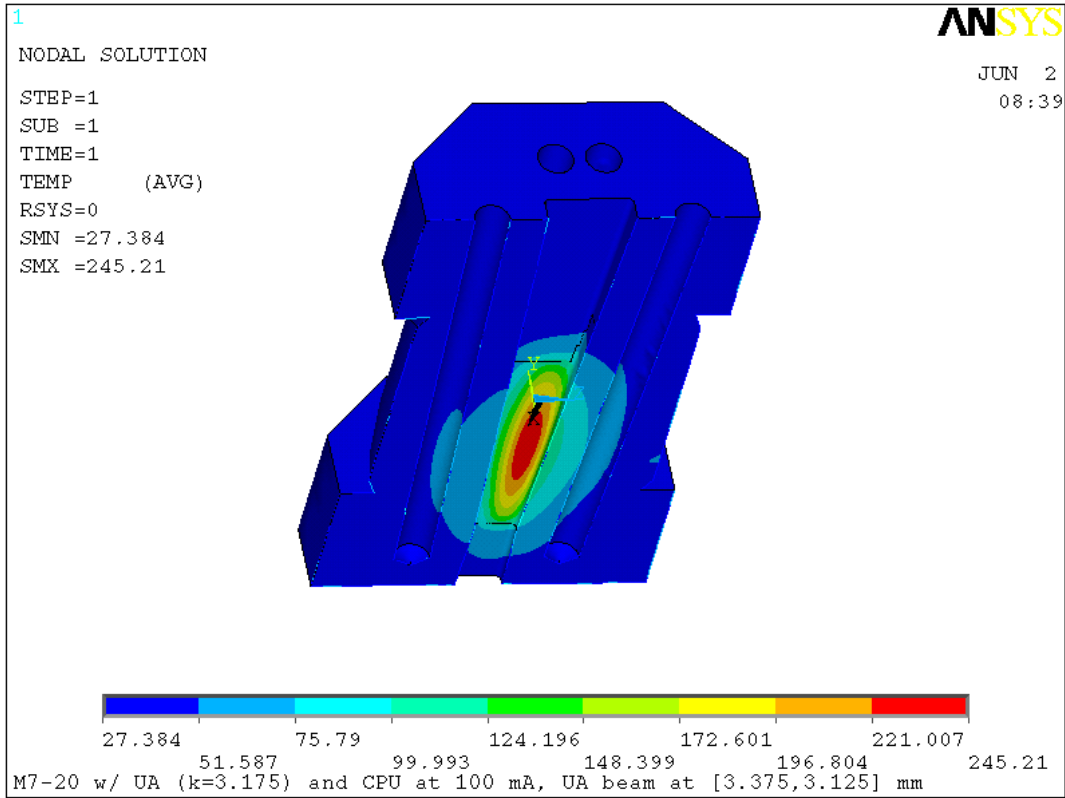


Figure 6.3-8 M7-20 temperature plot (°C), with undulator A and the CPU. UA beam near-corner missteering, UA beam center at [3.375, 3.125] mm.

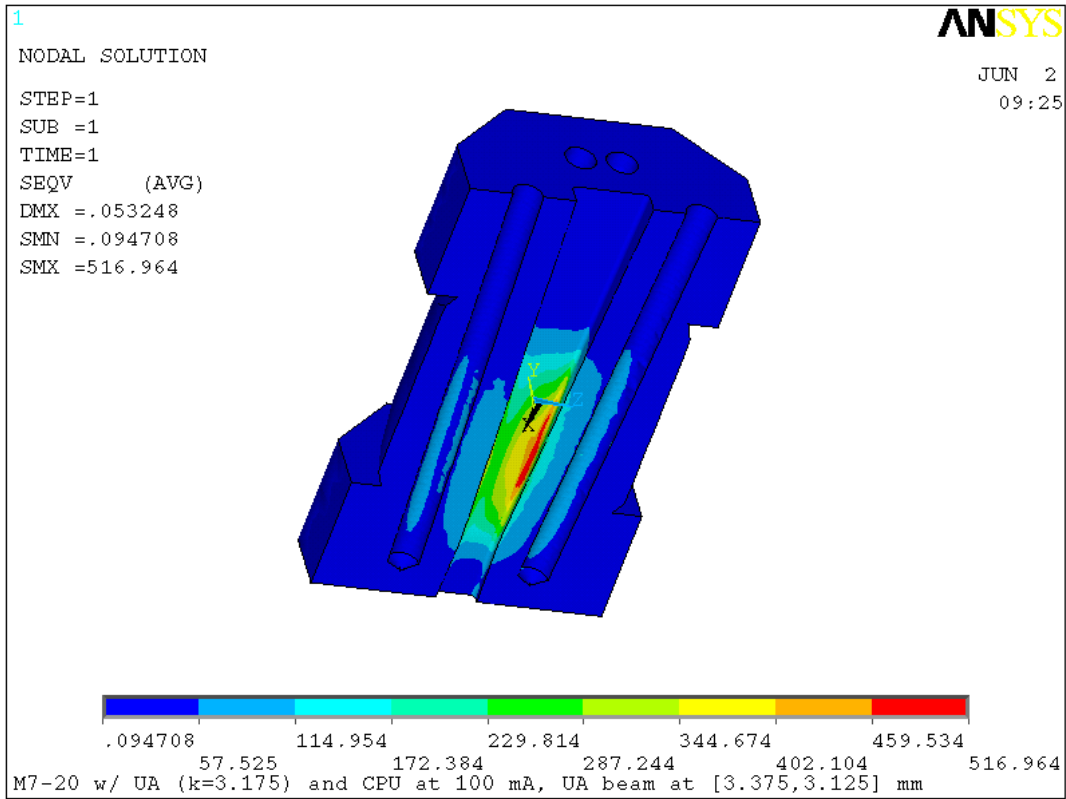


Figure 6.3-9 M7-20 von Mises stress plot (MPa), with undulator A and the CPU. UA beam near-corner missteering, UA beam center at [3.375, 3.125] mm.

The von Mises stress for M7-20 at 100 mA operation is almost equivalent to the exit mask L5-83 for undulator A at 11 mm gap at 130 mA. Thus 100 mA is the maximum beam current that 4-ID can operate. The gap of undulator A needs to be opened with any beam current larger than 100 mA.

7. Summary and Conclusion

Generally speaking, both FEv1.2u and FEv1.5 front ends can operate with a single undulator A at 11 mm gap at a maximum current of 130 mA under the current failure criteria. For FEv1.2u, the maximum beam current allowed is limited by the photon shutters, first fixed mask and the exit mask. For FEv1.5 the maximum beam current allowed is limited by the fixed masks and the exit mask. If the new failure criteria defines separate criteria for shutters and masks and allows higher stress limit on masks, then the maximum allowed beam current for FEv1.5 will be higher. Special cases with two IDs such as 2-ID, 3-ID and 4-ID are restricted to 100 mA. At a higher current run, these sectors should only run with a single undulator or run with both undulators at a restricted gap. 2-ID is currently operated by limiting the combined total power to a certain limit from both undulators. The 11-ID elliptical multipole wiggler (EMW) has a much lower power density compared to undulator A, so it is conservative to say that the maximum beam current for 11-ID is 130 mA. The 11-ID EMW will be replaced with a different ID in the near future, so it is not necessary to study 11-ID for a higher current run.

7.1. FE Components and Source Summary

Table 7.1-1 summarizes all the data, including the front-end type, FE components, ID source, maximum allowed beam current and maximum temperature and stress under the maximum allowed beam current.

Table 7.1-1 Summary table of sector, FE type, source, FE components, maximum temperature and stress, maximum allowed beam current

Sector	ID source	Type of FE	Front End Components							Max. allowed beam current	Comments
			FM1	FM2	FM3	PS1	PS2	Exit Mask	2 nd Exit Mask		
1,5,6,7,8,9,10,12,13,14,15,17,18,19,20,33,34	U-3.3, k=2.62	FEv1.2u	M1-30	M2-30	N/A	P1-20	P2-20	L5-83	M4-30	130 mA	M4-30 installed in sector 1,7,10 only
	T _{max} at 130mA (°C)		314.1	260.9		291.1	302.6	240.1	126.4		
	σ _{vm,max} at 130mA (MPa)		541.2	398.1		397.9	396.8	506.2	209.7		
16,22,31,32	U-3.3, k=2.62	FEv1.5	M1-40	M2-40	M2-50	P2-30	P2-30	M4-40	N/A	130 mA	PS2 is the same as PS1, PS2 data not calculated
	T _{max} at 130mA (°C)		258.6	252.7	254.3	175.5	<PS1	246.6			
	σ _{vm,max} at 130mA (MPa)		453.8	424.5	402.6	229.1	<PS1	475.5			
2-ID	U-3.3 US U-5.5 DS	FEv1.2u	M1-30	M2-30	N/A	P1-20	P2-20	L5-83	N/A	100 mA	Limit combined total power
3-ID	U-2.7 US U-2.7 DS K=1.697	FEv1.2u	M1-30	M2-30	N/A	P1-20	P2-20	L5-83	N/A	100 mA	Maximum beam current based on photon shutters
	T _{max} at 100mA (°C)					282	301				
	σ _{vm,max} at 100mA (MPa)					404	416				
4-ID	CPU US U-3.3 DS k=3.175	FEv1.2u & FEv1.5 mix	M1-40	M2-40	M2-50	P1-20	P2-20	M7-20	N/A	100 mA	Max. current based on photon shutters and exit mask
	T _{max} at 100mA (°C)					297	308	247			
	σ _{vm,max} at 100mA (MPa)					410	403	516.9			
11-ID	EMW	FEv1.2w	M1-20	M2-30	N/A	P1-20	P2-20	N/A	N/A	130 mA	
21,23,24	Two U-3.3-N62 1.0 mrad	CUFE	FM1	FM2	N/A	PS1	PS2	Exit mask	N/A	200 mA	See CUFE design report [1]
26-ID	Two inline U-3.3, k=2.76	High heat load FE	FM1	FM2	FM3 and FM4	PS1	PS2	Exit mask	N/A	180 mA	See high heat load FE design report [2]
30-ID	3 inline U-3.0	High heat load FE	FM1	FM2	FM3 and FM4	PS1	PS2	Exit mask	N/A	120 mA	

Acknowledgments

The author thanks Dr. Mati Meron of CARS-CAT for providing the synchrotron source calculation source code SRUFF. The author also thanks Dana Capatina, Michelle Givens and Erika Rossi of the Design & Drafting Group for modeling the components' geometry in ProEngineer. The author also thanks Susan Picologlou for editing this paper.

References

- [1] M. Sanchez del Rio and R. J. Dejus, "XOP: A Multiplatform Graphical User Interface for Synchrotron Radiation Spectral and Optics Calculations," SPIE Proc., vol. 3152, 148-157, 1997.
- [2] Mati Meron, CARS-CAT, "SRUFF: A Comprehensive Package for Synchrotron Radiation Spectral and Optics Calculations," unpublished, 2001.
- [3] "GlidCop Grade AL-15 Dispersion Strengthened Copper," Technical data, SCM Metal Products, Inc., 1988.
- [4] H.L.T. Nian, T. M. Kuzay, I. C. A. Sheng, "Thermo-Mechanical Optimization of Photon Shutter 1 for APS Front Ends," APS Light Source Note LS-205, July 1992.
- [5] H. L. T. Nian, T. M. Kuzay, and I. C. A. Sheng, "Thermo-Mechanical Parametric Studies of Fixed Mask 1 and Photon Shutter 2 for APS Front Ends," APS Light Source Note LS-208, September 1992.
- [6] H. L. Thomas Nian, D. Shu, I. C. Albert Sheng, Tuncer M. Kuzay, "Thermo-mechanical analysis of fixed mask 1 for the advanced photon source insertion device front ends," Nuclear Instrum. Methods, A347 (1994) 657-663.